



Université catholique de Louvain
École Polytechnique de Louvain
Earth and Life Institute

How modeling tools can inform coral reef management in the Florida Reef Tract

Doctoral dissertation presented by

Thomas Dobbelaere

in partial fulfillment of the requirements for the degree of

Doctor in Engineering Science

Thesis committee:

Prof. Emmanuel Hanert (Supervisor)	Université catholique de Louvain
Prof. Eric Deleersnijder	Université catholique de Louvain
Dr. Jonathan Lambrechts	Université catholique de Louvain
Prof. Claire B. Paris-Limouzy	University of Miami
Dr. Christopher Thomas	Université catholique de Louvain ^a

^aPresent address: Risk Management Solutions, London, UK

Louvain-la-Neuve, March 2022

Abstract

The population of corals throughout the world has declined dramatically under the effect of rising water temperature and many coral species are now listed as threatened. In addition to ocean warming, other threats to corals include (but are not limited to) disease outbreaks, intensifying hurricanes and sediment disturbances. In particular, Florida's Coral Reef (FCR) is currently facing a multi-year outbreak of the stony coral tissue loss disease (SCTLD). First observed in 2014 during the monitoring of dredging operations in the Port of Miami, the disease has now spread through the entirety of FCR and has been observed in numerous territories of the Caribbean. Furthermore, hurricanes tend to strike Florida during the reproduction period of the corals, when thousands of larvae are released in the water column. In addition to causing physical harm to corals, hurricanes significantly modify ocean currents and might therefore disturb larval exchanges between reefs. A high resolution ocean model, SLIM, is used to build a biophysical model to study the aforementioned threats to FCR. First, a coupled epidemi-hydrodynamic model is developed to study both the onset and the propagation mechanisms of the SCTLD. Furthermore, a coupled wave-current model is devised to study the impact of Hurricane Irma (2017) on transport processes in the Florida Keys. This study brings new insight on the impact of hydrodynamics on the propagation of SCTLD as well as the impact of hurricane on coral ecosystem.

Remerciements

Lorem ipsum dolor sit amet, consectetuer adipiscing elit. Ut purus elit, vestibulum ut, placerat ac, adipiscing vitae, felis. Curabitur dictum gravida mauris. Nam arcu libero, nonummy eget, consectetuer id, vulputate a, magna. Donec vehicula augue eu neque. Pellentesque habitant morbi tristique senectus et netus et malesuada fames ac turpis egestas. Mauris ut leo. Cras viverra metus rhoncus sem. Nulla et lectus vestibulum urna fringilla ultrices. Phasellus eu tellus sit amet tortor gravida placerat. Integer sapien est, iaculis in, pretium quis, viverra ac, nunc. Praesent eget sem vel leo ultrices bibendum. Aenean faucibus. Morbi dolor nulla, malesuada eu, pulvinar at, mollis ac, nulla. Curabitur auctor semper nulla. Donec varius orci eget risus. Duis nibh mi, congue eu, accumsan eleifend, sagittis quis, diam. Duis eget orci sit amet orci dignissim rutrum.

Nam dui ligula, fringilla a, euismod sodales, sollicitudin vel, wisi. Morbi auctor lorem non justo. Nam lacus libero, pretium at, lobortis vitae, ultricies et, tellus. Donec aliquet, tortor sed accumsan bibendum, erat ligula aliquet magna, vitae ornare odio metus a mi. Morbi ac orci et nisl hendrerit mollis. Suspendisse ut massa. Cras nec ante. Pellentesque a nulla. Cum sociis natoque penatibus et magnis dis parturient montes, nascetur ridiculus mus. Aliquam tincidunt urna. Nulla ullamcorper vestibulum turpis. Pellentesque cursus luctus mauris.

Nulla malesuada porttitor diam. Donec felis erat, congue non, volutpat at, tincidunt tristique, libero. Vivamus viverra fermentum felis. Donec nonummy pellentesque ante. Phasellus adipiscing semper elit. Proin fermentum massa ac quam. Sed diam turpis, molestie vitae, placerat a, molestie nec, leo. Maecenas lacinia. Nam ipsum ligula, eleifend at, accumsan nec, suscipit a, ipsum. Morbi blandit ligula feugiat magna. Nunc eleifend consequat lorem. Sed lacinia nulla vitae enim. Pellentesque tincidunt purus vel magna. Integer non enim. Praesent euismod nunc eu purus. Donec bibendum quam in tellus. Nullam cursus pulvinar lectus. Donec et mi. Nam vulputate metus eu enim. Vestibulum pellentesque felis eu massa.

Quisque ullamcorper placerat ipsum. Cras nibh. Morbi vel justo vitae lacus tincidunt ultrices. Lorem ipsum dolor sit amet, consectetuer adipiscing elit. In hac habitasse platea dictumst. Integer tempus convallis augue. Etiam facilisis. Nunc elementum fermentum wisi. Aenean placerat. Ut imperdiet, enim sed gravida sollicitudin, felis odio placerat quam, ac pulvinar elit purus eget enim. Nunc vitae tortor. Proin tempus nibh sit amet nisl. Vivamus quis tortor vitae risus porta vehicula.

Contents

Contents	vii
1 Introduction	1
2 Modeling the spread of SCTLD in Florida	7
2.1 Introduction	8
2.2 Methods	10
2.3 Results	19
2.4 Discussion and conclusions	23
3 Transmission of SCTLD from the Marquesas to the Dry Tortugas	27
3.1 Introduction	28
3.2 Methods	30
3.3 Results	32
3.4 Discussion and conclusion	35
4 The onset of the SCTLD outbreak and the PortMiami Deep Dredge Project	39
4.1 Introduction	40
4.2 Methods	42
4.3 Results	45
4.4 Discussion	48
4.5 Conclusion	51
5 Impacts of hurricanes on wave-induced ocean transport processes	53
5.1 Introduction	54
5.2 Methods	56
5.3 Results	65
5.4 Discussion	69
5.5 Conclusion	74
6 Conclusions and perspectives	75
Bibliography	79

Introduction

Lorem ipsum dolor sit amet, consectetuer adipiscing elit. Ut purus elit, vestibulum ut, placerat ac, adipiscing vitae, felis. Curabitur dictum gravida mauris. Nam arcu libero, nonummy eget, consectetuer id, vulputate a, magna. Donec vehicula augue eu neque. Pellentesque habitant morbi tristique senectus et netus et malesuada fames ac turpis egestas. Mauris ut leo. Cras viverra metus rhoncus sem. Nulla et lectus vestibulum urna fringilla ultrices. Phasellus eu tellus sit amet tortor gravida placerat. Integer sapien est, iaculis in, pretium quis, viverra ac, nunc. Praesent eget sem vel leo ultrices bibendum. Aenean faucibus. Morbi dolor nulla, malesuada eu, pulvinar at, mollis ac, nulla. Curabitur auctor semper nulla. Donec varius orci eget risus. Duis nibh mi, congue eu, accumsan eleifend, sagittis quis, diam. Duis eget orci sit amet orci dignissim rutrum.

Nam dui ligula, fringilla a, euismod sodales, sollicitudin vel, wisi. Morbi auctor lorem non justo. Nam lacus libero, pretium at, lobortis vitae, ultricies et, tellus. Donec aliquet, tortor sed accumsan bibendum, erat ligula aliquet magna, vitae ornare odio metus a mi. Morbi ac orci et nisl hendrerit mollis. Suspendisse ut massa. Cras nec ante. Pellentesque a nulla. Cum sociis natoque penatibus et magnis dis parturient montes, nascetur ridiculus mus. Aliquam tincidunt urna. Nulla ullamcorper vestibulum turpis. Pellentesque cursus luctus mauris.

Nulla malesuada porttitor diam. Donec felis erat, congue non, volutpat at, tincidunt tristique, libero. Vivamus viverra fermentum felis. Donec nonummy pellentesque ante. Phasellus adipiscing semper elit. Proin fermentum massa ac quam. Sed diam turpis, molestie vitae, placerat a, molestie nec, leo. Maecenas lacinia. Nam ipsum ligula, eleifend at, accumsan nec, suscipit a, ipsum. Morbi blandit ligula feugiat magna. Nunc eleifend consequat lorem. Sed lacinia nulla vitae enim. Pellentesque tincidunt purus vel magna. Integer non enim. Praesent euismod nunc eu purus. Donec bibendum quam in tellus. Nullam cursus pulvinar

lectus. Donec et mi. Nam vulputate metus eu enim. Vestibulum pellentesque felis eu massa.

Quisque ullamcorper placerat ipsum. Cras nibh. Morbi vel justo vitae lacus tincidunt ultrices. Lorem ipsum dolor sit amet, consectetur adipiscing elit. In hac habitasse platea dictumst. Integer tempus convallis augue. Etiam facilisis. Nunc elementum fermentum wisi. Aenean placerat. Ut imperdiet, enim sed gravida sollicitudin, felis odio placerat quam, ac pulvinar elit purus eget enim. Nunc vitae tortor. Proin tempus nibh sit amet nisl. Vivamus quis tortor vitae risus porta vehicula.

Fusce mauris. Vestibulum luctus nibh at lectus. Sed bibendum, nulla a faucibus semper, leo velit ultricies tellus, ac venenatis arcu wisi vel nisl. Vestibulum diam. Aliquam pellentesque, augue quis sagittis posuere, turpis lacus congue quam, in hendrerit risus eros eget felis. Maecenas eget erat in sapien mattis porttitor. Vestibulum porttitor. Nulla facilisi. Sed a turpis eu lacus commodo facilisis. Morbi fringilla, wisi in dignissim interdum, justo lectus sagittis dui, et vehicula libero dui cursus dui. Mauris tempor ligula sed lacus. Duis cursus enim ut augue. Cras ac magna. Cras nulla. Nulla egestas. Curabitur a leo. Quisque egestas wisi eget nunc. Nam feugiat lacus vel est. Curabitur consectetur.

Suspendisse vel felis. Ut lorem lorem, interdum eu, tincidunt sit amet, laoreet vitae, arcu. Aenean faucibus pede eu ante. Praesent enim elit, rutrum at, molestie non, nonummy vel, nisl. Ut lectus eros, malesuada sit amet, fermentum eu, sodales cursus, magna. Donec eu purus. Quisque vehicula, urna sed ultricies auctor, pede lorem egestas dui, et convallis elit erat sed nulla. Donec luctus. Curabitur et nunc. Aliquam dolor odio, commodo pretium, ultricies non, pharetra in, velit. Integer arcu est, nonummy in, fermentum faucibus, egestas vel, odio.

Sed commodo posuere pede. Mauris ut est. Ut quis purus. Sed ac odio. Sed vehicula hendrerit sem. Duis non odio. Morbi ut dui. Sed accumsan risus eget odio. In hac habitasse platea dictumst. Pellentesque non elit. Fusce sed justo eu urna porta tincidunt. Mauris felis odio, sollicitudin sed, volutpat a, ornare ac, erat. Morbi quis dolor. Donec pellentesque, erat ac sagittis semper, nunc dui lobortis purus, quis congue purus metus ultricies tellus. Proin et quam. Class aptent taciti sociosqu ad litora torquent per conubia nostra, per inceptos hymenaeos. Praesent sapien turpis, fermentum vel, eleifend faucibus, vehicula eu, lacus.

Pellentesque habitant morbi tristique senectus et netus et malesuada fames ac turpis egestas. Donec odio elit, dictum in, hendrerit sit amet, egestas sed, leo. Praesent feugiat sapien aliquet odio. Integer vitae justo. Aliquam vestibulum fringilla lorem. Sed neque lectus, consectetur at, consectetur sed, eleifend ac, lectus. Nulla facilisi. Pellentesque eget lectus. Proin eu metus. Sed porttitor. In hac habitasse platea dictumst. Suspendisse eu lectus. Ut mi mi, lacinia sit amet, placerat et, mollis vitae, dui. Sed ante tellus, tristique ut, iaculis eu, malesuada ac, dui. Mauris nibh leo, facilisis non, adipiscing quis, ultrices a, dui.

Morbi luctus, wisi viverra faucibus pretium, nibh est placerat odio, nec commodo wisi enim eget quam. Quisque libero justo, consectetur a, feugiat vitae, porttitor eu, libero. Suspendisse sed mauris vitae elit sollicitudin malesuada. Mae-

cenas ultricies eros sit amet ante. Ut venenatis velit. Maecenas sed mi eget dui varius euismod. Phasellus aliquet volutpat odio. Vestibulum ante ipsum primis in faucibus orci luctus et ultrices posuere cubilia Curae; Pellentesque sit amet pede ac sem eleifend consectetur. Nullam elementum, urna vel imperdierit sodales, elit ipsum pharetra ligula, ac pretium ante justo a nulla. Curabitur tristique arcu eu metus. Vestibulum lectus. Proin mauris. Proin eu nunc eu urna hendrerit faucibus. Aliquam auctor, pede consequat laoreet varius, eros tellus scelerisque quam, pellentesque hendrerit ipsum dolor sed augue. Nulla nec lacus.

Suspendisse vitae elit. Aliquam arcu neque, ornare in, ullamcorper quis, commodo eu, libero. Fusce sagittis erat at erat tristique mollis. Maecenas sapien libero, molestie et, lobortis in, sodales eget, dui. Morbi ultrices rutrum lorem. Nam elementum ullamcorper leo. Morbi dui. Aliquam sagittis. Nunc placerat. Pellentesque tristique sodales est. Maecenas imperdierit lacinia velit. Cras non urna. Morbi eros pede, suscipit ac, varius vel, egestas non, eros. Praesent malesuada, diam id pretium elementum, eros sem dictum tortor, vel consectetur odio sem sed wisi.

Sed feugiat. Cum sociis natoque penatibus et magnis dis parturient montes, nascetur ridiculus mus. Ut pellentesque augue sed urna. Vestibulum diam eros, fringilla et, consectetur eu, nonummy id, sapien. Nullam at lectus. In sagittis ultrices mauris. Curabitur malesuada erat sit amet massa. Fusce blandit. Aliquam erat volutpat. Aliquam euismod. Aenean vel lectus. Nunc imperdierit justo nec dolor.

Etiam euismod. Fusce facilisis lacinia dui. Suspendisse potenti. In mi erat, cursus id, nonummy sed, ullamcorper eget, sapien. Praesent pretium, magna in eleifend egestas, pede pede pretium lorem, quis consectetur tortor sapien facilisis magna. Mauris quis magna varius nulla scelerisque imperdierit. Aliquam non quam. Aliquam porttitor quam a lacus. Praesent vel arcu ut tortor cursus volutpat. In vitae pede quis diam bibendum placerat. Fusce elementum convallis neque. Sed dolor orci, scelerisque ac, dapibus nec, ultricies ut, mi. Duis nec dui quis leo sagittis commodo.

Supporting publications

- Dobbelaere T.**, E.M. Muller, L. J. Gramer, D. M. Holstein and E. Hanert (2020), Coupled Epidemio-Hydrodynamic Modeling to Understand the Spread of a Deadly Coral Disease in Florida. *Frontiers in Marine Science*, 7, 1-16.
- Dobbelaere T.**, M. Curcic, M. Le Hénaff and E. Hanert (2021), Impacts of Hurricane Irma (2017) on ocean transport processes, *Ocean Modelling*, accepted.
- Dobbelaere T.**, D. M. Holstein, E.M. Muller, L. J. Gramer, L. McEachron, S.D. Williams and E. Hanert (2021), Connecting the dots: Transmission of stony coral tissue loss disease from the Marquesas to the Dry Tortugas. *Frontiers in Marine Science*, accepted.
- Purkis S.J., A.M. Oehlert, **T. Dobbelaere**, E. Hanert and P. Harris (2020), Always a White Christmas in the Bahamas - Ocean Chemistry and Hydrodynamics Focus Winter Mud Production on Great Bahama Bank, *Sedimentology*, in revision.
- Alaerts L., **T. Dobbelaere**, P.M. Gravinese and E. Hanert (2022), Climate change will fragment Florida stone crab communities. *Frontiers in Marine Science*, submitted.
- Hanert E., Aboobacker V.M., Veerasingam S, **Dobbelaere T.**, Vallaey V. And E. Hanert (2021) A multiscale ocean modelling system for the central Arabian Gulf: From basin-scale circulation patterns to flow-structure interactions. *Estuarine, Coastal and Shelf Science*, submitted.
- Anselain T., **T. Dobbelaere**, E. Heggy and E. Hanert (2022) Qatar oil spill vulnerability threatens both its national water security and the global gas market. *Nature Communications*, in preparation.

Public presentations

- D. Vincent**, O. Karatekin, V. Dehant, E. Deleersnijder, 2015 Numerical simulations of tides in Ontario Lacus. European geoscience Union - General Assembly, Vienna.
<http://hdl.handle.net/2078.1/158392>
- D. Vincent**, O. Karatekin, V. Dehant, E. Deleersnijder, 2016, Modelling of tidal flows between Titan's seas Kraken Mare and Ligeia Mare. Titan surface meeting, Paris.
- D. Vincent**, O. Karatekin, V. Dehant, E. Deleersnijder, 2016, Modelisation of tidal flows between Titan's seas Kraken Mare and Ligeia Mare. European geoscience Union - General Assembly, Vienna.
<http://hdl.handle.net/2078.1/173566>
- D. Vincent**, O. Karatekin, V. Dehant, E. Deleersnijder, Eric, 2017, Study of liquid exchanges between Titan's seas Kraken Mare and Ligeia Mare. European

- geoscience Union - General Assembly, Vienna.
<http://hdl.handle.net/2078.1/185118>
- D. **Vincent**, O. Karatekin, V. Dehant, E. Deleersnijder, Eric, 2017, Modelling the tides of Titan's liquid bodies. TECLIM Seminar, Louvain-la-Neuve.
- D. **Vincent**, O. Karatekin, J. Lambrechts, V. Dehant, E. Deleersnijder, 2018, Tides and eigenmodes of an idealized subsurface global ocean on Titan. European geoscience Union - General Assembly, Vienna.
<http://hdl.handle.net/2078.1/196902>
- H. A. Le, X. H. D. Vu, J. Lambrechts, S. Ortaleb, V. Vallaeyns, D. **Vincent**, N. Gratiot, S. Soares Frazao, E. Deleersnijder, 2018, A new wetting – drying algorithm integrated in SLIM, with an application to the Tonle Sap lake, Mekong. European geoscience Union - General Assembly, Vienna.
<http://hdl.handle.net/2078.1/196904>

Modeling the spread of SCTLD in Florida

This chapter is based on the following article:

Dobbelaere, T., Muller, E. M., Gramer, L. J., Holstein, D. M., & Hanert, E. (2020). Coupled epidemio-hydrodynamic modeling to understand the spread of a deadly coral disease in Florida. *Frontiers in Marine Science*, 7, 1016. doi: 10.3389/fmars.2020.591881.

Abstract

For the last six years, the Florida Reef Tract (FRT) has been experiencing an outbreak of the Stony Coral Tissue Loss Disease (SCTLD). First reported off the coast of Miami-Dade County in 2014, the SCTLD has since spread throughout the entire FRT with the exception of the Dry Tortugas. However, the causative agent for this outbreak is currently unknown. Here we show how a high-resolution bio-physical model coupled with a modified patch Susceptible-Infectious-Removed epidemic model can characterize the potential causative agent(s) of the disease and its vector. In the present study, the agent is assumed to be transported within composite material (e.g., coral mucus, dying tissues, and/or resuspended sediments) driven by currents and potentially persisting in the water column for extended periods of time. In this framework, our simulations suggest that the SCTLD is likely to be propagated within neutrally buoyant material driven by mean barotropic currents. Calibration of our model parameters with field data shows that corals are diseased within a mean transmission time of 6.45 days, with a basic reproduction number slightly above 1. Furthermore, the propagation speed of the disease through the FRT is shown to occur for a

well-defined range of values of a disease threshold, defined as the fraction of diseased corals that causes an exponential growth of the disease in the reef site. Our results present a new connectivity-based approach to understand the spread of the SCTLD through the FRT. Such a method can provide a valuable complement to field observations and lab experiments to support the management of the epidemic as well as the identification of its causative agent.

2.1 Introduction

Coral diseases are a major threat to coral reef ecosystems and have led to significant declines in coral cover especially within the Caribbean region (Richardson et al., 1998b; Sutherland et al., 2004; Aronson and Precht, 2001; Harvell et al., 2007; Miller et al., 2009; Brandt and McManus, 2009). Indeed, the Florida Reef Tract (FRT), which was dominated by *Acropora palmata* and *Acropora cervicornis*, and often had 30% coral cover until the 1970s/80s (Dustan and Halas, 1987; Porter and Meier, 1992), is now dominated by bare substrate, octocorals, and macroalgae with only approximately 5% stony coral cover remaining (Ruzicka et al., 2013). The loss of the branching Acroporid species was attributed primarily to a disease outbreak, termed white band disease (Aronson and Precht, 2001), but several other threats such as habitat reduction, eutrophication, overfishing, hurricanes, and bleaching likely all contributed to these species decline (Team, 2005). Subsequent losses of coral cover within the region were often linked to additional disease incidences and repeated regional coral bleaching events as a result of global climate change (Kuta and Richardson, 1996; Richardson et al., 1998b; Sutherland et al., 2004; Gardner et al., 2003; Aronson and Precht, 2006; Kuffner et al., 2015; Manzello, 2015). A novel coral disease outbreak, termed Stony Coral Tissue Loss Disease (SCTLD), is now threatening the last vestiges of coral throughout the Florida Reef Tract (FRT).

SCTLD was first documented off the coast of Miami-Dade County in the summer of 2014 by Precht et al. (2016) and has since spread throughout the entire FRT with the exception of the Dry Tortugas. To date, SCTLD has been observed affecting over 20 different stony corals species. A case definition of SCTLD has been compiled to describe the visual appearance and ecology of SCTLD (NOAA, 2018). Briefly, the gross morphology of SCTLD is described as focal or multifocal, with locally extensive to diffuse areas of acute to subacute tissue loss distributed basally, peripherally, or both. In some cases, tissues bordering areas of chronic tissue loss show indistinct bands (1–5 cm) of pallor, progressing to normal pigmentation away from the denuded skeleton. There is also a range in coral susceptibility to SCTLD, with species categorized as highly susceptible (e.g., *Dendrogyra cylindrus*, *Dichocoenia stokesii*, *Meandrina meandrites*), moderately susceptible (e.g., *Orbicella* spp., *Montastraea cavernosa*, *Siderastrea siderea*, *Stephanocoenia intersepta*), or tolerant (e.g., *Porites* spp., *Acropora* spp.). Unfortunately, SCTLD has not remained isolated in the FRT and has now been recorded in Mexico (Alvarez-

Filip et al., 2019), the US Virgin Islands (Blondeau et al., 2020) and several other locations around the Caribbean (Kramer et al., 2019). The continued persistence of the outbreak, the high number of species affected, and the large geographical range of reports consistent with the case definition suggests that SCTLD is the largest coral disease outbreak on record

Large-scale spatial epidemiologic analyses showed that the reefs in Florida with SCTLD are clustered, supporting a contagious mode of transmission (Muller et al., 2020). Similarly, aquaria-based experiments indicate SCTLD can be transmitted through direct contact or indirectly through the water column (Aeby et al., 2019) suggesting water can function as a SCTLD vector, at least within a controlled setting. The initial exponential increase in spread among reefs from the disease epicenter (Precht et al., 2016) and the persistent subsequent linear rate of spread of SCTLD (Muller et al., 2020), north along South Florida reefs and south into the Florida Keys, indicates that water currents may play a role in disease transmission. Furthermore, the rate of spread, estimated at 100 m per day, suggests surface currents are likely too fast to have spread SCTLD within the region. These results imply that either the middle layer or the bottom boundary layer, which are both significantly slower than surface currents, may be the vertical location in which transmission occurs (Muller et al., 2020). However, to date, there have been no attempt to link local hydrodynamic modeling efforts with the spatio-temporal dynamics of SCTLD in Florida.

Estimating the transport of the disease causative agent from reef to reef by currents cannot be performed empirically. However, experimentally-calibrated numerical models that simulate currents can provide a realistic picture of the dispersal of disease agents. Nonetheless, accurately modeling water circulation at the spatial scales that affect this dispersal remains a key challenge, as small-scale flow features such as recirculation eddies around reefs and islands strongly impact exchanges between reefs (Wolanski, 1994; Burgess et al., 2007; Figueiredo et al., 2013). In this context, models that can explicitly simulate flow features down to the reef scale are needed. This represents a spatial resolution of the order of 100-1,000 m in dense reef systems. As of today, most regional ocean models using traditional numerical methods cannot achieve such resolution because of the computational resources it requires. To our knowledge, the best resolution currently available among these models in the FRT is ~ 900 m with the FKEYS-HYCOM model that has been developed for the Florida Keys region (Kourafalou and Kang, 2012; Sponaugle et al., 2012; Vaz et al., 2016). Unstructured-mesh ocean models offer a potential solution to this resolution issue by locally increasing the model resolution close to reefs and islands (Lambrechts et al., 2008; Thomas et al., 2014, 2015), in order to focus the computational resources where they are most needed. High resolution bio-physical dispersal models can be used to build the potential connectivity between reefs and therefore approximate exchanges between colonies in the complex topography of the coral reef systems (Frys et al., 2020a).

Marine diseases differ significantly from better studied terrestrial diseases, namely due to the potential for long environmental residence times, during which pathogens

may survive and disperse through the water (Harvell et al., 2007; Sokolow et al., 2009). Several recent studies have attempted to adapt traditional epidemic models (Susceptible-Infectious-Recovered, or SIR models) to coral reef systems (Sokolow et al., 2009; Bidegain et al., 2016a,b). Novel approaches have included developing pathogen pools (Bidegain et al., 2016a,b), and to model at the metapopulation scale, rather than at the scale of coral holobionts (Sokolow et al., 2009). Both of these approaches are attempting to address the same issue: disease occurs between patches of entirely sessile animals, through the dispersal of pathogen(s). Thus, there are internal within-patch disease dynamics and metapopulation-scale between-patch dynamics occurring simultaneously. The epidemic model developed in the present study utilizes the same basic architecture of previous coral reef SIR models, but rather than assume pathogen pools (e.g. Bidegain et al. (2016a,b)) or ignore internal patch dynamics (e.g. Sokolow et al. (2009)), we have modeled both within-patch disease dynamics and the dispersal of pathogenic agents explicitly using potential connectivity networks.

The objective of the present study is to deduce the probable propagation mechanism of the SCTLD throughout the FRT by developing an experimentally-calibrated epidemio-hydrodynamic model. With a resolution of about 100 m, this model can capture potential exchanges of disease-carrying material, further denominated as "infectious" in our modeling framework, between reefs that would be ignored by coarser models. By reproducing the observed spread of disease between 1st May 2018 and 1st April 2019, we provide insight on the characteristics of the disease agent and its vector. Ultimately, our model, coupled with lab and field studies, provide novel insight into the management of the epidemic, the identification of its causative agent, and mode of transmission.

2.2 Methods

2.2.1 Modeling reef connectivity

In the present study, we focused on the exchanges of infectious material between coral reefs driven by ocean currents, which therefore have to be accurately simulated. An ocean model should provide a realistic large-scale circulation while also resolving small-scale flow features down to the scale of individual reefs. In this context, we used the unstructured-mesh depth-integrated coastal ocean model *slim*¹ to simulate ocean currents over an area that includes the FRT but also the Florida Strait and part of the Gulf of Mexico (Fig. 2.1). By using an unstructured mesh, we increased the model resolution only over the FRT and hence concentrate computational resources where they were most needed. *slim* has already been successfully applied in complex coastal systems such as the Great Barrier Reef (Lambrechts et al., 2008; Thomas et al., 2014) and is well suited to shallow-water flows. Details of the model formulation and validation are provided in Frys et al. (2020a).

¹<https://www.slim-ocean.be>

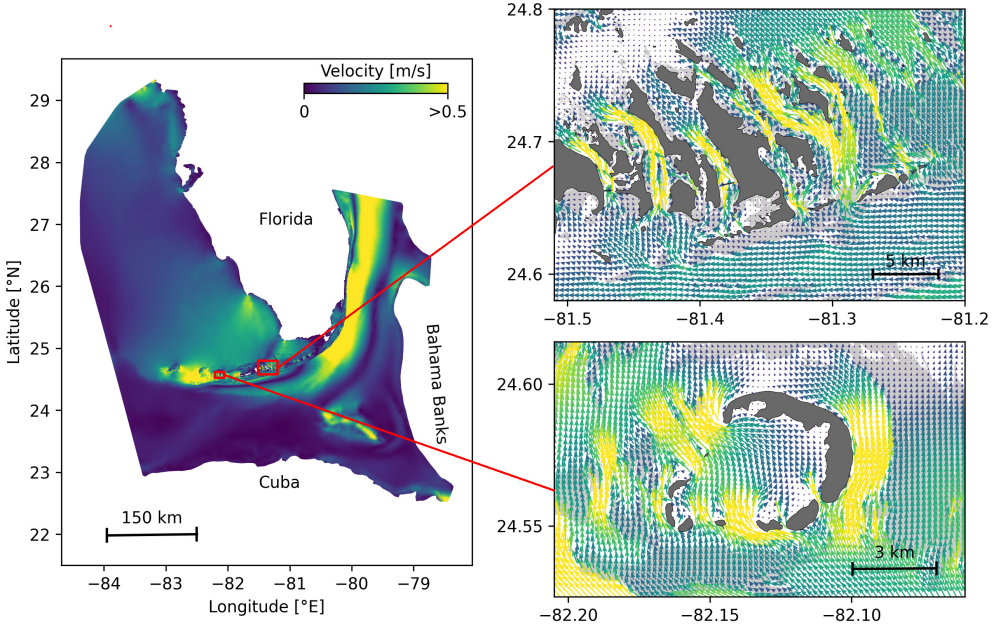


Fig. 2.1: Model computational domain and close-up views of the mesh with snapshots of the currents on May, 25 2018 at 00:00, for the Marquesas Keys (bottom) and the Lower Keys (top). This illustrates the benefits of unstructured meshes to represent the fine-scale details of the topography and hence simulate currents down to the scale of individual reefs (shown in light grey) and islands (shown in darker grey).

The mesh resolution depended only on the distance to the coast, but we distinguished between the coastlines along the FRT where we imposed a maximum resolution of 100 m and the other coastlines along which the finest resolution was 2500 m. The mesh was generated with the open-source mesh generator GMSH (Geuzaine and Remacle, 2009) and is composed of approximately 7×10^5 elements. The coarsest elements, far away from the FRT, had a characteristic length size of about 10 km. Fig. 2.1 depicts how a 100-m spatial resolution mesh simulated fine-scale details of the ocean currents, such as recirculation eddies and currents within the dense reef system in the Lower Keys that consist of many individual reefs with narrow passages in between.

The simulated currents were then used to model dispersal of disease agents throughout the FRT. In this study, 3 types of potential vectors carrying the disease causative agent were considered: positively buoyant (e.g. mucus and surfactant), neutrally buoyant (e.g. fines, pelagic organisms) and negatively buoyant (e.g. sediments, composites, demersal organisms). As SLIM is a depth-averaged model, the mean currents it generates are well suited to model the dispersal of neutrally buoyant material remaining within the water column. However, these currents must be modified to correctly represent the dynamics of material evolving in the surface and bottom boundary layers. Therefore, surface current response to winds was estimated by adding 1.5% of the wind speed to SLIM currents with a stress-layer veering angle of 45° to the right for positively buoyant particles. Such

parameterization is shown to be an accurate approximation of wave-induced Stokes drift and quasi-Eulerian surface currents by Arduin et al. (2009). For negatively buoyant material, bottom currents were obtained by taking 60% of SLIM currents velocity with a veering angle of 15° to the left. This is an approximation based on observations of bottom currents and whole water column current profiles in the shallow waters (<15 m) of Hawk Channel in the middle Florida Keys by Smith (2009), as well as observations obtained during the Atlantic Ocean Acidification Testbed project (Gramer, pers. comm.). This application is also consistent with the theory of current veering in the bottom Ekman layer, albeit that was previously observed in deeper (30-90 m) coastal waters, e.g., by Perlin et al. (2007) and Kundu (1976).

Using these three velocity fields, virtual particles were then released on all the reefs composing the FRT to model the dispersal of material carrying the disease causative agent. The locations of the reefs of Florida were extracted from the "coral reefs and hardbottom" layer of the Unified Florida Reef Tract Map (FWC-FWRI, 2017). The polygons of this reef map were then further divided into 500 m × 500 m squares in order to track the propagation of the disease with a finer geographical resolution, generating a total of 16,823 polygons. At the beginning of each simulated month and for each type of current, a total of about 1.5×10^6 particles were released over all the reef polygons. These particles had a state composed of their polygon of origin as well as their mass, that they lose at a constant rate γ as they were moved by surface, mean or bottom currents. The value of γ was chosen so that particles had a half-life of 30 days. When the particles were brought over a reef polygon by currents, the amount of disease mass that landed on the polygon was recorded in monthly potential connectivity matrices, whose entries are denoted C_{ij} . The matrix rows correspond to the source reefs and the columns correspond to the destination reefs. Hence C_{ij} represents the mass of diseased material originating from sub-reef i that had settled on sub-reef j . This matrix was then normalized by dividing each of its rows i by the total mass of particles released on polygon i in order to obtain the normalized potential connectivity matrix \tilde{C} , whose entry \tilde{C}_{ij} gives the probability that disease agents produced on sub-reef i settle on sub-reef j . Connectivity matrices were computed for each type of current and for each month of the simulated period.

These connectivity matrices are more easily handled by interpreting them as large graphs whose vertices are sub-reefs and whose edges represent connectivity pathways. They were analyzed using graph theory tools. In the present study, four potential connectivity measures were used to interpret the monthly computed graphs. These indicators are described in Table 2.1. The first indicator is the weighted connectivity length (WCL), which gave the average dispersal distance from origin to destination for material produced on a given reef. The weighted connectivity of reef polygon i is expressed as:

$$WCL_i = \frac{\sum_j \tilde{C}_{ij} L_{ij}}{\sum_j \tilde{C}_{ij}} \quad (2.1)$$

where L_{ij} is the distance between origin reef i and destination reef j . Another

Indicators	Description	What it shows
Weighted connectivity length (WCL)	Average dispersal distance from origin to destination reef for all disease agents released over a reef	Average distance that disease agents from a reef travels successfully to another reef
Out-degree	Number of out-going connections originating from a given reef multiplied by the total mass exchanged	Overall potential for a reef to spread the disease
Fraction exchanged	Fraction of disease agents produced on a given reef that settles on other reefs	Relative likelihood of successful spread of the disease to other reefs
Self-recruitment	Fraction of disease agents settling on a given reef that has been released on the same reef	Relative likelihood of unsuccessful spread of the disease from other reefs

Table 2.1: Indicators used to analyze the modeled exchanges of infected material for each considered type of currents and for each simulated month.

measure of the spreading potential of reef j is its out-degree, i.e. the product of the number of connections originating from reef j by the quantity of disease agents it sent to the network. This indicator was obtained by computing the number of non-zero entries of row i in the potential connectivity matrix C and multiplying it with $\sum_j C_{ij}$. The information given by the out-degree was complemented by the fraction of disease agents produced on reef i that successfully settled on a reef, called the fraction exchanged of reef i . This indicator is given by $\sum_j \tilde{C}_{ij}$. Finally, the isolation of reef i in the network was given by its self-recruitment, i.e. the fraction of disease agents settling on reef i that originated from reef i , computed by $C_{ii} / \sum_j C_{ji}$. A large self-recruitment value indicates that little infectious material produced elsewhere settled on the reef and thus that it was isolated from the rest of the network. However, due to its relative nature, high self-recruitment could still be coupled with a large amount of exogenous diseased agents reaching the reef, although this quantity would be considered proportionally small in regard to the total mass of diseased material settling on the reef.

2.2.2 Epidemiological modeling

2.2.2.1 Model equations

The spread of the SCTLD throughout the FRT was simulated using a connectivity-based Kermack and McKendrick (1927) SIR model. SIR models are among the most standard epidemiological models. They divide individuals into three compartments: susceptible (S), infectious (I) and removed (R). When affected by the disease, susceptible individuals become infectious and infect other susceptible individuals until they are removed from the system, either through recovery or death. Such models usually rely on the hypothesis of an homogeneous, well-mixed population. To account for the spatial heterogeneity of the FRT, the basic SIR formulation was modified by considering the fractions of susceptible (S_j), infectious (I_j) and removed (R_j) corals of each sub-reef j . Although the pathogen of SCTLD has not been identified, studies suggest a contagious mode of transmission (Aeby et al., 2019; Muller et al., 2020). Here, we use 'infectious' to denote disease agents that could be passed from individual to individual, which are responsible for causing disease signs. We note that the disease agents could be biological or non-biological in nature. In the present study's epidemiological model, individual reefs interact through the exchange of disease agents as represented by the different connectivity matrices. For each sub-reef j and at any time, the following relations hold: $0 \leq S_j, I_j, R_j \leq 1$ and $S_j + I_j + R_j = 1$. The evolution of these fractions through time is governed by the following equations:

$$\begin{aligned}\frac{dS_j}{dt} &= -\beta \sum_i \frac{A_i}{A_j} I_i \tilde{C}_{ij} S_j - \beta'(I_j) S_j I_j \\ \frac{dI_j}{dt} &= \beta \sum_i \frac{A_i}{A_j} I_i \tilde{C}_{ij} S_j + \beta'(I_j) S_j I_j - \sigma I_j \\ \frac{dR_j}{dt} &= \sigma I_j\end{aligned}\tag{2.2}$$

where \tilde{C}_{ij} is the entry corresponding to reef pair (i, j) of the normalized potential connectivity matrix [-], A_i is the area of reef polygon i [km^2], σ is the mortality rate [day^{-1}], and β and $\beta'(I_j)$ are the inter- and intra-reef disease transmission rates [day^{-1}], respectively. In this model, diseased corals of sub-reef i can 'infect' corals of sub-reef j if there is non-zero probability of disease agents exchange from sub-reef i to sub-reef j , given by \tilde{C}_{ij} . Moreover, to account for coral resistance to the disease, the intra-reef transmission function $\beta'(I_j)$ has the shape of a smooth step function of the fraction of infectious corals I_j and is expressed as follows:

$$\beta'(I_j) = \frac{\beta'_0}{2} (1 + \tanh[(I_j - I_0)/\tau]),\tag{2.3}$$

where I_0 is a threshold on the infection population above which intra-reef transmission becomes significant, and τ is a measure of the interval over which the transition from low to high transmission occurs. As long as the fraction of infectious corals on sub-reef j is below I_0 , the only infection mechanism taking place

is connectivity-driven transmission at rate β . Once the threshold is approached, intra-reef transmission with rate β'_0 is activated. A larger value of threshold I_0 corresponds to a greater resistance of corals to the disease, and therefore a slower spread of the disease within reef j . Coral reproduction and natural (*i.e.* non SCTLD-related) death rates are not taken into account in this model, which amounts to assume that they balance each other. For this study the same values were used for β and β'_0 .

2.2.2.2 Calibration

Transmission and removal parameters β'_0 and σ were fitted to disease prevalence observations averaged over all colonies from 6 permanent monitoring sites in the Lower Keys to accurately simulate the temporal evolution of S_j, I_j, R_j on each diseased reef polygon. Three focal reef sites were established in the lower Florida Keys, one offshore (Acer 17/18), one mid-channel (Wonderland), and one nearshore reef (N. Birthday). Sites were established in May 2018, when all colonies appeared healthy. Within each site, two $10\text{ m} \times 10\text{ m}$ quadrats were established. Quadrats were generally set up from east to west although N. Birthday was established with one quadrat further north of the other two to better capture coral cover in the site. All coral colonies $> 10\text{ cm}$ in size were mapped using self-contained underwater breathing apparatus (SCUBA). Each coral was given an (x, y) coordinate, identified to species, and maximum diameter was noted. After the initial data collection surveys, each site was visited every two to three weeks for rapid assessments to determine whether SCTLD was present. During these site visits, two divers conducted a visual assessment at each of the 6 quadrats. Disease was first observed in early October 2018. Detailed surveys were conducted every two to four weeks until December 2019. During the surveys, each individual coral was visually assessed for signs of SCTLD, including discoloration and tissue loss. Prevalence of diseased, apparently healthy, and dead were assessed for each time period. To relate our model framework to the compiled data, Eqs. 2.2 were simplified to a single-reef SIR model:

$$\begin{aligned}\frac{dS}{dt} &= -\beta'_0 SI \\ \frac{dI}{dt} &= \beta'_0 SI - \sigma I \\ \frac{dR}{dt} &= \sigma I\end{aligned}\tag{2.4}$$

Due to the low values of the entries in the normalized connectivity matrix \tilde{C}_{ij} , intra-reef transmission, when activated, is the dominant infection mechanism of Eqs. 2.2. Consequently, Eqs. 2.4 gave a reasonable approximation of the evolution of the disease on sub-reefs for which $I_j \geq I_0$. Using this approximation, the ratio β'_0/σ was estimated by matching the modeled fraction of susceptible corals remaining after the disease activity had stopped (S_∞) with observations. A standard property

of a SIR model solution is such that

$$S_\infty - \frac{\sigma}{\beta'_0} \log(S_\infty/S(t=0)) = 1 \quad (2.5)$$

where the initial fraction of susceptible corals ($S(t=0)$) was taken equal to $1 - I_0$ (see for instance Murray (2007)). In the framework of Eqs. 2.4, the ratio β'_0/σ gave the value of the basic reproduction number R_0 , defined as the average number of secondary cases produced by one infected individual introduced into a population of susceptible individuals (Keeling and Rohani, 2007). This number is used in epidemiological models to determine whether an emerging infectious disease can spread in a population ($R_0 > 1$) or not ($R_0 < 1$). The basic reproduction number that was obtained was then used to express σ in terms of β'_0 and calibrate its value to reproduce, as well as possible, the temporal evolution of the colonies-averaged susceptible population shown in Fig. 2.5.

2.2.2.3 Initialization

In order to solve Eqs. 2.2, initial conditions were needed, *i.e.* fractions of susceptible, infectious and recovered corals at the beginning of the simulated period. This information was constructed from 9 different field-collected datasets: (i) Coral Reef Evaluation and Monitoring Project (CREMP; 2014–2017), (ii) CREMP Presence/Absence Data (CREMP P_A; 2016–2017), (iii) Southeast Florida Coral Reef Evaluation and Monitoring Project (SECREMP; 2014–2017), (iv) Florida Reef Resilience Program Disturbance Response Monitoring (FRRP; 2014–2017), (v) Hurricane Irma Rapid Reef Assessment (IRMA; 2017, Viehman et al. (2018)), (vi) the Southeast Florida Action Network citizen science program (SEAFAN; 2014–2017), and (vii) the Southefrn Coral Disease Margin field effort (2017 and 2018; Neely (2018)), (viii) Mote Marine Laboratory's Field operations data (2018-2019) and (ix) data compiled through the citizen science BleachWatch program (2018). Every dataset provided data on the presence or absence of the SCTLD (or tissue loss consistent with the SCTLD case definition) within each survey. Some also provided detailed disease metrics such as the species affected and the disease prevalence, which was subsequently compiled into presence/absence of SCTLD data by surveyed site. The locations of these observations are shown in Fig. 2.2. Using this information, we first delineated the diseased zone by constructing the concave hull of the points where the disease was observed before May 2018. The reefs diseased prior to the beginning of our simulated period were then defined as the reefs located inside the constructed zone. The time of disease observation was then spatially interpolated on each reef of the diseased zone by kriging with a Gaussian semivariogram using Python pyKrig module (Murphy, 2014). Assuming an initial state $(S, I, R) = (1 - I_0, I_0, 0)$ when the disease was observed, the fractions of susceptible, infectious and removed corals on each reef of the diseased zone on the 1st May 2018 was finally approximated using Eqs. 2.4. Reefs outside of the diseased zone were initialized with an entirely susceptible population.

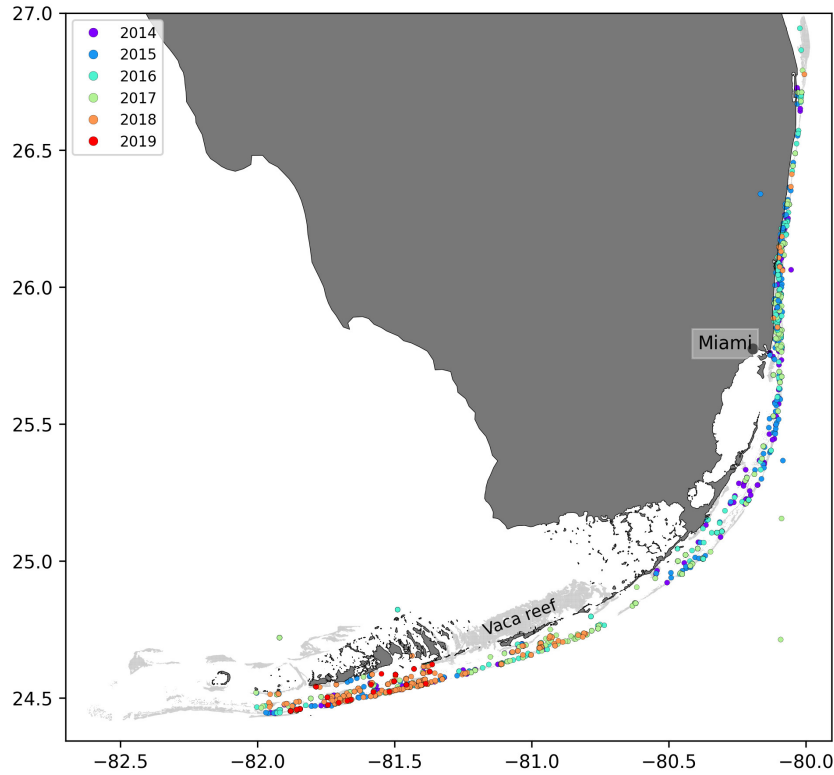


Fig. 2.2: Locations of the disease observations between 2014 and 2019 recorded in the data sets used in this study.

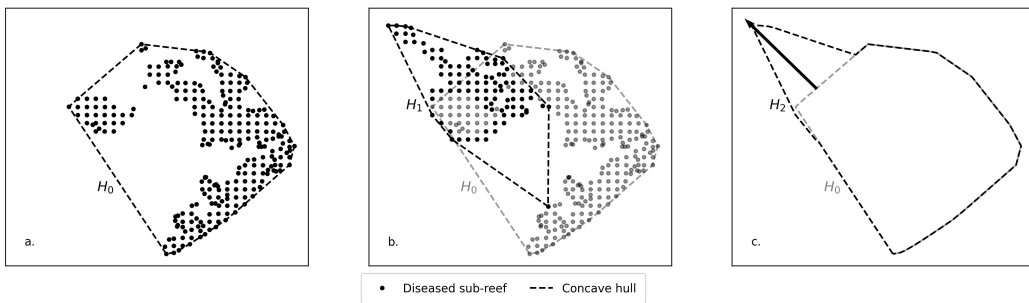


Fig. 2.3: Method used to compute the disease front displacement during a simulated time interval. **a.** Concave hull H_0 of the diseased sub-reefs at the beginning of the simulated period. **b.** Concave hull H_1 of the sub-reefs diseased during the simulated time interval. **c.** Arrow showing the computed front displacement during simulated time interval between H_0 and H_2 , the union of H_0 and H_1 .

2.2.2.4 Computation of front speed

Muller et al. (2020) estimated the speed of the spreading STCLD epidemics at around 92 m/day in the southern section of the FRT. In order to assess our simulation results in regard to this value, we developed a methodology to compute the displacement of the disease front during a given time interval within our simulated

period. First, the concave hull H_0 of the diseased polygons at the beginning of the time interval was delineated. Then the concave hull H_1 of the polygons diseased during the time interval was computed while the concave hull H_2 was defined as the union of H_0 and H_1 . This methodology is illustrated in Fig. 2.3. The distance traveled by the disease front was then obtained by computing the maximum distance between all pairs of points of H_0 and H_2 . The epidemic's front speed was finally obtained by dividing the resulting distance by the number of days in the simulated time interval.

2.2.3 Sensitivity analysis

Disease agents and their vector were assumed to have a half-life of 30 days in the water column, governed by parameter γ while inter- and intra-reef infection were assumed to occur at the same rate β . Although the sensitivity of our model to these two parameters was not extensively investigated in the present study, some additional simulations were performed to estimate how variations of their value might impact our results. To assess the influence of mass loss rate γ , additional connectivity matrices were computed using particles with a half-life of 15 days (γ increased with a factor 2) in our dispersal model. Connectivity indicators were then computed for these matrices and their value was compared with the ones derived from 30-day-half-life connectivity matrices. Moreover, to evaluate whether the 'infectiousness' of disease agent might be reduced during its journey from reef to reef, epidemiological model simulations were performed with reduced inter-reef 'infection' rate $\beta = \frac{1}{2}\beta_0'$.

2.2.4 Transmission experiments

In parallel to this modeling study, laboratory-based transmission experiments of SCTLD were conducted by several independent groups for various end points including transmission dynamics and samples for molecular and histological analysis. Requests for transmission data were sent to members of the 'Transmission' sub-group of the Florida Disease Advisory Committee's 'Research' working group as well as any other additional researchers that may have been conducting transmission studies on SCTLD. Data that was requested and subsequently provided included the location, dates, and duration of the experiment, the species used as the diseased colony (donor of disease agents) and apparently healthy colony (exposed to disease agents), the number of successful transmissions as well as the 'incubation' period following a contact with disease agents prior to disease signs. Additional information included the size of the colonies used in the experiment, the percent tissue loss of the diseased (donor) colony at the beginning of the experiment, and whether the apparently healthy (exposed) fragment was touching the diseased colony or not.

The average probability of successful disease transmission was determined by taking the mean of the number of colonies exposed to the disease in each study divided by the total number of coral colonies exposed to diseased colonies. The

'incubation' period was identified as the average number of days after an apparently healthy coral colony was exposed to a diseased colony before visual disease signs occurred (i.e., active tissue loss). Only corals that eventually showed disease signs were integrated within the 'incubation' period calculation.

Data were provided from 8 different research groups representing 15 institutions and 19 total collaborators providing a total of 109 data points. After amalgamating the contributed data, the mean probability of transmission of SCTLD to an apparently healthy coral had a likelihood of approximately $44.8 \pm 3.6\%$. The probability of transmission ranged from 0 to 100% depending on the experiment. Additionally, the time between exposure of an apparently healthy coral to a diseased coral and subsequently showing initial signs of tissue loss (i.e., 'incubation' period) was 9.7 ± 1 days.

2.3 Results

2.3.1 Exchanges of infected material

Among the three modes of transport, bottom currents exhibited the lowest propagation range as they generated the networks with the smallest weighted connectivity length (Fig. 2.4). However, disease agents transported by bottom currents had the largest settlement success rate as these currents produced the graphs with the largest fraction exchanged. Therefore, bottom currents tend to transport more disease agents to closer reefs compared to the two other modes of transport. Mean and surface currents, on the other hand showed similar spreading ranges with mean WCL of 20.63 km and 21.39 km respectively. However, the disease agents that surface currents transported had the lowest probability of settling successfully on reefs. Consequently, surface currents and bottom currents produced networks with similar mean out-degree, although surface currents have the potential to transport disease agents across larger distances. Nonetheless, networks had larger median out-degree with bottom currents than with surface currents, which suggests that surface currents have a lower spreading potential than bottom currents. As a result of their large WCL and fraction exchanged, barotropic currents on the other hand exhibited the largest mean out-degree, which indicates that they have the strongest dispersal potential.

Self-recruitment gives the fraction of disease agents settling on a reef that was produced on the same reef. The greater the self-recruitment value, the more the reef was isolated from the rest of the network. Since diseased material is less likely to settle on isolated reefs, self-recruitment informs on the potential for the disease to reach a given reef, whereas all three other indicators inform on the reef spreading potential. As mentioned before, self-recruitment is a relative measure and it might thus not give a complete picture of the amount of diseased material coming from upstream reefs that settles on a given reef. This is particularly true when considering reefs with different areas and coral cover. However, in the present study, we assumed a uniform coral cover and divided all the reefs into

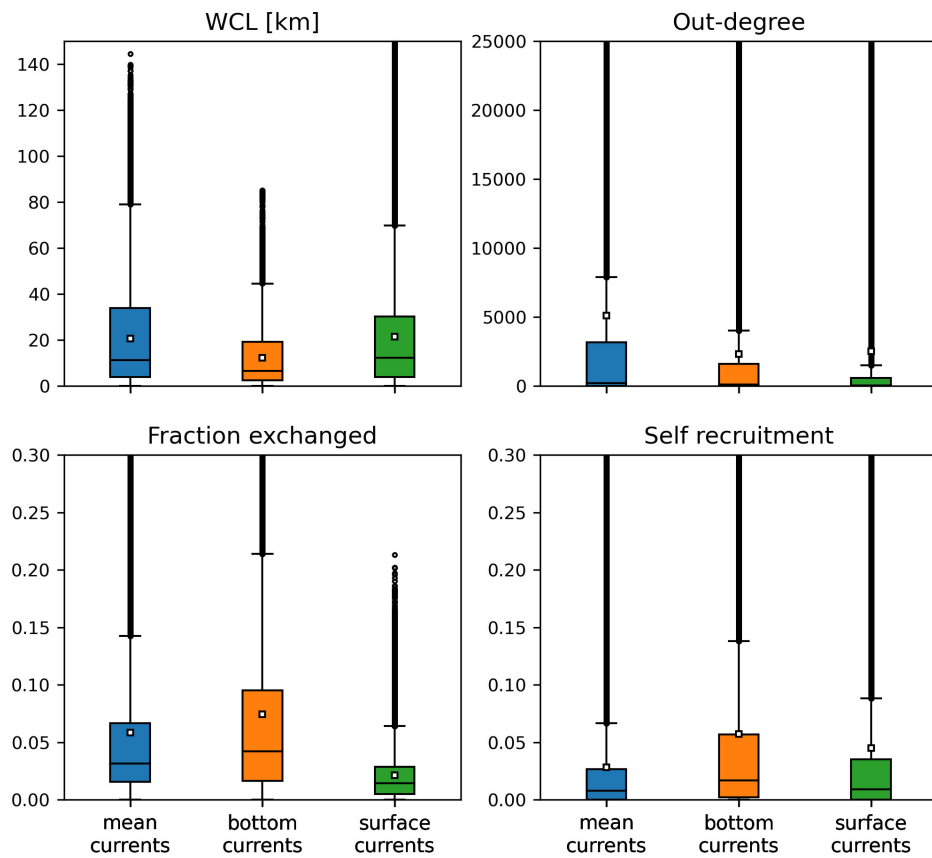


Fig. 2.4: Distribution of the indicators derived from the monthly connectivity matrices computed for each type of current during our simulated period. Mean values are indicated by white squares.

square sub-reefs with the same area. It is therefore reasonable to assume that sub-reefs with high self-recruitment act as weak sinks for diseased material. Fig. 2.4 shows that the disease was more likely to settle on the reefs of networks generated by mean currents. This result is consistent with the values of the other connectivity measures, as reefs tended to be more strongly connected with mean currents. On the other hand, reefs were more isolated with bottom currents, as they produced the graphs with lowest WCL and out-degree. Finally, surface currents generated larger self-recruitment values than mean currents as they exhibited the lowest fraction exchanged. Therefore, although bottom currents exhibited stronger spreading potential than surface currents, reefs were more likely to become diseased with surface currents.

2.3.2 Epidemiological model results

As aggregated observations showed a fraction of susceptible individuals of about 85% after a year, a basic reproduction number $R_0 = \beta'_0/\sigma = 1.0345$ was found with Eq. 2.5. Using this ratio, best fit to averaged disease prevalence observations

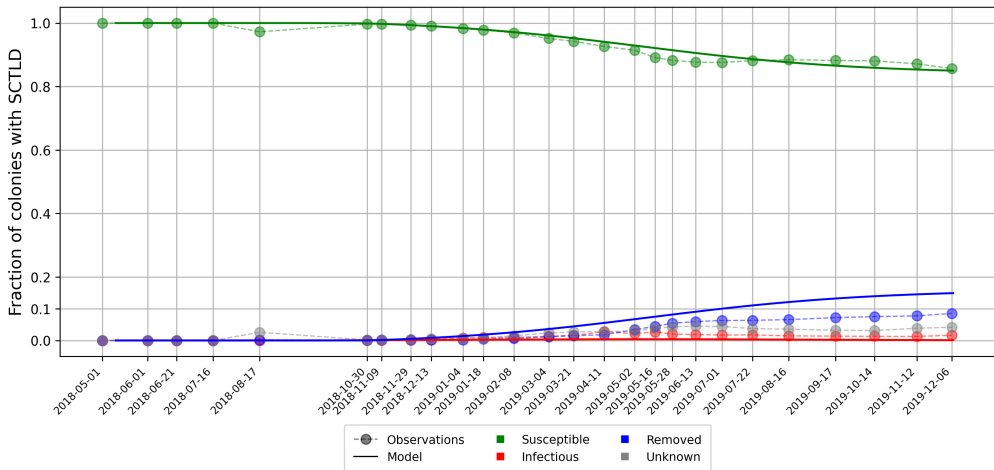


Fig. 2.5: Disease prevalence averaged over all monitored sites over time as modeled by Eqs. 2.4 using calibrated transmission and removal parameters $\beta'_0 = \frac{1}{6.45} \text{ days}^{-1}$ and $\sigma = \frac{1}{6.99} \text{ days}^{-1}$.

was obtained with transmission rate $\beta'_0 = \frac{1}{6.45} \text{ days}^{-1}$ and mortality rate $\sigma = \frac{1}{6.99} \text{ days}^{-1}$. Comparison of the evolution of the state described by Eqs 2.4 with observations is shown in Fig. 2.5. Our model results accurately reproduced the observed fraction of susceptible individuals on colonies through time. However, the modeled fraction of removed individuals overestimated observations by about 5%. These discrepancies might be explained by the presence of "Unknown" values in our data sets as well as the simplifying assumptions of SIR models. Since 'infection' and removal occur at very close rates, the instantaneous fraction of diseased individuals on the reefs remained low through the outbreak, with a maximum value of about 0.4%.

Once the model was calibrated, epidemic-hydrodynamic model simulations were performed from 1st May 2018 to 1st April 2019 for each type of current and different values of the 'infection' threshold I_0 . Two metrics were used to assess the accuracy of the model. First, the modeled front speed was compared to the reference rate of 92 m/day derived by Muller et al. (2020). Furthermore, we computed the mean of the distances between each point where SCTLD had been observed during our simulated period (extracted from the 2018-2019 data sets described in section 2.2.2.3) and the centroid of the closest reef polygon predicted to be diseased by our model during the same period (Fig. 2.6). Bottom currents produced the slowest modeled disease propagation with a maximum front speed of ~ 20 m/day, while simulations performed with surface currents spread the disease at a maximum speed of about 60 m/day. However, surface currents tended to propagate the disease to the north, rather than westward, along the Florida Keys. This explains why bottom currents predict disease occurrence closer to field observations despite exhibiting slower front speed. Finally, mean barotropic currents outperform other types of current predictions regarding both criteria with a front speed of 107 m/day and a mean geographical accuracy of ~ 1.2 km. This

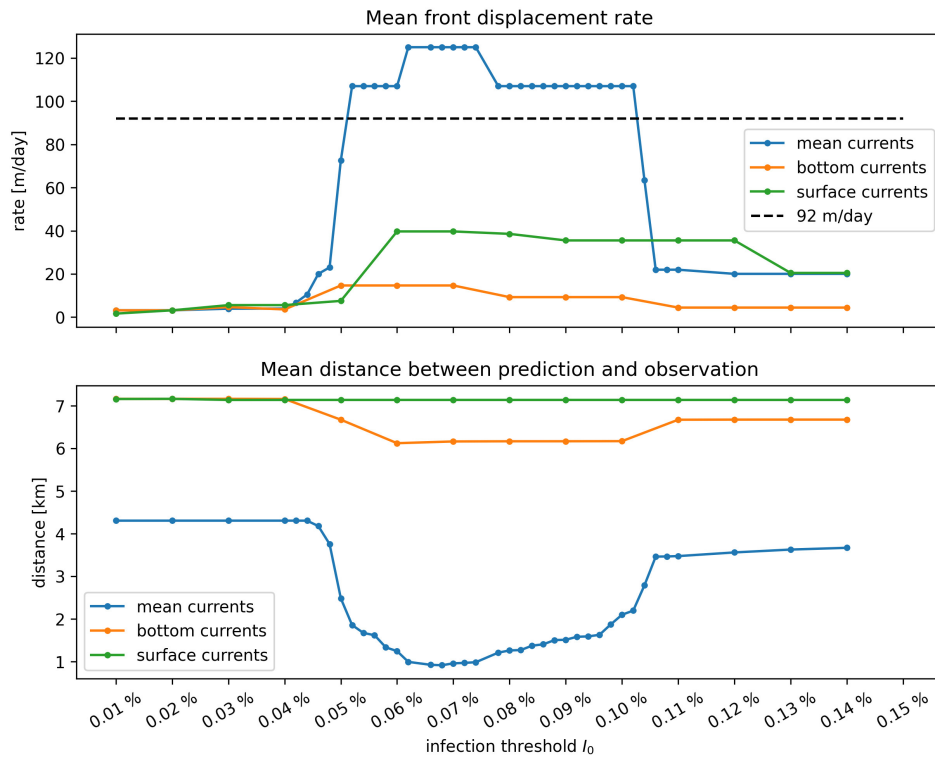


Fig. 2.6: Summary of epidemiological model simulations with calibrated transmission parameters. **Top:** Modeled disease front speed for each type of current with respect to intra-reef 'infection' threshold I_0 . **Bottom:** Mean distance between predicted diseased reefs and observed disease points. These results show that mean barotropic currents outperformed other modes of transport at reproducing the observed spread of the disease. The appearance of a plateau suggests that the modeled spread of the disease occurs for a well-defined range of values of I_0 .

suggests that the disease agents of SCTLD may be transported within neutrally buoyant material driven from reef to reef inside the water column by mean currents.

Moreover, Fig. 2.6 shows a strong dependence of the model results to 'infection' threshold I_0 , that gives the fraction of diseased individual that colonies can withstand before exponential disease growth is triggered on the reef. Front speeds of both mean and bottom currents reached a plateau for values of the threshold between $I_0 = 0.05\%$ and $I_0 = 0.1\%$, while the minimal prediction error was reached around $I_0 \approx 0.078\%$ with mean currents. For $I_0 > 0.1\%$, intra-reef 'infection' was strongly impeded and populations of 'infectious' individuals on diseased reefs were not able to become sufficiently large to infect other colonies on connected reefs. For values of I_0 lower than 0.05% on the other hand, intra-reef 'infection' dominated and coral populations on diseased reefs were removed too fast to efficiently spread the disease through the network. Since disease propagation throughout the FRT only occurred for fairly small values of I_0 in our model, corals are expected to have low resistance to the causative agent of the SCTLD.

The results shown in Fig. 2.6 were obtained by removing the large reef lo-

cated North to Vaca key, denoted Vaca reef in Frys et al. (2020a), from our reef polygons. Preliminary simulations showed that this reef had close to no impact on the modeled spread of the disease to the rest of the FRT, as it sent very few disease agents to southerly and easterly neighboring reefs. Moreover, Vaca reef has a low coral coverage (0 – 10%), which strongly impedes disease spread on the reef. However, as coral coverage was not taken into account in our epidemiological model, propagation of the disease on the reef was overestimated. This led to unrealistically strong modeled front speed variations due to the large size of the reef. Consequently, and in the absence of SCTLD observations on Vaca reef, this area was removed from our reef polygons in order to avoid overestimating the front speed.

2.3.3 Sensitivity analysis

Connectivity matrices computed using particles with a half-life of 15 days exhibited shorter range connectivity. However, the impact of increasing mass loss rate γ in our dispersal model remained limited with variations in connectivity indicator values weaker than 10%. However, reducing inter-reef 'infection' rate β by a factor 2 had a significant impact on epidemiological model outputs as predicted disease front speed did not exceed 20 m/day, far less than the observed speed of the disease front. This strong decrease can be explained by the interplay between inter- and intra-reef disease activity. Reducing inter-reef transmission rates decreases the fraction of diseased corals on reefs attained by disease agents, which in turn reduces the amount of disease agents sent to the rest of the network.

2.4 Discussion and conclusions

We developed an epidemio-hydrodynamic model to simulate the spread of the SCTLD throughout the entire FRT. Calibrating our model with colony-averaged prevalence observations, we estimated the species-averaged reproduction number R_0 to be slightly larger than one. Our model simulations suggest that barotropic currents best reproduce the observed spread of the disease among reefs in the lower Florida Keys. Bottom current did not spread disease agents far enough while surface currents did not allow disease agents to reside within the reefs long enough to ensure disease transmission that matched field observations. The results, therefore, suggest the causative agent of SCTLD is likely to be transported within neutrally buoyant particles in the water column. With this mode of transport, the propagation of the disease from reef to reef only occurred for a well-defined range of values of the 'infection' threshold I_0 . This threshold is defined as the fraction of all sub-reef colonies that were diseased which triggered a rapid spread of the disease over the entire sub-reef area. Our results suggest that this occurred once 0.05 – 0.1% of the colonies were diseased. These results suggest that, on average, corals appear to have a low resistance to SCTLD.

After calibration, we estimated the species-averaged basic reproduction number β'_0/σ to be equal to 1.0835. This value, being close to 1, suggests modeled diseased individuals were removed from the system almost as fast as susceptible individuals became diseased. This situation caused the fraction of infectious corals on the reefs to remain fairly low (*i.e.* $\leq 0.4\%$) through time. These results suggest that only a small fraction of the colonies caused the disease to spread on the reef during the outbreak. The observation-based species-averaged transmission period of 6.45 days used in the model was a reasonable estimation of the disease transmission dynamics, being of the same order of magnitude as the experimentally-derived mean incubation period of 9.7 days. The difference between the two values can be explained by field measurement uncertainties as well as the inability to perfectly mimic field conditions in laboratory. In the present study, the same values were used for inter- and intra-reef 'infection' rates β and β'_0 , *i.e.* disease agents 'infectiousness' was assumed to remain unchanged during their journey from reef to reef. This assumption is consistent with sensitivity analysis results, which showed that reducing the value of β strongly impeded disease propagation through the network. This outcome suggests that, to reproduce the observed spread, inter- and intra-reef transmission rates must have similar magnitude, *i.e.* that the causative agent is not degraded while traveling from reef to reef. Given that the etiology of SCTLD is still unknown, the lack of degradation of the SCTLD causative agent over distances of tens of kilometers between reefs may help to narrow the search.

The fact that mean barotropic currents outperformed the other modes of transport can be explained by considering the trajectories of the particles used to model the transport of the disease causative agent. Due to the impact of winds on positively buoyant material, particles driven by surface currents are likely to be blown away from the reefs. Moreover, even when winds are pushing particles along the reef line, these particles spend less time over the same region than particles driven by mean and bottom currents. Smaller amounts of particle mass will therefore settle on reef polygons, leading to lower connection strengths in the potential connectivity matrix, *i.e.* lower exchange of infectious material between reefs. Hence, despite being able to transport the disease over greater distances, surface currents are less efficient to drive the propagation of the disease. Particles driven by bottom currents, on the other hand, remain over the same region longer, producing larger entries of the potential connectivity matrix. Due to these large exchange probabilities between reefs, bottom currents are better at propagating the disease (Fig. 2.6). Nevertheless, because bottom currents are slower, exchanges of disease agents occur within a more limited geographical range. Mean barotropic currents that carry particles greater distances while allowing for sufficiently large amounts of diseased material to settle on reef polygons, were thus best suited to propagate the disease at a speed similar to field-collected data (Fig. 2.6).

Since mean currents were the only mode of transport that successfully reproduced the observed propagation speed of the disease in our model, the disease causative agent is expected to be transported within neutrally buoyant material inside the water column. Current-driven propagation seems reasonable as water-

borne transmission is an important spreading mechanism for multiple coral diseases, including white band disease, white plague disease, white pox disease, white syndrome disease, *Porites* ulcerative white spots diseases, and skeletal eroding band disease (Shore and Caldwell, 2019). These results suggest that coral mucus or sloughed off diseased coral tissue may directly transmit SCTLD if they remain suspended within mean currents. Aeby et al. (2019) showed that corals held within aquaria can transmit SCTLD to healthy colonies suggesting that these mechanisms may be occurring within reefs. Additionally, vectors such as zooplankton, phytoplankton, or even marine snow, may be transporting disease agents from reef to reef within the water column. Landsberg et al. (2018) used histology to show an association between the location of the in hospite symbiotic algae that reside within the coral gastrovascular cavity and the area of tissue necrosis occurring within SCTLD-affected corals. These results have led to the working hypothesis that SCTLD could be associated with the symbiotic algae or the process of heterotrophic feeding and ingestion. The causative agent could also be transported within fine sediments such as silt, as suggested by Rosales et al. (2020). Such sediments are easily eroded in shallow areas around coral reefs and would therefore be mostly transported inside the water column by mean barotropic currents. This hypothesis might be tested by adapting the deposition rate γ used in our experiments to be consistent with the sedimentation rate of silt. However, such modification of γ would alter the entries of our potential connectivity matrices. Nonetheless, sensitivity analysis of connectivity indicators suggest that such modifications would have a minor impact on model behavior and that the main results of this study would remain valid for larger deposition rates.

Coral resistance to SCTLD was represented by parameter I_0 , defined as the maximum fraction of the colony that can become diseased without causing the disease to spread to the rest of the sub-reef site. The plateau shown in Fig. 2.6 highlights the impact of this parameter on the modeled propagation of the disease. On the one hand, when corals were strongly susceptible to the disease, diseased individuals were removed from the system too fast to become sustainable sources of disease agents in the network. On the other hand, if corals were weakly susceptible to the disease, very few corals became diseased and the disease barely propagated. Our simulations suggest that this value of resistance must be fairly low (around 0.07%) in order to successfully spread the disease throughout the FRT. This seems to imply that susceptible coral species have very weak defense mechanisms against the causative agent of the disease.

As with any modeling study, it is important to understand the assumptions on which the model is based. Here, we have used a 2D barotropic ocean model forced by the 3D model HYCOM (Chassignet et al., 2007) in order to indirectly represent baroclinic phenomena. Such a model is well-suited to simulate the fate of neutrally-buoyant material in shallow regions. However, as depth-averaged currents do not accurately approximate the motion of particles in the bottom and surface layers, they have been modified to simulate the exchanges of negatively and positively buoyant material. In order to derive bottom and surface currents

from mean barotropic currents, we used parameterizations consistent with both observations and theory (Ardhuin et al., 2009; Perlin et al., 2007; Kundu, 1976; Smith, 2009). Although such parametric estimation of surface and bottom currents adds additional uncertainty to those simulations, using a 2D model as the basis for the study allowed for reef-scale resolution throughout the whole FRT with available computational resources. Such high-resolution allowed the simulation to explicitly represent recirculation eddies around islands and reefs, that significantly impact the weighted connectivity length as well as the local retention of pathogenic material on the reefs (Frys et al., 2020a).

The appearance of an interval of optimal values of threshold I_0 for the propagation of the disease in our results highlights the impact of coral resistance on the spread of SCTLD through the FRT. Therefore, a next step in our modeling approach would be further dividing coral populations of our polygons into highly susceptible (e.g. *Dichocoenia stokesii*, *Meandrina meandrites*), intermediately susceptible (e.g. *Orbicella faveolata*, *Montastrea cavernosa*), and weakly susceptible (e.g. *Acropora Palmata*, *Acropora cervicornis*) sub-populations. The fractions of susceptible, infectious and removed individuals within these sub-populations would then be modeled with specific transmission (β , β'_0) and removal (σ) rates as well as specific infection thresholds I_0 . Such approach would however require a detailed knowledge of the fine-scale distribution of the different coral species throughout the FRT. This knowledge about coral coverage could also be used to avoid over-estimation of the front propagation, as in the case of Vaca reef.

Despite the limitations of its current formulation, our model brings unprecedented perspectives on the propagation mechanism of SCTLD throughout the FRT. Using a reef-scale spatial resolution, we determined the most probable mode of transport for the vector of the disease agent and deduced its host-species-averaged reproduction number based on prevalence observations. In addition, our model formulation provides a framework to quantify coral resistance to the disease. This framework is a novel contribution to the study and modeling of marine diseases, as both inter- and intra-patch disease dynamics are modeled explicitly and realistically in time and space. As our model results are continuous through time, they can exhibit the variability of the propagation of SCTLD temporally and therefore bring additional insight into observation data. This study provides much-needed complementary insight into the identification of the causative agent of the SCTLD and the management of the crisis it generates. Furthermore, our modeling approach could be applied to other affected areas of the Caribbean, where there is still time to perform active management as the disease spreads throughout the region.

Transmission of SCTLD from the Marquesas to the Dry Tortugas

This chapter is based on the following article:

Dobbelaeere, T., Holstein, D. M., Muller, E. M., Gramer, L. J., McEachron L., Williams, S. D., & Hanert, E. (2022). Connecting the dots: Transmission of stony coral tissue loss disease from the Marquesas to the Dry Tortugas. *Frontiers in Marine Science*, 9. doi: 10.3389/fmars.2022.778938.

Abstract

For the last seven years, Florida's Coral Reef (FCR) has suffered from widespread and severe coral loss caused by stony coral tissue loss disease (SCTLD). First observed off the coast of Miami-Dade county in 2014, the outbreak has since spread throughout the entirety of FCR and some areas of the Caribbean. However, the propagation of the disease through FCR seemed to slow down when it reached the western end of the Marquesas in August 2020. Despite being present about 30 km (~20 miles) from the Dry Tortugas (DRT), SCTLD was not reported in this area before May 2021. As SCTLD transmission is likely to be waterborne, here we suggest that this apparently delayed propagation is related to eddy activity near the DRT under the influence of the Loop Current/Florida Current system. To quantify the impact of the local ocean circulation on the spread of SCTLD from the Marquesas and the DRT, we evaluated the hydrodynamic-predicted connectivity between these two regions using a high-resolution hydro-epidemiological model between May 2018 and May 2021. Our results suggest that the Marquesas and the DRT were not connected during February–October 2020 and January–May 2021. These

periods coincided with either the occurrence of Tortugas gyres and mean circulation with an eastward component between the Marquesas and the DRTD or the presence of southward currents. Our results suggest that disease agents probably reached the DRTD in November 2020 and that they most likely originated from southern or northwestern reefs of the Marquesas. This study provides novel insight into the role played by the hydrodynamics in the spread of SCTLD within the western-most edge of FCR, and in propagating the disease to uninfected locations.

3.1 Introduction

Over the last seven years, Florida's Coral Reef (FCR) has suffered from a widespread decline in living, reef-building corals due to a multi-year coral-disease outbreak (Precht et al., 2016; Walton et al., 2018), called stony coral tissue loss disease (SCTLD). First reported off the coast of Miami-Dade county in 2014, the disease has since spread through the entirety of FCR as well as other sites within the Caribbean (Alvarez-Filip et al., 2019; Kramer et al., 2019; Estrada-Saldívar et al., 2020) and affected more than 20 scleractinian coral species (NOAA, 2018). The range of species affected coupled with the large spatial and temporal extents of the outbreak make SCTLD the most severe disease outbreak to have affected coral reefs on record.

Previous study of the spatio-temporal dynamics of SCTLD between West Palm Beach and Marathon showed that the epizootic propagated at a rate of ~100 m/day to the north and ~92 m/day to the south, hitting the Middle Florida Keys in 2017 (Muller et al., 2020). The disease was then reported in the Lower Keys in summer 2018 (FRRP, 2018); near Key West in winter 2018 (FRRP, 2018); on the easternmost boundary of the Marquesas subregion in October 2019 (FRRP, 2019); and at its western end, approximately 11 km. west of halfmoon shoal, in August 2020 (FRRP, 2020). SCTLD was observed propagating faster than 100 m/day within the Marquesas between October 2019 and August 2020 and would have reached the reefs of the Dry Tortugas (DRTD) by February 2021 if it had spread at a similarly high propagation rate (Kramer et al., 2019). These propagation rates were observed in a relatively dense shallow-water reef system and mostly occurred through transmission from neighbor to neighbor. Disease agents then had to cross 30 km (~20 miles) of open waters to reach the reefs of the DRTD. The disease was ultimately observed in May 2021 (Kramer et al., 2019) in the southeast of the DRTD. To date, questions remain about the timing of the spread of the disease to the DRTD as well as the role played by hydrodynamics in the process.

The DRTD coral reefs are among the most preserved, but also vulnerable, marine ecosystems of the continental United States (Kourafalou et al., 2018). They are part of the Florida Keys National Marine Sanctuary (FKNMS), under the jurisdiction of the Tortugas Ecological Reserve that covers around 566 km² of no-take marine reserves (Ault et al., 2006). Since the establishment of DRTD in July 2001, fish populations within the managed areas have significantly increased in

size, adult abundance, and occupancy rates, therefore favoring the establishment of sustainable fisheries (Ault et al., 2013). Furthermore, because of their location and hydrodynamics, DRTO reefs are believed to be important sources of recruitment for coral-reef fishes downstream in the Florida Keys (Domeier, 2004) and thus significantly contribute to the overall resilience of the Florida Keys coral-reef ecosystem.

Although the pathogen responsible for the disease remains unknown to date, hydrodynamics are likely to play an important role in its propagation. Modeling studies suggest that the observed spread of the disease can be reproduced by simulating the dispersal of neutrally buoyant particles (Dobbelaere et al., 2020), while ex situ experiments show evidence of waterborne disease transmission (Aeby et al., 2019; Eaton et al., 2021; Meiling et al., 2021). Accounting for the underlying ocean circulation is therefore important to understand the evolution of the propagation of the disease. The observed apparent stalling of the spread of SCTLD from the Marquesas to DRTO reefs may be explained by ephemeral or persistent oceanographic features in the area that initially prevented the transmission of disease agents further west.

The ocean circulation between the Marquesas and the DRTO is strongly driven by the Loop Current (LC). This ocean current brings warm waters from the Caribbean Sea through the Yucatan Channel, loops anti-cyclonically through the northeastern Gulf of Mexico (GoM) and finally exits through the southern Straits of Florida, where it forms the Florida Current (FC). The northward penetration of the LC through the GoM varies throughout the year, and sporadically an anticyclonic ring separates from the current (Leipper, 1970; Maul, 1977; Vukovich, 1988). The dominant mesoscale feature near the DRTO is the formation of quasi-stationary eddies with a diameter of 100-200 km (Lee et al., 1994; Fratantoni et al., 1998), usually called Tortugas gyres or eddies. Fratantoni et al. (1998) hypothesized that the formation of these eddies as well as their lifespan was linked to the generation of anticyclonic rings from the LC in the GoM, while Kourafalou and Kang (2012) showed the relation between eddy formation dynamics near the DRTO and meandering of the FC. These eddies can remain up to 120 days near the DRTO before moving eastward at a speed of 5 km/day under the action of LC frontal eddies (Maul, 1977). Tortugas gyres have been identified as an important mechanism for the potential retention of larvae of invertebrates and fishes on the southwest Florida shelf (Lee et al., 1994; Sponaugle et al., 2005; Kourafalou and Kang, 2012) and might therefore have impacted the dispersal of disease agents from the Marquesas to the DRTO.

The objective of the present study was to apply the same modeling tools as Dobbelaere et al. (2020) to determine the potential impact of the circulation in the GoM on the delayed propagation of SCTLD between the Marquesas and the DRTO. This was performed by evaluating the evolution of the hydrodynamic-predicted connectivity between these two regions between May 2018 and May 2021. We then assessed how large-scale ocean circulation features, such as Tortugas gyres, could have prevented the transport of potential disease agents from the

Marquesas to the DRTO. Ultimately, this study aims to provide novel insight on the role hydrodynamics have played in the spread of SCTLD throughout the western-most area of FCR, which further informs how it has, and will continue to, spread throughout the tropical western Atlantic.

3.2 Methods

Stony Coral Tissue Loss Disease data was obtained by using the Florida Reef Resilience Program's Disturbance Response Monitoring Report for 2019 and 2020 (FRRP, 2019, 2020) as well as the Atlantic and Gulf Rapid Reef Assessment (AGGRA) resources for SCTLD reported throughout the Caribbean, an open access spatial and temporal database curated by experts in Caribbean coral reef ecology (Kramer et al., 2019). Assumptions associated with SCTLD included the following: (i) SCTLD is different from other tissue loss diseases previously reported on corals (i.e. white plague, white syndrome) based on its ecology and case definition (NOAA, 2018), (ii) SCTLD is transmitted, in part, by ocean currents (Aeby et al., 2019; Muller et al., 2020; Eaton et al., 2021) and (iii) SCTLD was along the western most reef area of the Lower Florida Keys in October 2019, reached the western most part of the Marquesas in August 2020, and did not occur in DRTO until May 2021 based on curated data provided by the FRRP reports and the AGGRA open access database.

We studied the transmission patterns of SCTLD between the Marquesas and the DRTO by using the hydro-epidemiological model of Dobbelaere et al. (2020). This model relies on the multi-scale ocean model SLIM¹ to simulate the hydrodynamics over the entirety of FCR. The computational domain includes the Florida Straits as well as part of the GoM (Fig. 3.1a). SLIM is coupled with the large-scale ocean model HYCOM in order to correctly represent the dynamics of the FC which is a major western boundary current that flows out of the GoM, as a continuation of the Loop Current, before joining the Gulf Stream. SLIM uses an unstructured mesh whose resolution can be locally increased in order to accurately represent fine-scale flow features. Here we used the same mesh as Dobbelaere et al. (2020), composed of 7×10^5 elements, and with resolution that reaches 100 m over reefs and along the coastline (Fig 3.1a). By using such a fine resolution, we can explicitly represent circulation and resolve tides at the reef scale, such as around the Marquesas island group (Fig. 3.1a, inset), while also representing the large-scale flow features within the FC (Fig 1b and c). Further details on the model formulation and validation are provided by Frys et al. (2020b).

We simulated the dispersal of disease agents throughout FCR between May 2018 and May 2021. As in Dobbelaere et al. (2020), disease agents were modeled as passive particles transported by depth-averaged currents which constantly lost mass with a half-life of 30 days. We ran the particle transport model for every month between May 2018 and May 2021 and hence obtained monthly normal-

¹<https://www.slim-ocean.be>

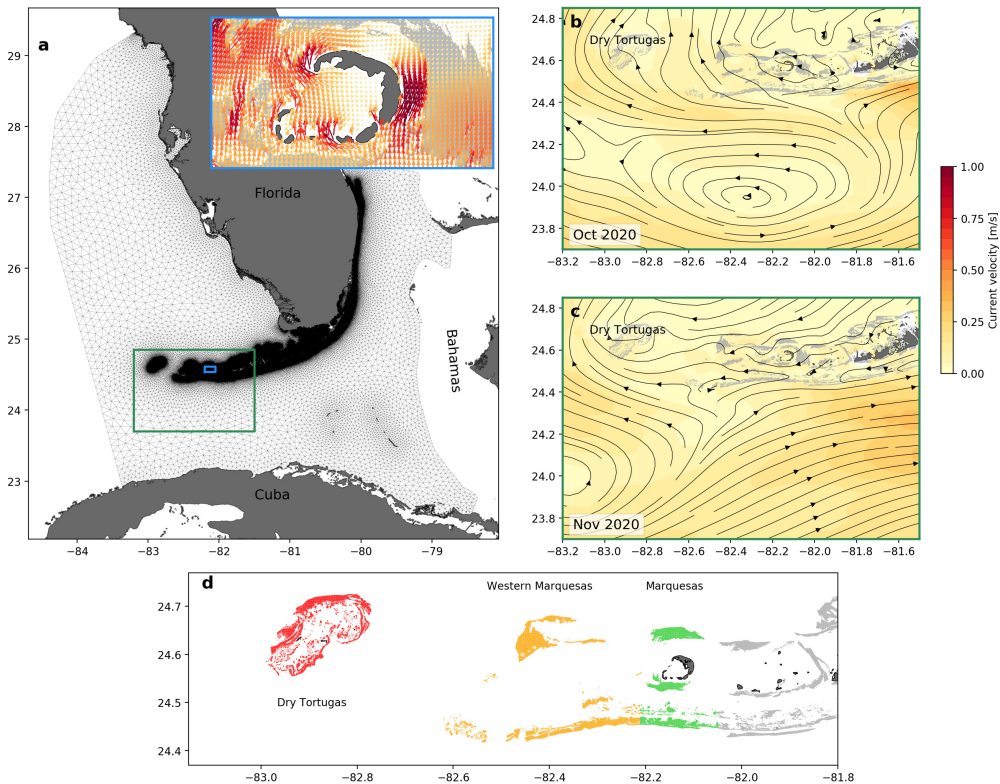


Fig. 3.1: (a) Mesh of the computational domain and close-up view of the instantaneous currents on November 15, 2020 at 12:00 in the Marquesas (inset), (b) close-up view of the monthly-averaged circulation between the Marquesas and the DRTO in October 2020, and (c) November 2020. (d) Reefs of the areas of the DRTO, the Western Marquesas and the Marquesas, as defined in this study. Land is shown in dark gray and reefs in light gray, except in panel (d) where reefs from the Marquesas, the Western Marquesas and the DRTO are respectively shown in green, yellow and red. Streamlines indicate the presence of the Tortugas gyre in October 2020, which leads to northward currents between the Marquesas and the DRTO. In November, the gyre left its static location to transit through the Straits of Florida and currents between the Marquesas and DRTO became westward.

ized connectivity matrices. An entry C_{ij} of the connectivity matrix represents the probability that disease agents produced on sub-reef i settle on sub-reef j . These sub-reefs were defined by extracting polygons from the “coral reefs and hard bottom” layer of the Unified Florida Reef Tract Map (FWC-FWRI, 2017) and further dividing them into $500 \text{ m} \times 500 \text{ m}$ squares, generating a total of 16,823 sub-reef polygons. Since the connectivity matrices had more than 200 million entries, they were not directly interpreted. Instead, they were represented as large networks where nodes corresponded to sub-reefs of FCR and edges corresponded to nonzero entries in the connectivity matrix. Graph-theory algorithms were then used to analyze the properties of the connectivity networks.

To quantify the connectivity between the Marquesas and the DRTO, we defined

3 sub-regions within the sub-reefs of the western part of FCR: (*i*) the Marquesas, (*ii*) the Western Marquesas and (*iii*) the DRTO (Fig. 3.1d). The sub-region of the Marquesas was defined as all the sub-reefs whose centroid is located between -82.21° and -82.05° longitude; the Western Marquesas included all sub-reefs between -82.73° and -82.21° ; and the DRTO were composed of all the sub-reefs in our domain located west of -82.73° longitude. We evaluated the exchanges between two given sub-regions by identifying all edges connecting any sub-reef from one sub-region to any sub-reef from the other sub-region in our monthly connectivity networks. We then defined a connectivity indicator by multiplying the number of these direct edges by their mean connection probability. This indicator was computed monthly between May 2018 and May 2021 to evaluate the connectivity (*i*) from the Marquesas to the DRTO, (*ii*) from the Western Marquesas to the DRTO and (*iii*) from the Marquesas to the Western Marquesas.

The spatial information of the network can be used to predict which part of the DRTO was likely to be first exposed to potential disease agents via hydrodynamic connections. We built a monthly spatial vulnerability indicator by summing the probabilities of all edges connecting sub-reefs of the Marquesas and the Western Marquesas to a given sub-reef of the DRTO. Sub-reefs of the DRTO with larger values of this indicator would have a larger cumulative likelihood of being infected during the simulated month. Such areas would thus be more likely to be the "entry points" of SCTLD in the DRTO during the month, as they were the destination of more pathways with larger exchange probabilities. A similar indicator can be computed for the Marquesas and the Western Marquesas by summing the probabilities of the edges connecting a given sub-reef of these sub-regions to the DRTO. Sub-reefs with higher value of this source indicator would be more likely to initiate the propagation of the disease to the DRTO, as they were the origin of more connectivity pathways with larger exchange probabilities. Model predictions were then compared to actual observations of the first cases of SCTLD in the DRTO collected on the interactive map of Kramer et al. (2019).

To understand the effect of the ocean circulation on disease transmission, we computed the monthly-averaged circulation for each simulated month. These residual currents were used to visually assess the presence of a Tortugas gyre during that month, i.e. the presence of eastward moving eddies persisting on temporal and spatial scales consistent with the description of Lee et al. (1994) in the vicinity of the DRTO. Moreover, we defined an axis from the Marquesas to the DRTO over which we averaged the monthly residual currents. These temporally and spatially averaged currents were used as a proxy of the circulation between the Marquesas and the DRTO during each simulated month.

3.3 Results

The evolution of the monthly connectivity indicator suggests that there were no exchanges from the Marquesas and the Western Marquesas to the DRTO between February and October 2020, and between January and May 2021 (Fig. 3.2a).

This is quite remarkable as outside of these periods of low connectivity, there were no periods greater than four months without exchange from both the Marquesas and the Western Marquesas between May 2018 and May 2021. Furthermore, February–October 2020 and March 2021 were the only months characterized by mean currents with an eastward component between the Marquesas and the DRTD (Fig. 3.2b). These periods of low connectivity and circulation inversion appeared correlated with the presence of eddies near the DRTD, as Tortugas gyres were observed during most months with no simulated connections to the DRTD. Additionally, no exchange occurred in September 2019 or from January to February 2021, during which a strong southward mean circulation occurred between the Marquesas and the DRTD (Fig. 3.2b). This suggests that southward currents might also act as a barrier to disease propagation by flushing away disease agents south to the GoM. Connectivity from the Marquesas to the Western Marquesas was never completely interrupted during our simulated period (Fig 2a). Nonetheless, periods of low connectivity to the DRTD occurred in the presence of Tortugas eddies (April–June 2020) and southward circulation (February 2021). This suggests that propagation of disease agents from the Marquesas to the Western Marquesas was routinely possible, even though exchanges may have been hindered by the local circulation. This latter result is consistent with the observed westward propagation of the disease in the Marquesas between October 2019 and August 2020.

We analyzed the spatial patterns of hydrodynamic-predicted disease connectivity to the DRTD in November 2020 in more detail as the model suggested this was the month with the highest transmission probability due to high hydrodynamic connectivity. The most probable pathways to the DRTD originated mainly from southern reefs located between the Marquesas and the Western Marquesas, as well as from reefs of the northwestern end of the Western Marquesas (Fig. 3.3). This suggests that sub-reefs of these areas were more likely to send disease agents to the DRTD in November 2020. Conversely, no connection with large probability originated from the southwestern tip of the Western Marquesas, suggesting that they had very low potential to spread the disease to the DRTD. The reefs with the highest vulnerability indicator value in November 2020 were mostly located on the eastern part of the DRTD, suggesting that these reefs were more likely to be affected during this month (Fig. 3.4a). More specifically our results suggest that an area of higher vulnerability was present in the vicinity of the locations where SCTLD was observed in May 2021. Vulnerability was the lowest on inner sub-reefs of the DRTD as they are not directly connected to the reefs of the Western Keys. This suggests that the disease must first spread through the outer reefs to reach them. The source indicator values confirm that disease transmission to the DRTD is more likely to originate from southern reefs at the interface between the Marquesas and the Western Marquesas, and reefs on the northwestern end of the Western Marquesas.

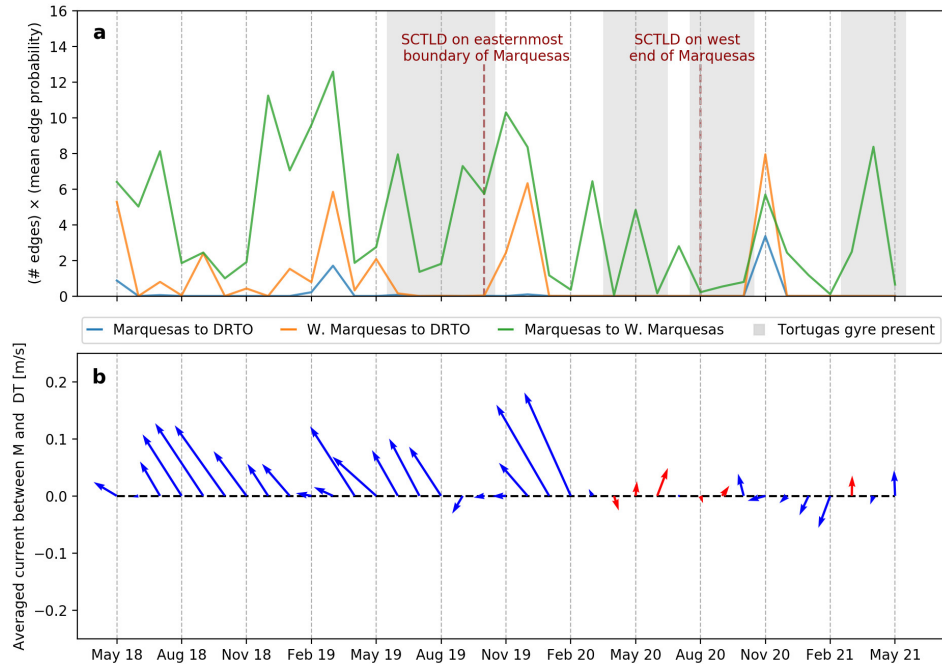


Fig. 3.2: (a) Monthly connectivity indicator between the Marquesas and the DRTO (blue), the Western Marquesas and the DRTO (orange) and the Marquesas and the Western Marquesas (green) between May 2018 and May 2021. Months during which Tortugas gyres were observed in the ocean model outputs are highlighted in grey. Milestones of the observed propagation of the SCTLD through the Marquesas are indicated by dark red dotted lines. (b) Monthly mean currents between the Marquesas and the DRTO between May 2018 and May 2021. Mean ocean circulation with an eastward component is highlighted by red arrows.

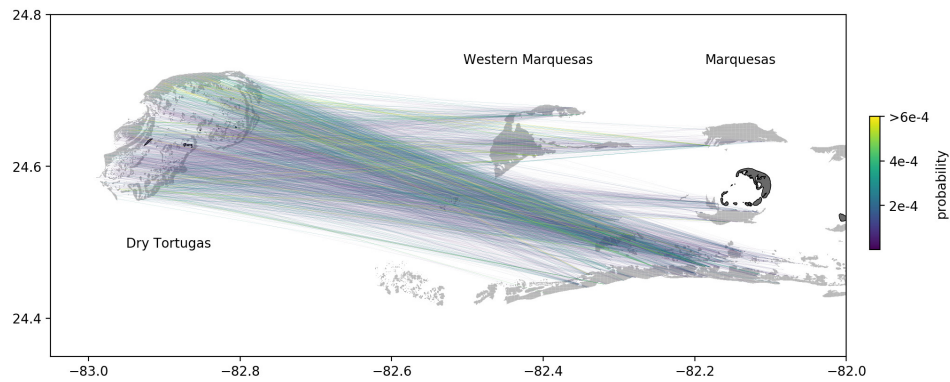


Fig. 3.3: Edges with largest connection probability to each sub-reef of the DRTO from the Marquesas and the Western Marquesas in November 2020. Connections mostly originated from the southern reefs between the Marquesas and Western Marquesas, and from the northwestern reefs of the Western Marquesas. Reefs are highlighted in light gray while islands are shown in dark gray.

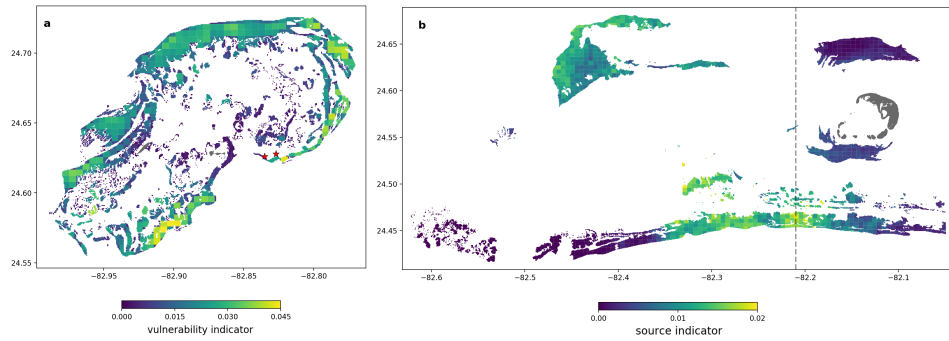


Fig. 3.4: (a) Vulnerability indicator value of all sub-reefs of the DRTO in November 2020. Eastern reefs of the DRTO appear most vulnerable to the disease. Locations where the SCTLD was observed in the DRTO are indicated by red stars (b) Source indicator value in November 2020 for every sub-reef of the Marquesas and the Western Marquesas. Northwestern reefs of the Western Marquesas and southern reefs between the Marquesas and the Western Marquesas show a higher transmission potential to the DRTO. Main islands are shown in dark grey, separation between the Marquesas and the Western Marquesas is indicated by a dashed line.

3.4 Discussion and conclusion

Our results show that the eddies generated by the LC/FC system strongly influence the connectivity between the Marquesas and the DRTO. Mesoscale eddies modify the westward coastal currents by breaking them through strong cross-shore flow regime (Kourafalou and Kang, 2012), as illustrated for October 2020 in Fig. 3.1. Lee et al. (1994) hypothesized that such cross-shore flow could impact the transport of larvae spawned in the Florida Keys and cause their retention on the West Florida Shelf for periods on the order of 6 months. As Tortugas eddies may remain stationary near the DRTO for up to 120 days (Fratantoni et al., 1998), they may thus act as barriers for the exchanges between the Marquesas and the DRTO for extended periods of time. Moreover, the passage of mesoscale eddies was identified as one of the physical mechanisms likely to deliver larvae from the DRTO to the Upper Keys, therefore opposing exchanges from the Marquesas to the DRTO. Our results confirm the role of mesoscale eddies as potential barriers to connectivity between these two regions as most months during which Tortugas eddies were present correspond to a vanishing connectivity indicator. The fact that no eddies were observed at the beginning of our simulation might be related to the identification method, based solely on visual assessment of the residual currents. A comprehensive identification of all Tortugas eddies during our simulated period would require the analysis of sea surface temperature and elevation, which is beyond the scope of the present study. While our approach might miss some Tortugas gyres, it filters out submesoscale eddies with lifespan of the order of several days. Consequently, when horizontally elongated mesoscale cyclonic streamlines are present in the computed monthly-averaged currents, they can be identified as Tortugas eddies with sufficient certainty.

The connectivity from the Marquesas to the DRTO does not seem to follow any clear seasonality and exhibits high interannual variability. Although a longer simulation period might be required to rigorously assess the presence of seasonal variations, no clear seasonal patterns were observed over the 3-year simulated period for both the connectivity indicator and the mean currents (Fig. 3.2). In this regard, the boundary of the West Florida Shelf significantly differs from the inner shelf, which exhibits a robust cycle between summer and winter months (Liu and Weisberg, 2012). Furthermore, our results indicate that the connectivity from the Marquesas to the DRTO strongly varies from year to year. This is best illustrated in March-September 2020, during which no connectivity was observed for an extended period of time and the dominant currents between the Marquesas and the DRTO had an eastward component. Such behavior was not observed during the rest of the simulation. These results are consistent with the strong variability of the LC/FC system, which strongly impacts circulation near the DRTO. Lee et al. (1994) and Fratantoni et al. (1998) first described the influence of the LC penetration and ring shedding dynamics in the GoM on the formation of eddies near the DRTO. Kourafalou et al. (2018) then further identified that LC eddy separation events were related to the formation of southward currents over the Pulley Ridge reefs and the perturbation of the slope stratification on the Southwestern Florida Shelf. The detachment of anticyclonic eddies from the main LC affects in turn the position of the FC, which strongly impacts eddy activity near the DRTO and the Marquesas, either through the formation of local eddies or the retention of remote eddies near the DRTO (Kourafalou and Kang, 2012). These variations of the FC position have been shown to have no seasonal pattern with strong interannual variability and generate complex eddy to eddy interactions (Kourafalou and Kang, 2012). Furthermore, the DRTO area was identified as a region of significant importance for the ecology of the West Florida Shelf, as contacts with the LC cause the inflow of nutrients that modify water properties on the shelf (Weisberg and He, 2003; Liu et al., 2016). Weisberg and Liu (2017) further hypothesized that these contacts might in turn impact the penetration of the LC in the GoM.

We have shown that the ocean circulation, and in particular the presence or absence of eddies shed from the Florida Current, coincides with the timing of initial SCTLD observations and likely transmission to the DRTO. However, it is important to note that it is currently not possible to determine whether SCTLD is caused by a novel pathogenic agent or simply a variant of a previously existing disease that causes tissue loss on corals. The DRTO has experienced episodic outbreaks of tissue loss in years prior to 2020 (see FRRP, 2018). These previously documented tissue loss events occurred during the summer months within isolated reef sites and primarily affected one genus of corals, *Orbicella*. Although the ecology of SCTLD documented from 2014 to the present differs from these previous reports, until pathogenic agents are identified, the positive identification of a particular coral disease, such as SCTLD, will remain presumptive. However, past studies indeed suggest SCTLD is likely caused by a waterborne agent regardless of the particular pathogen at play. As such, intense eddy activity between February 2020 and

May 2021 would have largely prevented the exchange of disease agents westward, with the exceptions of November and December 2020. During those two months, the residual circulation on the southwestern Florida shelf turned westward, and thus would have allowed disease agents to reach the DRTO. The transmission of disease agents to the DRTO was most likely to occur in November 2020, when the connectivity indicator was the largest. The developed vulnerability indicator indicates that sub-reefs on the eastern part of the DRTO were more likely to be affected by the disease. These results are consistent with observation as the locations where SCTLD was observed in the DRTO are located near sub-reefs identified as highly vulnerable by our model (Kramer et al., 2019). Nonetheless, the area predicted to be vulnerable exceeds the extent of the region where signs of the disease were first observed. These discrepancies might be explained by the fact that our vulnerability indicator accounts for all potential connections to a given sub-reef. In practice, these connections only yield the transmission of disease agents if the sub-reef they originate from is affected by SCTLD. Our model might therefore overestimate the vulnerability of some sub-reefs. Moreover, due to the lack of data on coral distribution in FCR, an uniform coral density was assumed over all reefs. The impact of some reefs with low coral cover might thus be overestimated by the model. Nonetheless, we argue that our model remains a valuable tool to assess the (absence of) connectivity between the Marquesas and the DRTO.

Model results suggest a time lag of 5 to 6 months between the moment the hydrodynamics predicted that disease agents reached the DRTO and the moment SCTLD symptoms were observed in the DRTO. This seems to contradict the results of previous modeling and experimental studies that found SCTLD transmission times of 10 days or less (Dobbelaere et al., 2020; Meiling et al., 2021). However, several elements might explain a slower development of the disease on the DRTO. First, *in situ* conditions might significantly differ from the ones of a controlled tank environment, potentially leading to differences in the time required for the first disease lesions to appear. Furthermore, disease transmission in the Florida Keys might occur faster as reefs can receive disease agents from several affected neighboring reefs. In the case of disease agents reaching the fully susceptible population of the DRTO, such interactions with neighboring affected colonies do not take place and the outbreak might therefore require more time to develop. Furthermore, our results suggest that corals of the DRTO could only be exposed to agents coming from the Marquesas in November and December 2020, while exposure to incoming disease agents was continuous in the Keys due to the density of the reef system. Additionally, the epidemiological parameters of Dobbelaere et al. (2020) were calibrated on species-averaged prevalence data in the Florida Keys, which might not be representative of the colony composition and environmental conditions in the DRTO. Finally, observational data is dependent on the frequency and spatial distribution of field missions and might therefore give an incomplete picture of the situation on the field. For example, fine scale observations of SCTLD in the Lower Florida Keys found low disease incidence (< 10 colonies) starting in October, and then disease incidence peaked in April 2019 (Williams et al., 2021).

Alternatively, one might argue that this lag between the modeled transmission of the disease agents to the DRTO and the first observations of the SCTLD indicates that the propagation of the disease was not caused by local currents. In that case, another vector, such as ballast waters, might have to be considered. However, such investigations are beyond the scope of the present study.

It is important to note that the time and location of the first observations of an outbreak do not necessarily correspond to its initiation. An epidemic might grow unnoticed during its first stages, as it first develops at a linear rate before growing exponentially. Tools such as the ones developed in the present study might therefore have helped to mitigate the SCTLD during the first stages of its development in the DRTO, before May 2021. Furthermore, this study has shown that strong eddy activity near the DRTO was likely to interrupt connectivity from the Western Florida Keys to the DRTO. Therefore, monitoring eddy activity through satellite observations of sea surface temperature and sea surface elevation anomaly (Kourafalou et al., 2018) might serve as a proxy for reef managers to estimate connectivity between these two areas. The implications of our connectivity results are not limited to the propagation of disease agents and apply to the spread of any type of propagules from the Marquesas and the DRTO. This study therefore brings additional insight on the physical and environmental connectivity in the southwestern part of FCR.

The onset of the SCTLD outbreak and the PortMiami Deep Dredge Project

This chapter is based on the following article:

Dobbelaere T., other co-authors TBD, & E. Hanert, 2022, Early transmission dynamics of SCTLD and its connection with the PortMiami Deep Dredge Project. (planned submission to *Marine Pollution Bulletin*)

Abstract

For the last 8 years, Florida's Coral Reef (FCR) has suffered from severe coral loss caused by stony coral tissue loss disease (SCTLD). The outbreak reportedly initiated near Virginia Key in September 2014, during the deepening of the Port of Miami (PoM) shipping channel, that took place between November 20, 2013 and March 16, 2015. The disease then spread to the entirety of FCR, likely through waterborne transmission. Although the causative agent of SCTLD remains unknown, there is evidence that sediment can act as vector for the disease. The goal of this study is therefore to evaluate whether sediments produced or resuspended during dredging operations might have been transported to reefs where disease was reported and to assess whether the timing of these sediment fluxes was consistent with the observed spread of the disease. We evaluated the transport of sediments caused by the expansion of PoM between November 2013 and September 2014 using a quasi-3D sediment transport model forced by currents from the high-resolution coastal ocean model SLIM. Our result suggested that the dredging had close to no direct impact on the

coral reefs of Virginia Key. However, a significant fraction of the sediments produced reached monitoring sites where the disease was reported prior to September 2014, suggesting that the dredging might have played a role in the onset of the outbreak at these sites. Furthermore, using a biophysical disease agent transport model suggests that waterborne transmission from one of these sites to Virginia Key was possible before September 2014. This study brings new insight on the role that the deepening of PoM might have played in the onset of one of the worst coral outbreaks on record in the Caribbean.

4.1 Introduction

Coral diseases are a major threat to coral reef ecosystems and have led to significant declines in coral cover especially within the Caribbean region (Richardson et al., 1998a; Sutherland et al., 2004; Aronson and Precht, 2001; Harvell et al., 2007; Brandt and McManus, 2009). One of the latest and the most damaging outbreak to date in Florida's Coral Reef (FCR) is the stony coral tissue loss disease (SCTLD) (NOAA, 2018). First observed off the coast of Miami in 2014 by Precht et al. (2016), the disease has since spread through the entire FCR (Muller et al., 2020; Dobbelaere et al., 2022) and has been observed in several territories of the Caribbean (Kramer et al., 2019; Meiling et al., 2021; Estrada-Saldívar et al., 2021; Heres et al., 2021). Although the causative agent of the disease remains unknown, hydrodynamics are likely to play an important role in its propagation as both modeling studies and ex situ experiments show evidence of waterborne disease transmission (Aeby et al., 2019; Dobbelaere et al., 2020; Eaton et al., 2021; Meiling et al., 2021). Furthermore, recent studies showed evidence that sediments can act as a vector for the SCTLD (Rosales et al., 2020; Studivan et al., 2022).

Some of the first signs of SCTLD were reported in September 26th, 2014, near Virginia Key by Precht et al. (2016). They derived a relationship between the time of the first outbreak at monitored reefs and their geographic distance to Virginia Key. It was therefore hypothesized that the epidemic started near Virginia Key and then spread to the neighboring reef, both north and south. However, earlier signs of diseases were already reported north of Virginia Key in June 2014, at the monitoring site of N. Sunny Isles (Precht et al., 2016). All these observations occurred during the deepening of the Port of Miami (PoM) shipping channel, that took place between November 20, 2013 and March 16, 2015. The dredging was monitored twice-weekly at 26 permanent monitoring stations established within the Miami-Dade County, making it one of the most complete datasets related to a dredging project (Gintert et al., 2019). Interestingly, disease signs were also reported at one of these monitoring stations in May 2014.

While operating in a conventional way, dredged materials were pumped from the dredge to a spider barge and then transported to the US Environmental Protection Agency designated Ocean Dredge Material Disposal Site (ODMDS) located 4.7 nautical miles offshore. However, the suction mechanism was turned off during

non-conventional rock-chopping activities in order to pre-treat very hard rock contained in the Anastasia and Fort Thompson formations between December 2013 and May 2014 (Miller et al., 2016). The Army Corps commissioned a report that provides a back-of-the-envelope estimating this practice could have resulted in up to 33 cm deposition over 874,121 m² of reef surrounding the outer entrance channel (U.S. Army Corps of Engineers, 2017). Additionally, several studies reported that the impact of the dredging was widespread (Miller et al., 2016), causing the death of > 560,000 corals within 0.5 km of the channel (Cunning et al., 2019) and producing sediment plumes covering up to 11 km² of coral area within 5-10 km of the dredging (Barnes et al., 2015).

Sediments released by dredging can affect the biological functions of corals in numerous ways through turbidity and sedimentation (Erfemeijer et al., 2012; Jones et al., 2015). Increased turbidity caused by the suspended sediments reduces the light available to symbiotic zooxanthellae, leading to reduced coral cover and growth. Sedimentation, on the other hand, can cause smothering or burial of coral polyps (Erfemeijer et al., 2012). Furthermore, both sedimentation and turbidity can significantly reduce larval recruitment by inhibiting settlement and reducing larval survival in the water column (Jones et al., 2015). These effects are stronger with fine-grained sediments, as they cause a stronger light reduction (Fournier and Figueiredo, 2017). Additionally, fine-grained sediments such as silts have high nutrient contents, which can lead to an increased microbial activity, eventually causing anoxic conditions in the immediate vicinity of corals (Weber et al., 2012). As they release finer sediments over significantly longer periods than natural events such as hurricanes, dredging activities can thus be more harmful to corals and reef habitat compared to other types of sedimentation (Cunning et al., 2019).

Nonetheless, Gintert et al. (2019) argued that the reported coral mortality during the dredging project was dominated by the regional outbreak of SCTLD. Further, they suggested that the onset of the disease might have been linked to a leaking discharge pipe of the Miami Central District Municipal Wastewater Treatment Plant (WWTP) located off Virginia Key. However, as sediments can act as vector for SCTLD (Studivan et al., 2022), there is also a possibility that the causative agents of the disease was transported to the monitoring site of Virginia Key on sediments released by the dredging. This possibility can be evaluated using a hydrodynamic model simulating the transport of sediments produced during the dredging project. As coastal reef ecosystems are characterized by the complex topography of the coastline and the presence of islands, reefs and artificial structures, such a model would require high spatial resolution to accurately represent the transport of sediments at the reef-scale. In this context, unstructured-mesh models are particularly well suited, as they can easily adapt to the topography (Fringer et al., 2019) and can capture small-scale circulation features around reefs and islands (Lambrechts et al., 2008).

The goal of this study is therefore to simulate the trajectories of the sediments released during the entirety of the PortMiami Deep Dredge Project (PMDDP) using a high-resolution hydrodynamic model coupled with a sediment transport

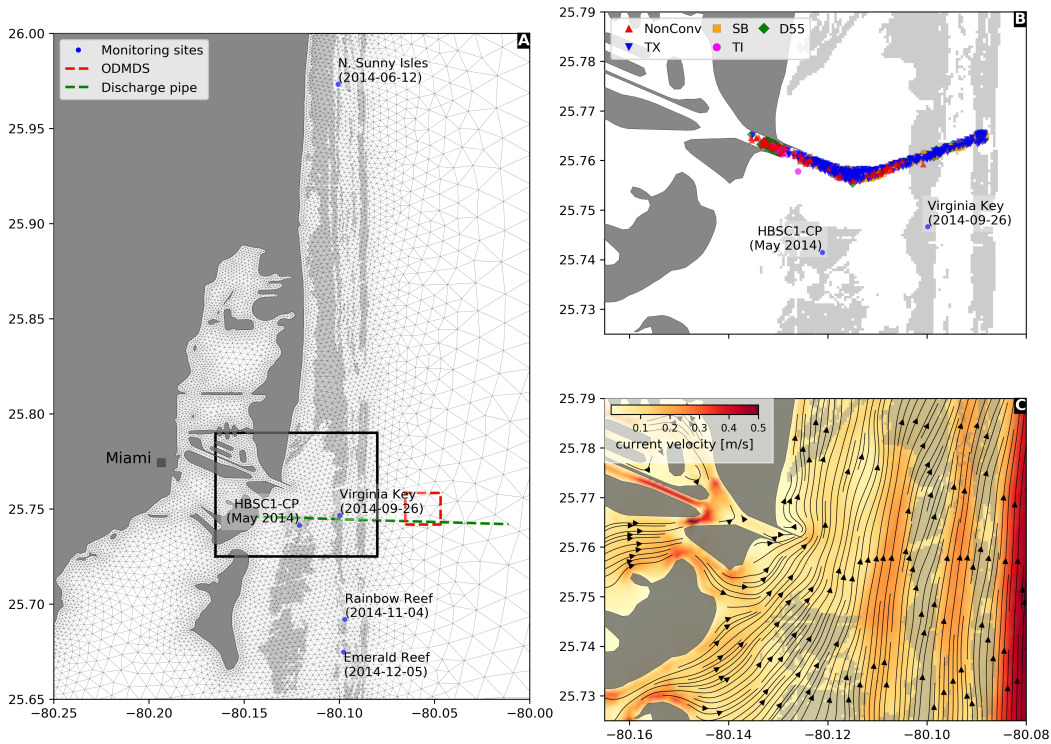


Fig. 4.1: **A:** Model mesh near the dredged channel. Elements have a characteristic length of 100 m over reefs (in light grey) and along the coasts (in dark gray). The monitoring sites considered in the present study are shown by blue dots. The date where SCTLD was first observed at these sites is given between brackets. The Ocean Dredge Material Disposal Site (ODMDS) is shown in red and the discharge pipe of the Miami Central District Municipal Wastewater Treatment Plant in green. **B:** Close up view of the dredged channel. The locations of the different types of dredging that took place during the expansion of PoM are shown by colored markers. **C:** Snapshot of the modeled currents in the vicinity of the dredged channel. Small-scale flow features such as the acceleration of currents between reefs and islands are well reproduced by the model.

model. Specifically, our goal is to answer the following questions: (1) Which reefs were impacted by PMDDP ? (2) Is the impact on these reefs consistent with the observed timing of the onset of SCTLD ?

4.2 Methods

The hydrodynamics of the entire FCR was modeled using the multi-scale ocean model SLIM¹, which has already been extensively validated in the area (Frys et al., 2020a; Dobbelaere et al., 2020, 2022). SLIM uses an unstructured mesh whose resolution can be locally increased in order to accurately represent fine-scale flow features. The mesh used in this study was built following the same methodology

¹<https://www.slim-ocean.be>

as Dobbelaere et al. (2020), with a local refinement near PoM and in the Bay of Biscayne to achieve a resolution of 100 m in the vicinity of the dredged channel (Fig. 4.1A). It was made up of approximately 3.5×10^5 triangles and was generated with the seamsh² Python library, which is based on the open-source mesh generator GMSH (Geuzaine and Remacle, 2009). The model was run between October 15, 2013 and September 26, 2014 to cover the whole dredging period prior to the first observation of SCTLD by Precht et al. (2016). Figure 4.1C depicts how a 100-m spatial resolution mesh simulated fine-scale details of the ocean currents, such as the flow acceleration between reefs and islands.

The transport of sediments released from the channel was then modeled using a Lagrangian particle tracking model, forced by the simulated currents. The sediment model is inspired by the Particle Transport Model (PTM), developed by the US Army Corps of Engineers (MacDonald et al., 2006). In this model, particles undergo a combination of horizontal and vertical motions. The vertical is mostly driven by gravity, with heavier particles sinking faster. Once they have settled, particles can be resuspended when shear stress exceeds the critical Schields parameter, as parameterized by Soulsby et al. (1997). The horizontal motion of the suspended particles is derived from the 2D model velocity by assuming a vertical log profile, hence yielding a quasi-3D approach. When sediment particles enter the near-bed zone, their horizontal velocity is greatly reduced and sediments are transported with the bedload.

As sediment dispersion is dependent on the grain size, we modeled the dispersal of five sediment classes to represent the impact of fine- to coarse-grained particles: (i) 5-50 μm , (ii) 50-100 μm , (iii) 100-200 μm , (iv) 200-300 μm , and (v) 300-400 μm . We performed a different simulation for each class, with the grain size randomly drawn from a uniform distribution over the corresponding size range. The density of each sediment particle was derived from their size using the formula of Hamilton and Bachman (1982). Furthermore, all particles were differentiated based on the type of dredge that produced them. Five types of dredge were considered in our modeling study (Fig. 4.1B): (a) Texas cutterhead (TX), (b) non-conventional dredging, i.e TX with suction mechanism turned off (NonConv), (c) Spider Barge (SB), (d) Terrapin Island hopper (TI), and (e) Dredge 55 clamshell (D55).

Dredging operations performed during the expansion of PoM were characterized in our dataset by a date, a location and a type of dredging operation (Fig. 4.1B). In the absence of information about the exact time of the dredging, sediment particles were released from the dredging location during a whole day at a rate of 80 particles/hour in the model. To account for the motion of spider barges between the dredging site and disposal site, particles were released every 500 m along a straight line joining the dredging location to the ODMDS (see Fig. 4.1A) for every dredging operation labelled as SB.

The outputs of the sediment model were then used to evaluate the turbidity and sedimentation generated by the expansion of PoM over coral reefs. The occurrence of high turbidity over reefs was assessed based on the concentration of suspended

²<https://pypi.org/project/seamsh/>

sediment particles in the model. This concentration was computed by counting the number of suspended particles inside the cells of a regular $200\text{ m} \times 200\text{ m}$ grid over our computational domain. The modeled occurrence of plume was then compared against daily data of plume detection. This dataset was derived from satellite imagery by Cunning et al. (2019)³ following the methods of Barnes et al. (2015) at sites located within 15 km of the dredged channel. As in these two previous studies, we computed the simulated plume frequency by dividing the number of days during which plumes occurred by the total number of simulated days for all grid cells. The impact of sedimentation was quantified by computing the cumulated concentration of settled particles within the same computational grid. This cumulated concentration was normalized by the total number of simulated time steps to obtain an averaged concentration of deposited particles over the simulated period. Higher values of this indicator would indicate larger sediment deposition over longer cumulated time.

The potential impact of dredging on the onset of the SLD outbreak was more specifically assessed at five monitoring sites where signs of disease were reported. Four sites were reefs where disease was reported in 2014 by Precht et al. (2016). The fifth site was monitoring station HBSC1-CP of the monitoring of the expansion of PoM, where signs of disease were already reported in May 2014 (Fig. 4.1A, see pictures in Appendix). The impact of dredging was assessed by counting the number of sediment particles originating from each dredging that were transported within 500 m of all five sites. This distance was chosen to match the scale of the $500\text{ m} \times 500\text{ m}$ reef polygons used in the model (Dobbelaere et al., 2020). The obtained number of particles was then divided by the total number of sediment particles released by each type of dredge. Larger values of this indicator would suggest a greater impact of a given type of dredging operation at a given monitoring sites.

Finally, as previous studies showed evidence of waterborne transmission of SCTLD (Aeby et al., 2019; Dobbelaere et al., 2020; Eaton et al., 2021; Meiling et al., 2021), there is a possibility that the disease propagated to Virginia Key from other diseased reefs affected prior to September 2014. To evaluate this possibility, we computed monthly disease connectivity matrices following the methodology of Dobbelaere et al. (2020) during our simulated period. These connectivity matrices can be interpreted as large graphs whose vertices are $500\text{ m} \times 500\text{ m}$ reef areas and whose edges represent disease connectivity pathways. Evaluating the possibility of disease propagation from any sub-reef A to any sub-reef B is therefore equivalent to evaluating the existence of paths, i.e. sequences of connected vertices in the network starting from A and reaching B . As computing all possible paths is not computationally tractable, we limited ourselves to the computation of shortest paths from any given reefs to the Virginia Key monitoring site. This was performed using the function `get_all_shortest_paths` of the Python `python-igraph` package (Csardi et al., 2006). Such function requires the definition of a weight w_{ij} for the edge connecting reef i to reef j . We chose $w_{ij} = 1 - \tilde{C}_{ij}$, where \tilde{C}_{ij} is the

³datasets available at <https://github.com/jrcunning/pom-dredge/>

probability of disease propagation from reef i to reef j , so that "shorter" edges of the networks ($i.e.$ connectivity pathways with smaller weights) correspond to connections with larger disease propagation probability. The probability of a given path was then defined as the mean connection probability of the edges composing this path.

Finally, the 2D mode of the particle tracking model was used to assess the impact of wastewater leaking from the discharge pipe mentioned by Gintert et al. (2019). This model simulates the transport of neutrally buoyant material driven by mean current within the water column (Dobbelaere et al., 2020). Without clear information about the location of the leak, particles were continuously released every 100 m along a straight line between Miami Central District Municipal WWTP, located on Virginia Key and the ocean discharge outfall located at $25^{\circ}44'31''N$ $80^{\circ}05'10''W$ (Koopman et al., 2006). The impact of wastewater released from the different potential leak locations was then evaluated by computing the fraction of released wastewater particles that were transported within 500 m of the site of Virginia Key.

4.3 Results

$5-50\ \mu m$ was the only grain size that produced plumes consistent with the observations of Barnes et al. (2015) and Cunning et al. (2019) (Fig. 4.2A). For larger grain sizes, particles settled in the direct vicinity of the channel. For these heavier particles, suspended sediments were only observed offshore, closer to the Florida Current, where the current velocity was sufficiently strong to prevent deposition. This suggests that the observed turbidity was mostly due to fine silts. The modeled occurrence of plumes within 15 km of the dredged matched the presence/absence data of Cunning et al. (2019) in 82.7% of cases and the total area where plumes were observed was about $230\ km^2$, consistent with the $\sim 228\ km^2$ estimated by Barnes et al. (2015). Modeled plumes mostly occurred north of the dredged channel, as particles were driven northward under the action of the Florida Current, with plume frequencies of about 20% near the monitoring site of N. Sunny Isles. Plume frequencies were lower ($\sim 5\%$) over offshore reefs but reached up to 50% over alongshore reefs. These alongshore reefs correspond to regions of important sedimentation (Fig. 4.2B), which is consistent with the correlation between plumes and sedimentation highlighted in Cunning et al. (2019). The plume frequency was about 1% at site of HBSC1-CP while no plume occurred at other southern monitoring sites during the simulation.

Deposition results are shown for grain sizes corresponding to silts, which are more likely to carry organic matter and therefore more likely to carry SCTL agents (Erfemeijer et al., 2012)(Fig. 4.2B,C). Sedimentation mostly occurred on reefs located north of the dredge channel. For grain sizes smaller than $5-50\ \mu m$, sediments mostly settled on inshore reefs while sedimentation mostly took place on offshore reefs for grain size larger than $50\ \mu m$. When increasing grain sizes, the spatial distribution of sedimentation shifted southward, with a decrease of

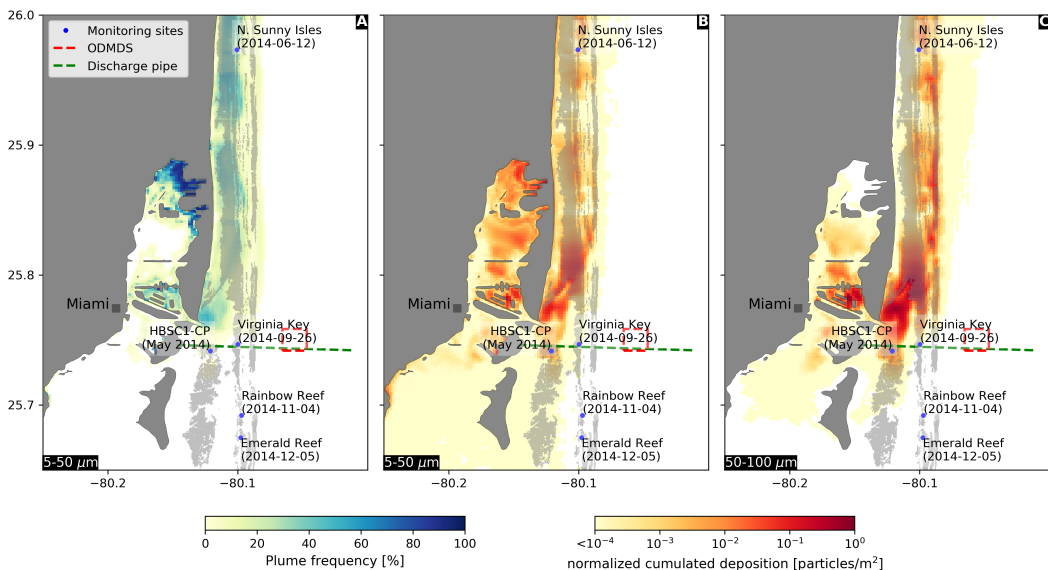


Fig. 4.2: **A:** Plume frequency for grain size in the range $5\text{-}50 \mu\text{m}$. The averaged concentration of deposited sediments are shown for grain sizes more likely to carry the disease: $5\text{-}50 \mu\text{m}$ (**B**) and $50\text{-}100 \mu\text{m}$ (**C**). Most modeled turbidity and sedimentation occurred north of the dredged channel. Non negligible sediment deposition occurred at site HBSC1-CP.

sedimentation near N. Sunny Isles and an increase of the concentration of settled sediments near HBSC1-CP and Virginia Key. The normalized cumulated deposition was around $0.01 \text{ particles}/\text{m}^2$ at site HBSC1-CP for all grain sizes while it increased from 2.5×10^{-7} to 1.6×10^{-3} with grain size at Virginia Key. For all grain sizes, no sedimentation occurred near Rainbow Reef and Emerald Reef. However, sediments settled at similar latitudes west to these sites for grain sizes below $100 \mu\text{m}$.

The evaluation of the impact of dredging at the monitoring sites indicated that dredging did not significantly impact the stations located south of the dredge channel, except at site HBSC1-CP (Fig. 4.3). In contrast, up to 40% of the released sediment particles reached the northern site of N. Sunny Isles. The impact of dredging at this site decreased with sediment size and the fraction of sediment particles reaching the N. Sunny Isles dropped below 2% for grain sizes larger than $200 \mu\text{m}$. However, for grain sizes finer than $50 \mu\text{m}$, N. Sunny Isles was heavily impacted by TX dredging. Indeed, the number of particles produced by TX reaching N. Sunny Isles was 50% larger than the cumulated number of particles produced by other dredging operations reaching the monitoring site for the same grain size. Such large impact can be explained by the fact that TX was one of the most frequent type of dredging during the simulations, with 268 simulated operations (Fig. 4.3C). However, SB events occurred at an equivalent frequency but resulted in 4 times fewer particles to reach N. Sunny Isles. For grain sizes below $100 \mu\text{m}$, between 10% and 30% of the sediments released by non conventional dredging reached N. Sunny Isles. This fraction dropped below 1% for grain sizes larger than $200 \mu\text{m}$. The fraction of sediments produced by non conventional dredging reaching

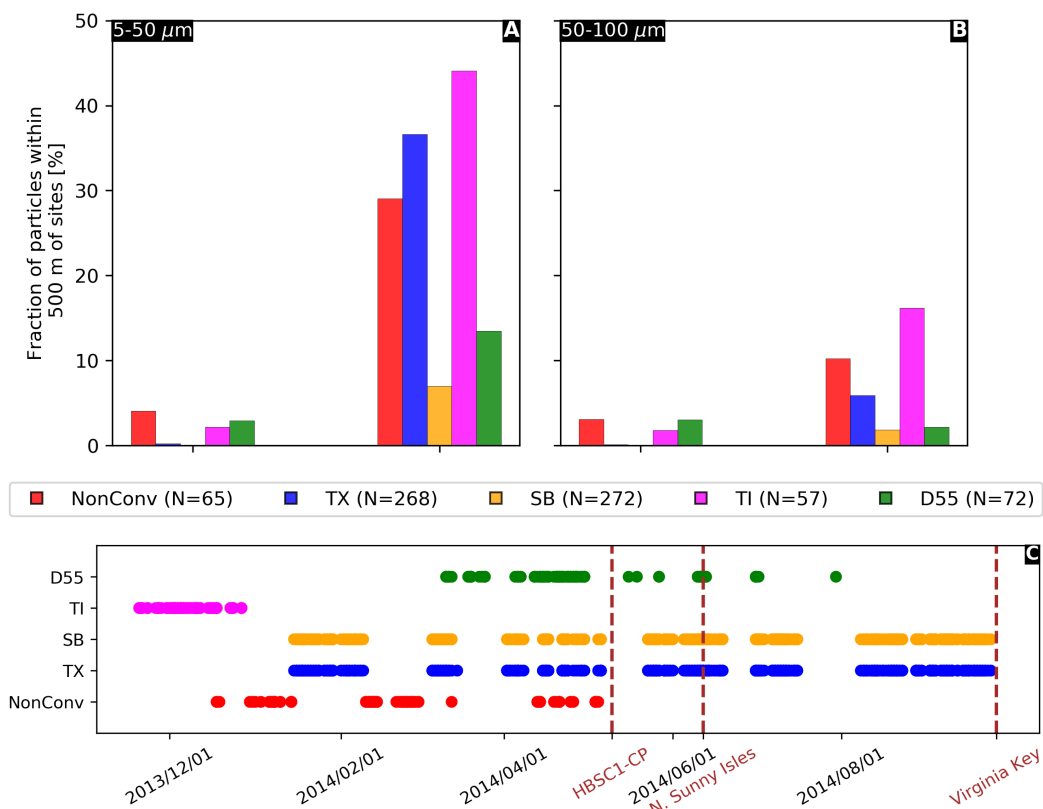


Fig. 4.3: Fraction of sediment particles released by each type of dredge that drifted within 500 m of HBSC1-CP and N. Sunny Isles with grain sized of 5-50 μm (**A**) and 50-100 μm (**B**). **C:** Temporal distribution of the simulated dredging operations. The dates of the first reported disease signs at each monitoring site are shown in brown. With the exception of HBSC1-CP, sites located south to the dredged channel were barely impacted by the dredging. However, a significant fraction of the released sediment particles reached the northern site of N. Sunny Isles. The number of simulated dredging operations is given between brackets for each dredging type

site HBSC1-CP remained between 1% and 5% for all grain sizes. For grain sizes below 100 μm , D55 and NonConv were the main sources of sediments reaching HBSC1-CP. Above 100 μm , the main source of sediments to the site became TI. The fraction of sediments produced by SB reaching HBSC1-CP remained negligible for all grain sizes. No sediment particles reached the sites of Rainbow Reef and Emerald Reef for all grain sizes. However, some particles reached Virginia Key for grain sizes larger than 100 μm . These sediments particles almost entirely originated from SB. Nonetheless, the impact of the dredging on Virginia Key remained limited with less than 1% of the released particles reaching the site.

Applying the same analysis to the discharge pipe of Miami Central District Municipal WWTP suggests that only wastewater released from a leak in the direct vicinity of the Virginia Key could have impacted the site. Fig. 4.4 shows the fraction of released wastewater particles that reached the site of Virginia key for

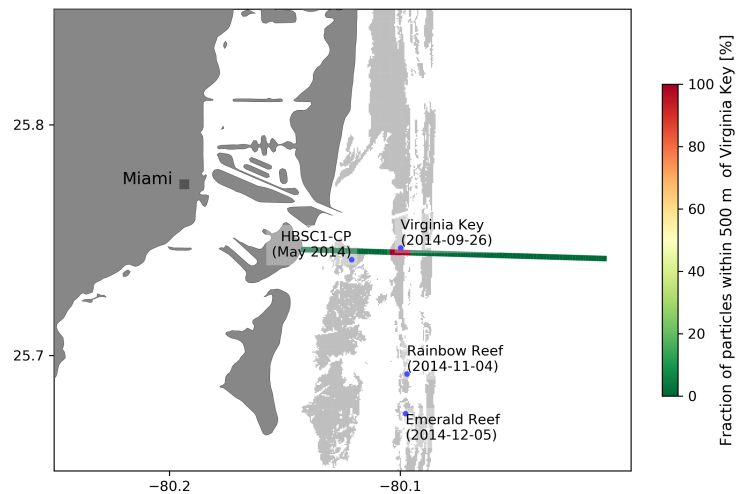


Fig. 4.4: Fraction of wastewater particles reaching the site of Virginia Key for potential leak positions located every 100 m along the discharge pipe. Only particles released in the direct vicinity of Virginia Key could reach the monitoring site.

every 100 m segments of the discharge pipe. The fraction of particles that drifted within 500 m of Virginia Key was: 100% for particles released within 500 m of the site; 0-1% for particles released between 500 m and 1.5 km away from the site; and 0% for all other sources of wastewater particles. As HBSC1-CP was also located near the discharge pipe, a similar analysis was conducted for this monitoring site and gave similar results.

As signs of disease were observed at site HBSC1-CP in May 2014, before the first observations of SCTLD in Virginia Key in September 2014, we assessed the presence of shortest paths from HBSC1-CP to Virginia Key in the modeled monthly disease connectivity networks between May and September 2014 (Fig. 4.5). We found connectivity pathways connecting the two sites during all months of May-September 2014, with the exception of July. This suggests that there was a possibility of disease propagation from HBSC1-CP to Virginia Key during most of these 5 months. However, we found no direct pathway connecting the two sites. Southern intermediary reefs were systematically needed as stepping stones for the propagation of the disease. This suggests that several months might have been required for disease agents to reach Virginia Key from HBSC1-CP. Moreover, shortest paths in June, August and September 2014 had many sub-reef stepping stones in common. These similar connectivity patterns indicate favorable conditions for disease propagation over several months from HBSC1-CP to Virginia Key during this period.

4.4 Discussion

The quasi-3D sediment model forced by currents from the high-resolution coastal ocean model SLIM reproduced a sediment dynamics consistent with plume obser-

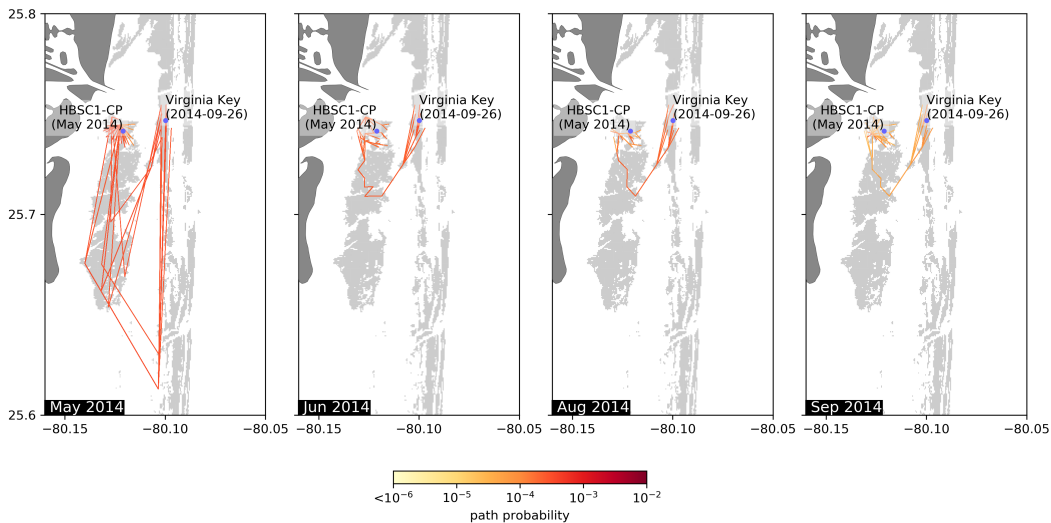


Fig. 4.5: Shortest path from HBSC1-CP to Virginia Key in the monthly disease connectivity networks between May and September 2014. July 2014 was the only month without modeled connectivity between the two sites between May and September 2014. Southern intermediary reefs were needed as stepping stones for the propagation of the disease from HBSC1-CP to Virginia Key.

vations derived from satellite imagery. It suggests that sediment particles produced by dredging were mostly transported northward under the influence of the Florida Current. No sediment particles reached the southern sites of Rainbow Reef and Emerald Reef while dredging had limited direct impact on Virginia Key, identified as the site where the outbreak of SCTLD was initiated in September 2014. Furthermore, our results indicate that it is unlikely that the site was affected by a leaking discharge pipe of Miami Central District Municipal WWTP, as suggested by Gintert et al. (2019). However, signs of disease were observed prior to September 2014 at the sites of N. Sunny Isles and HBSC1-CP, where the impact of dredging was greater. Up to 30% of silt particles produced by non-conventional dredging reached coral reefs of N. Sunny Isles while 5% of them reached site HBSC1-CP, where significant sedimentation occurred. Furthermore, analysis of monthly disease connectivity networks indicate disease transmission from HBSC1-CP to the site of Virginia Key was possible through waterborne transmission.

Our study confirms previous reports about the widespread impact of the expansion of PoM. As in Barnes et al. (2015), the total area of plumes in our model was about 230 km². Furthermore, the model results reproduced the presence/absence within 15 km of the dredged channel derived by Cunning et al. (2019) with an accuracy of 82.7%. Such good agreement was only obtained for grain sizes in the range 5-50 μm , suggesting that fine silts were the main drivers of the turbidity generated by dredging, which is consistent with previous studies (Fournier and Figueiredo, 2017). Despite this good agreement, the distribution of plumes predicted by our model tends to be shifted northward compared to these previous studies. These discrepancies might be explained by the fact that our approaches is

solely based on sediment concentration. However, turbidity depends on many local factors such as the water content of phytoplankton and organic matters (Gray, 2000; Thackston and Palermo, 2000). As reported by Cunning et al. (2019), the plumes mostly occurred in areas of high sedimentation. As such areas were mostly located over coral reefs, our results suggests that the expansion of PoM might have harmed coral populations over an extended area through increased turbidity and sedimentation. This sedimentation mostly took place on alongshore reefs for grain sizes smaller than $50\mu\text{m}$ and on offshore reefs for coarser grain sizes. Sediment settlement might be significantly harmful to offshore coral reefs populations as they are usually less accustomed to sedimentation than their inshore counterparts (Wolanski et al., 2005).

A limitation of our study is that the amount of released sediments might be overestimated, as conventional and non-conventional dredging are treated in the same way in the model. For all dredging types, sediment particles were released at the same rate in the model. Although conventional dredging was reported to release fine-grained sediments in the water column through dewatering and overflow from barges (Jones et al., 2016), the quantity of dredged material lost in the water was limited by the use of pumping mechanisms. By contrast, for non-conventional dredging, the suction mechanism was turned off, causing all chopped rock particles to be released in the water column. The numbers of particles reaching the monitoring sites were therefore likely overestimated for all sources but non conventional dredging. However, the fractions given in Fig. 4.3A,B remain valid as they are relative to the total number of sediments released in the water columns. Despite these overestimations, the coral reefs of N. Sunny Isles appeared to be highly sensitive to fine-grained sediments produced by dredging (Fig. 4.3). Furthermore, the non-conventional rock-chopping that took place between December 2013 and May 2014, was a non-negligible source of sediments to N. Sunny Isles, as up to 30% of the released particles reached the site. As sediments have the potential to act as a SCTLD vector (Rosales et al., 2020; Studivan et al., 2022), the dredging might therefore have contributed to the observed onset of the disease on the reefs of N. Sunny Isles in June 2014. Moreover, up to 5% of the fined-grained sediments produced by non-conventional dredging reached the site HBSC1-CP. Although this represents a more limited quantity of sediments, HBSC1 was within 2 km from the sites where non-conventional dredging took place, in a region where the model predicted an important sedimentation. Therefore, although fewer sediments reached HBSC1-CP, they had a higher probability to settle and to be in direct contact with corals. In addition to smothering corals and diverting their energy through sediment removal (Erfemeijer et al., 2012), these settled sediments are more likely to transmit the disease to the reefs.

In all simulations, the expansion of PoM had limited direct impact on Virginia Key, identified as the site where the outbreak initiated in September 2014 Precht et al. (2016). For all grain sizes, the fraction of sediment particles reaching Virginia Key remained below 1%. It is therefore unlikely that sediments produced by the deepening of the channel brought the disease to the site. Furthermore,

our simulation of leaking wastewater along the discharge pipe of Miami Central District Municipal WWTP suggests that currents were likely to flush wastewater away from Virginia Key. It was therefore unlikely that wastewater affected the site, except if the leak was located within hundreds of meters from the site. However, signs of disease were observed prior to September 2014 at the sites of N. Sunny Isles and HBSC1-CP, both of which were impacted by the dredging. Several studies showed evidence of waterborne transmission of SCTLD (Aeby et al., 2019; Dobbelaere et al., 2020; Eaton et al., 2021; Meiling et al., 2021). Disease agents might therefore have been transported by currents from one of the diseased sites to Virginia Key. As site HBSC-CP was the closest to Virginia Key, we built and analyzed monthly disease connectivity networks and found connectivity pathways from HBSC1 to Virginia Key in May, June, August and September 2014. This implied that the propagation of the disease from HBSC1-CP to Virginia Key through hydrodynamics-driven transport of disease agents was possible during these four months. However, these pathways used reefs located further southward as stepping stones. Therefore, the propagation of outbreak to reach Virginia Key starting from HBSC1-CP required these intermediary reefs to get first infected by disease agents released by disease colonies of HBSC1-CP. Once diseased, these colonies would then send diseased agents to affect the next colonies of the connectivity pathway until the outbreak reached Virginia Key. Assuming an averaged transmission time of the order of 5-10 days (Dobbelaere et al., 2020), disease propagation from HBSC1-CP to Virginia Key might have required several months. This is consistent with the 5 month period separating reports of diseased at the two sites. Moreover, the fact that June, August and September exhibited similar connectivity pathways suggests that disease propagation could indeed have occurred over several months without being interrupted by changing hydrodynamic conditions.

4.5 Conclusion

In the present study, we evaluated the impact of the dredging operations that took place the impact of the deepening of the Port of Miami shipping channel on the neighboring coral reefs. This evaluation was performed using a quasi-3D sediment model forced by high-resolution currents from the coastal ocean model SLIM. As the first signs of the SCTLD outbreak were reported during these expansion works near Virginia Key and knowing that sediments may serve as SCTLD vector, we aimed at answering two main questions. First, we wanted to evaluate the fraction of sediments produced by the PortMiami Deep Dredge Project that reached the site of Virginia Key. Second, we evaluated the possibility of waterborne transmission of SCTLD to Virginia Key from other reefs impacted by the dredging. Doing so, we paid a special attention to the sediments produced by non conventional rock chopping during which pumping mechanisms were turned off, causing all chopped rock particles to be directly released in the water column.

Our results suggest that the dredging works had close to no direct impact on the coral reefs of Virginia Key, indicating that disease transmission trough the produced

sediments was extremely unlikely. However, our results show the sediments released by the expansion works had a non-negligible impact on the sites of N. Sunny Isles and HBSC1-CP, where signs of disease were observed before the outbreak was first reported at Virginia Key, indicating that the sediments might have played a role in the onset of the disease at these two sites. Furthermore, using a previously developed bio-physical model that successfully reproduced the observed spread of SCTLD, we show that there was a possibility of waterborne disease propagation from HBSC1-CP to Virginia Key.

This study suggests that the expansion of the Port of Miami might have played a role in the onset of the outbreak of SCTLD in sites where the disease was reported during the first half of 2014. Furthermore, it shows that the disease could then have spread from these sites to Virginia Key, from where SCTLD was then reported to propagate both north and south to the neighboring reefs. Our work brings new insight on the impact of a major dredging project in Florida on the onset of one of the worst coral outbreaks on record in the Caribbean.

Impacts of hurricanes on wave-induced ocean transport processes

This chapter is based on the following article:

Dobbelaeere, T., Curcic, M., Le Hénaff, M., & Hanert, E. (2022). Impacts of Hurricane Irma (2017) on wave-induced ocean transport processes. *Ocean Modelling*, 101947. doi: 10.1016/j.ocemod.2022.101947.

Abstract

The intensity of major tropical cyclones has increased during the past decade. Their effect is particularly acute in coastal areas where they cause extensive damage leading to an influx of debris, sediments and waste to the sea. However, most operational coastal ocean models do not represent heavy-wind transport processes correctly if the hydrodynamics is not coupled with the wind-generated waves. This may lead to significant errors in ocean simulations under tropical cyclone conditions. Here, we investigate current-wave interactions during a major hurricane and assess their impact on transport processes. We do that by coupling the unstructured-mesh coastal ocean model SLIM with the spectral wave model SWAN, and applying it to the Florida Reef Tract during Hurricane Irma (September 2017). We show that the coupled model successfully reproduces the wave behavior, the storm surge and the ocean currents during the passage of the hurricane. We then use the coupled and uncoupled wave-current model to simulate the transport of passive drifters. We show that the wave radiation stress gradient alone can lead to changes of up to 1 m/s in the modeled

currents, which in turn leads to differences of up to 5 km in the position of drifting material over the duration of the hurricane. The Stokes drift however appears to cause deflections up to 4 times larger and hence dominates wave-induced transport. Wave-current interactions therefore strongly impact the transport of drifting material such as sediments and debris in the aftermath of a hurricane. They should thus be taken into account in order to correctly assess its overall impact.

5.1 Introduction

Major hurricanes are becoming more intense under the effect of global warming (Bhatia et al., 2019; Knutson et al., 2020). Better understanding their repercussions on coastal areas becomes therefore critical. However, estimating the impact of hurricanes on the coastal ocean circulation remains a challenge. Understanding wave-current interactions and representing their impact on coastal ocean transport processes is central to many coastal activities such as dredging, erosion management, oil and gas activities, search and rescue, and insurance (Bever and MacWilliams, 2013; Li and Johns, 1998; Breivik et al., 2013). All these activities require wave-current models to predict the impact of tropical cyclones on the coastal circulation and on the sea surface elevation.

Wave-current interactions during a cyclone are highly nonlinear and vary significantly in space and time (Wu et al., 2011). Wave-induced currents are generated by wave radiation stress gradients (Longuet-Higgins, 1970), affecting water levels near shorelines and wave breaking points (Longuet-Higgins and Stewart, 1964). Changes in water levels and currents, in turn, affect the motion and evolution of the waves (Sikirić et al., 2013). Coupled wave-current models hence require the calculation of the full directional wave spectrum in order to correctly reproduce the dynamics of wind-driven surface waves. This is usually achieved by spectral wave models, which describe the evolution of the wave energy spectrum. As of today, the most popular spectral wave models are the WAve Model (WAM) (WAMDI Group, 1988), Simulating WAve Nearshore (SWAN) (Booij et al., 1999), and WAVEWATCH III (Tolman et al., 2009). Among these models, SWAN has been specifically developed for coastal applications, as it represents depth-induced wave breaking and triad wave-wave interactions using numerical techniques adapted to small-scale, shallow water regions (Booij et al., 1999). WAVEWATCH III has also recently been equipped with new parallelization algorithm, domain decomposition and numerical schemes for high resolution coastal applications (WW3DG, 2019; Abdolali et al., 2020).

Coastal oceans are characterized by the complex topography of the coastline and the presence of islands, reefs and artificial structures. Traditional structured-grid models lack the flexibility to simulate near-shore processes at a sufficiently small scale. Although the use of nested structured grids allows local grid refinement (Warner et al., 2010), staircase-like representation of complex coastal topographies cannot be avoided. Instead, unstructured-mesh models easily adapt

to the topography and are hence better suited to coastal processes (Fringer et al., 2019). Capturing the impact of the topography on wave interactions becomes even more important in the case of tropical cyclones. Heavy winds generate large wind-waves and disturb ocean conditions (Liu et al., 2020) by causing coastal upwellings on continental shelves (Smith, 1982) and inducing strong currents, waves and storm surges in nearshore and coastal regions (Dietrich et al., 2010; Weisberg and Zheng, 2006).

Ocean waves act as the dynamical interface between the atmosphere and the ocean. Through this interface, tropical cyclones cause a cooling of the upper ocean layer by vertical mixing and heat transfer (Aijaz et al., 2017; Varlas et al., 2020). By altering the structure of the upper-ocean, hurricane can cause the disruption of major ocean currents such as the Florida Current and Gulf Stream (Oey et al., 2007). Interaction with hurricanes alters the thermal structure of these currents and can cause a significant decline of their flow, resulting in delayed increased coastal levels along their path, even in locations out of reach of the hurricane itself (Ezer et al., 2017; Ezer, 2018, 2020).

Near the storm, heavy wind conditions also affect material transport at the ocean surface. The transport of drifting objects or substances that are locally released is often best represented by a Lagrangian individual-based model. Such an approach is routinely used to model the dispersal of larvae, pollutants, sediments and many other tracers (e.g. Le Hénaff et al., 2012; Liubartseva et al., 2018; Figueiredo et al., 2013; Frys et al., 2020b). Although some transport model might take wave-induced currents into account, most of them neglect wave-current interactions, which can lead to significant errors in storm conditions (Röhrs et al., 2012; Curcic et al., 2016). Niu and Xia (2017) and Mao and Xia (2018, 2020) investigated the impact of wave-current interactions during storm event in lakes and inlets. However, to our knowledge, there have been no similar studies on the impact of hurricane-induced wave-current interactions in coastal environments such as the Florida Reef Tract (FRT), where changes in transport processes might significantly impact the biological connectivity.

The main questions we want to answer in this study are the following: (1) How important are wave-current interactions during a tropical cyclone? (2) What effect do they have on the transport of drifting material? We tackle these issues by investigating the transport of drifting particles on the Florida shelf during Hurricane Irma, one of the strongest and costliest tropical cyclones on record in the Atlantic Basin (Xian et al., 2018), which made landfall in Florida in September 2017. To do that, we developed an unstructured-mesh coupled wave-current model of the whole FRT to simulate the ocean circulation under hurricane conditions. Both modeled currents and waves were validated against field measurements and then used to simulate the transport of drifting material in the Florida Keys and over the Florida inner shelf. Model outputs were then compared with uncoupled simulation results in order to assess the impact of the radiation stress gradient and Stokes drift on the modeled currents and transport.

5.2 Methods

5.2.1 Study area and observational data

We study the ocean circulation in an area that covers the whole FRT and includes the northwestern end of the Gulf of Mexico and the Straits of Florida (Fig. 5.1). The large-scale ocean circulation around South Florida is dominated by the Florida Current (FC), which originates from the Loop Current (LC) where it enters the Florida Straits from the Gulf of Mexico, and, downstream, forms the Gulf Stream. The FC is a major western boundary current characterized by spatial variability and meandering, associated with the presence of cyclonic eddies between the core of the current and the complex reef topography of the FRT (Lee et al., 1995; Kourafalou and Kang, 2012). The variability of the FC extends over a large range of spatial and temporal scales, with periods of 30-70 days in the Lower Keys (Lee et al., 1995) and shorter periods of 2-21 days in the Upper Keys (Lee and Mayer, 1977), and exhibits significant seasonal and interannual cycles (Johns and Schott, 1987; Lee and Williams, 1988; Schott et al., 1988). Circulation on the West Florida Shelf (WFS), on the other hand, is forced by local winds and tidal fluctuations (Lee and Smith, 2002; Liu and Weisberg, 2012). Furthermore, due to its location relative to the warm waters of the North Atlantic, Florida is particularly vulnerable to tropical cyclones. On average, the state is hit by a hurricane every two years and strong hurricanes, some of which are among the most destructive on record, strike Florida on average once every four years (Malmstadt et al., 2009).

The state of the ocean around Florida is monitored by an extensive array of tide gauges, current meters and buoys. In this study, we used sea surface elevation measurements from the National Oceanic and Atmospheric Administration's (NOAA) Tides and Currents dataset. These measurements were taken at four locations: two in the Florida Keys (Key West and Vaca Key); one on the East coast of Florida (Virginia Key); and one on the West coast (Naples). For the currents, we used ADCP measurements from the University of South Florida's College of Marine Science's (USF/CMS) Coastal Ocean Monitoring and Prediction System (COMPS) for the WFS (Weisberg et al., 2009). More specifically, we used measurements from moorings C10, C12 and C13, respectively located at the 25, 50, and 50 m isobaths of the WFS (Liu et al., 2020). Finally, for the waves, we used measurements from four buoys of the NOAA's National Data Buoy Center (NDBC); two on Florida's eastern shelf and two on the WFS. The locations of all measurement stations are shown in Fig. 5.1.

5.2.2 Wind and atmospheric pressure during Hurricane Irma

Hurricane Irma made landfall in Florida on 10 September 2017 as a category 4 hurricane at Cudjoe Key (Florida Keys) and later as a category 3 hurricane on Marco Island, south of Naples (see hurricane track in Fig. 5.1). It then weakened to a category 2 hurricane as it moved further inland (Cangialosi et al., 2018). The

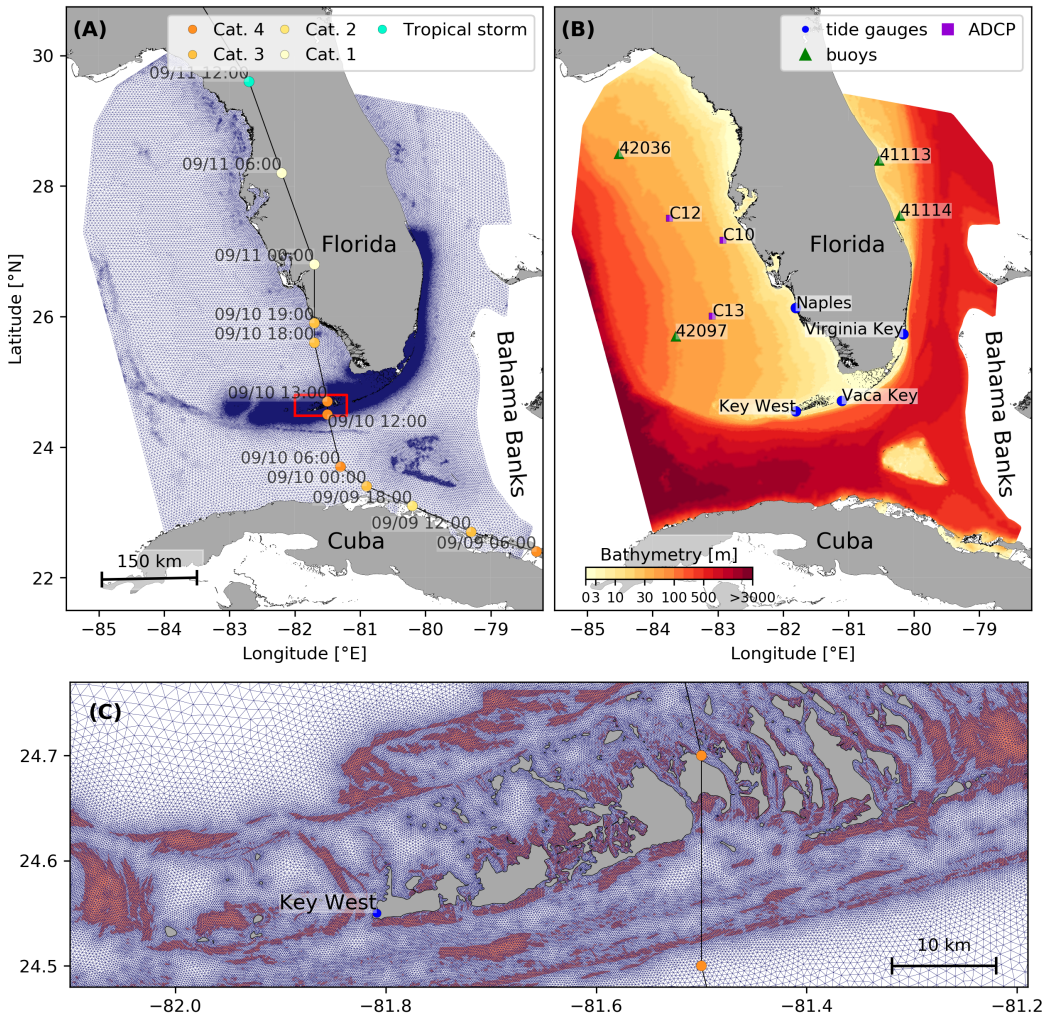


Fig. 5.1: (A) Mesh of the computational domain with the trajectory of Irma. The category of the hurricane is given by the Saffir-Simpson color scale. (B) Bathymetry of the domain with the location of stations used for the validation of the model outputs. (C) Close up view of the Lower Keys area (red box in (A)), where the mesh resolution reaches 100 m near reefs (shown in dark orange) and islands (shown in dark grey)

storm damaged up to 75% of the buildings at its landfall point in the Florida Keys, making it one of the strongest and costliest hurricanes on record in the Atlantic basin (Xian et al., 2018; Zhang et al., 2019). The strongest reported sustained winds on Marco Island were 50 m/s while the highest recorded storm surge was 2.3 m, although larger wind speed likely occurred in the Florida Keys (Pinelli et al., 2018). To reproduce the wind profile of Irma in our model, we used high-resolution H*Wind wind fields (Powell et al., 1998). As these data represent 1-min averaged wind speeds, we multiplied them by a factor 0.93 to obtain 10-min averaged wind speeds (Harper et al., 2010). This operation reduces the erratic values caused by the greater variance of mean winds measured over periods shorter than 10 minutes. Furthermore, H*Wind wind profiles did not cover the whole model extent during the

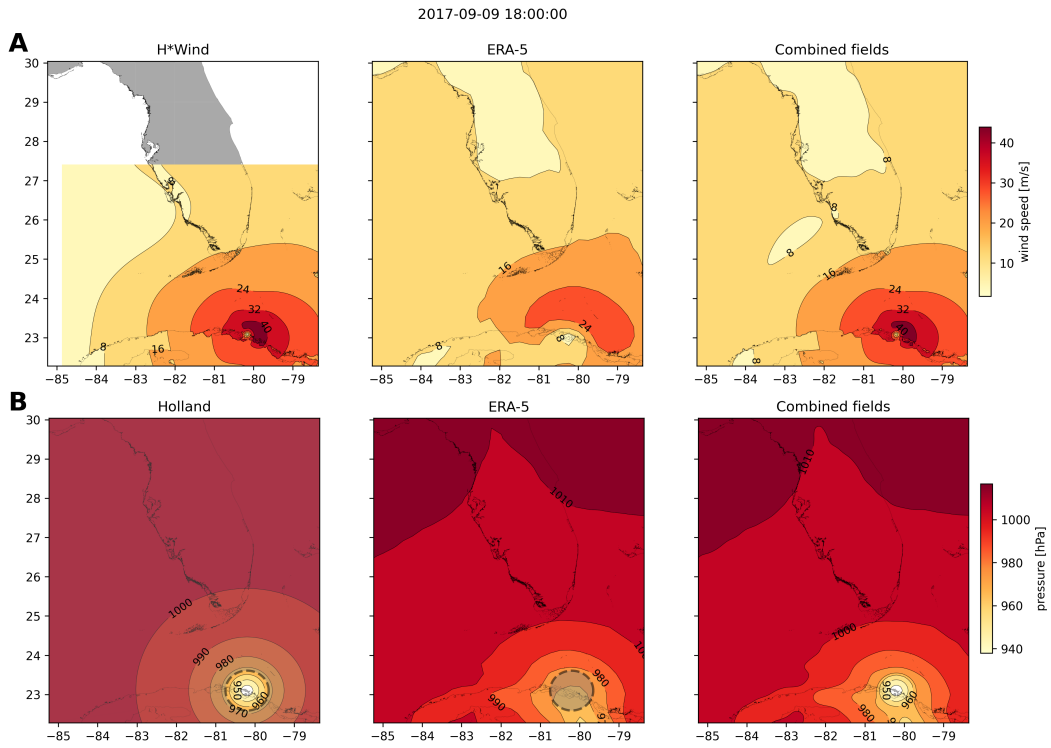


Fig. 5.2: Snapshot of the hybrid wind (**A**) and pressure (**B**) profiles constructed to capture the passage of Hurricane Irma at 1800 UTC on 9 September 2017. Wind profiles were obtained by combining high resolution H*Wind with coarser ERA-5 wind fields. The pressure field was built by combining the ERA-5 pressure field with an idealized Holland pressure profile based on the track of Irma in the HURDAT 2 database. Holland field was only used within the radius of maximum wind speed (dashed grey line) of the hurricane to capture its central depression.

passage of the hurricane and were thus blended within a coarser wind field extracted from the European Centre for Medium-Range Weather Forecasts (ECMWF) ERA-5 dataset (Fig. 5.2A). The pressure field during the passage of Hurricane Irma was also reconstructed using ERA-5 data. However, the coarse resolution of the dataset smoothes out the depression at the center of the hurricane, leading to an underestimation of the pressure gradient (Fig. 5.2B). To better capture the central depression of Irma, we therefore built a hybrid pressure field using the position and the minimal pressure of the core of the hurricane based on its track, as recorded in the HURricane DATabases (HURDAT) 2 (Landsea and Franklin, 2013). Based on this information, the hybrid pressure field was constructed by combining an idealized Holland pressure profile (Lin and Chavas, 2012) within the radius of maximum wind speed of Irma (Knaff et al., 2018) with ERA-5 pressure field. The transition from the Holland profile to ERA-5 data outside the radius of maximum wind speed data was performed using a smooth step function (Fig. 5.2).

5.2.3 Hydrodynamic model

Ocean currents generated during Hurricane Irma around South Florida were modeled using the 2D barotropic version of the unstructured-mesh Second-generation Louvain-la-neuve Ice-ocean Model¹ (SLIM) (Lambrechts et al., 2008). The model mesh covers an area similar to the model extent of Dobbelaere et al. (2020), that includes the FRT but also the Florida Straits and part of the Gulf of Mexico (Figure 5.1). However, this area has been slightly extended northeastward and westward in order to include the NOAA-NDBC buoys. Furthermore, to withstand potential cell drying during the hurricane, we solved the conservative shallow water equations with wetting-drying:

$$\begin{aligned} \frac{\partial H}{\partial t} + \nabla \cdot (\mathbf{U}) &= 0 , \\ \frac{\partial \mathbf{U}}{\partial t} + \nabla \cdot \left(\frac{\mathbf{U}\mathbf{U}}{H} \right) + f\mathbf{e}_z \times \mathbf{U} &= \alpha g H \nabla(H - h) - \frac{1}{\rho} \nabla p_{\text{atm}} + \frac{1}{\rho} \boldsymbol{\tau}_s \\ &\quad + \nabla \cdot (\nu \nabla \mathbf{U}) - \frac{C_b}{H^2} |\mathbf{U}| \mathbf{U} + \gamma (\mathbf{U}_{\text{ref}} - \mathbf{U}) , \end{aligned} \quad (5.1)$$

where H is the water column height and \mathbf{U} is the depth-averaged transport; f is the Coriolis coefficient; g is the gravitational acceleration; h is the bathymetry; α is a coefficient indicating whether the mesh element is wet ($\alpha = 1$) or dry ($\alpha = 0$) (Le et al., 2020); ν is the Smagorinsky viscosity; C_b is the bulk bottom drag coefficient; p_{atm} is the atmospheric pressure; $\boldsymbol{\tau}_s$ is the surface stress, usually due to wind; and γ is a relaxation coefficient towards a reference transport \mathbf{U}_{ref} . As this study focuses on transport processes and not coastal flooding, wetting-drying is only applied on wet grid cells that may become dry under the influence of the hurricane. As in Frys et al. (2020b) and Dobbelaere et al. (2020), SLIM currents were gradually relaxed towards the operational Navy HYbrid Coordinate Ocean Model (HYCOM) product (GOMI0.04², Chassignet et al. (2007)) in regions where the water depth exceeds 50 m. HYCOM's 3D currents were depth-integrated into 2D transports to be used as forcing in the model. Moreover, these transports as well as HYCOM's sea surface elevation were used as boundary condition in the model.

We adapted the parameterization of the wind-induced surface stress to storm conditions. At very high wind speeds, the white cap is blown off the crest of the waves. This phenomenon, also known as spume, has been hypothesized to generate a layer of droplets that acts as a slip layer for the winds at the ocean-atmosphere interface (Holthuijsen et al., 2012). It causes a saturation of the wind drag coefficient for strong winds (Powell et al., 2003; Donelan et al., 2004; Curcic and Haus, 2020). We take this saturation effect into account by using the wind drag parameterization of Moon et al. (2007). In this parameterization, the drag

¹<https://www.slim-ocean.be>

²<https://www.hycom.org/data/gom10pt04>

coefficient C_d depends on the wind speed at 10-m height U_{10} according to:

$$C_d = \kappa^2 \log \left(\frac{10}{z_0} \right)^{-2} \quad (5.2)$$

where κ is the von Karman constant and z_0 is the roughness length expressed as:

$$z_0 = \begin{cases} \frac{0.0185}{g} u_*^2 & \text{if } U_{10} \leq 12.5 \text{ m/s ,} \\ [0.085(-0.56u_*^2 + 20.255u_*) + 2.458] \times 10^{-3} & \text{if } U_{10} > 12.5 \text{ m/s ,} \end{cases} \quad (5.3)$$

with u_* the friction velocity. The relation between U_{10} and u_* is given by:

$$U_{10} = -0.56u_*^2 + 20.255u_* + 2.458 . \quad (5.4)$$

The mesh resolution depends on the distance to the coastlines and reefs following the approach of Dobbelaere et al. (2020). The mesh is then further refined according to bathymetry value and gradient, as suggested in the SWAN user-guide³. Such an approach improves the model efficiency as the mesh resolution is only increased where required by the currents and waves dynamics. The mesh was generated with the seamsh⁴ Python library, which is based on the open-source mesh generator GMSH (Geuzaine and Remacle, 2009). It is composed of approximately 7.7×10^5 elements. The coarsest elements, far away from the FRT, have a characteristic length of about 5 km whereas the finest elements have a characteristic length of about 100 m along the coastlines and over the reefs (Fig 5.1).

5.2.4 Wave model

Waves were modeled using the parallel unstructured-mesh version of the Simulating WAves Nearshore (SWAN) model (Booij et al., 1999), one of the most popular wave models for coastal areas and inland waters. It solves the action balance equation (Mei, 1989):

$$\frac{\partial N}{\partial t} + \nabla_x \cdot [(c_g + \mathbf{u})N] + \frac{\partial}{\partial \theta}[c_\theta N] + \frac{\partial}{\partial \sigma}[c_\sigma N] = \frac{S_{in} + S_{ds} + S_{nl}}{\sigma} , \quad (5.5)$$

where $N = E/\sigma$ is the wave action density and E is the wave energy spectrum; θ is the wave propagation direction; σ is the intrinsic wave frequency; c_g is the wave group velocity, $\mathbf{u} = \mathbf{U}/H$ is SLIM depth-averaged current velocity; c_θ and c_σ are the propagation velocities in spectral space due to refraction and shifting in frequency due to variations in depth and currents; and S_{in} , S_{ds} , and S_{nl} respectively represent wave growth by wind, wave decay and nonlinear transfers of wave energy through four and three-wave interactions, *i.e.* quadruplets and triplets. The wave

³<http://swanmodel.sourceforge.net/unswan/unswan.htm>

⁴<https://pypi.org/project/seamsh/>

spectra were discretized with 48 direction bins and 50 frequency bins logarithmically distributed from 0.03 to 2 Hz. Exponential wind growth was parameterized using the formulation of Janssen (1991), while dissipations by whitecapping and bottom dissipation followed the formulations of Komen et al. (1984) and Madsen et al. (1989), respectively.

Coefficients for exponential wind growth and whitecapping parameterizations were based on the results of Siadatmousavi et al. (2011), and significantly differ from SWAN's default settings. By default, SWAN implements the wind input formulation of Komen et al. (1984) and the steepness-dependent coefficient governing dissipation by whitecapping is a linear function of the wavenumber. In this study, this steepness-dependent coefficient is a quadratic function of the wavenumber, as it showed better predictions of the significant wave height in the study of Siadatmousavi et al. (2011). The choice of these formulations was motivated by the appearance of numerical instabilities in the region of the Gulf Stream when using SWAN's default parameter values. Finally, ERA-5 wave spectra was used as boundary condition for SWAN. Wave spectra is obtained from the ocean wave model WAM and is given on a $1^\circ \times 1^\circ$ grid with 24 directions and 36 frequencies.

Surface waves induce a net drift in the direction of the wave propagation, known as the Stokes drift (Van Den Bremer and Breivik, 2018; Stokes, 1880). This net drift has a significant impact on sediment transport in nearshore regions (Hoefel and Elgar, 2003), on the formation of Langmuir cells (Langmuir, 1938; Craik and Leibovich, 1976) as well as on the transport of heat, salt or pollutants such as oil or micro-plastic in the upper ocean layer (McWilliams and Sullivan, 2000; Röhrs et al., 2012; Drivedal et al., 2014). To correctly model the Stokes drift profile in mixed wind-driven sea and swell conditions, the full two-dimensional wave spectrum must be represented by a spectral wave model within a wave-current coupling (Van Den Bremer and Breivik, 2018). We therefore used SWAN modeled spectra to compute the Stokes drift as follows:

$$\mathbf{u}_s = \int_0^{2\pi} \int_0^{+\infty} \frac{\sigma^3}{h \tanh(2kh)} E(\sigma, \theta) (\cos \theta, \sin \theta) d\sigma d\theta , \quad (5.6)$$

where k is the norm of the wave vector; h is the water depth; and $E(\sigma, \theta)$ is the wave energy density. The computed Stokes drift velocity is then added to SLIM depth-averaged current velocity to transport drifting particles in the experiments described in section 5.2.6.

5.2.5 Coupled model

SLIM and SWAN are coupled so that they run on the same computational core and the same unstructured mesh. SLIM is run first and passes the wind velocity (\mathbf{U}_{10}), water level ($\eta = H - h$) and depth-averaged current ($\mathbf{u} = \mathbf{U}/H$) fields to SWAN, as well as a roughness length (z_0) for the bottom dissipation formulation of Madsen et al. (1989). This roughness length is computed from SLIM's bulk drag coefficient C_b following the approach of Dietrich et al. (2011) so that both

models have consistent bottom dissipation parameterizations. SWAN then uses these quantities to compute the wave radiation stress gradient, that is then passed to SLIM as the force exerted by waves on currents τ_{wave} (Fig. 5.3). SLIM then uses this quantity to update the value of the surface stress τ_s in Eq. (5.1), that now becomes the sum of wind and wave-induced stresses $\tau_s = \tau_{\text{wind}} + \tau_{\text{wave}}$. Here, the momentum flux from the atmosphere to the ocean is taken as the usual full wind stress τ_{wind} . Doing so, we neglect the momentum advected away from the storm by the waves, leading to a 10-15% overestimation of the momentum flux in hurricane winds (Curcic, 2015).

We followed the approach of Dietrich et al. (2012) by characterizing the wave-induced forces on currents using the radiation-stress (RS) gradient formalism, which has been successfully applied in both 2D and 3D coupled wave-current models under storm conditions (Hope et al., 2013; Sebastian et al., 2014; Brown et al., 2013). An alternative formalism is the vortex-force (VF) representation (McWilliams et al., 2004), that provides a clearer decomposition of the wave effect (Lane et al., 2007). Although both approaches were adopted by coastal modeling communities, there is an ongoing scientific debate over the correctness and applicability of the two concepts (Ardhuin et al., 2008; Mellor, 2013, 2015; Arduin et al., 2017). Xia et al. (2020) recently implemented the two formalisms in a 3D unstructured-grid model and compared them in three typical coastal systems, showing that the 3D RS algorithm could generate unrealistic offshore currents near shorelines. Despite these shortcomings, the 3D RS method reproduced most wave-induced currents and the 2D RS formalism remains a well-validated modeling approach. Furthermore, Mellor (2013) showed that the RS approach was valid when $[\frac{\partial H}{\partial x} / \sinh(kh)]^2$ is smaller or of the same order as $(ka)^2$, where a is the wave amplitude. We evaluated these quantities and verified that the validity criterion was met in our model domain. Additionally, since the VF and RS approaches are formally equivalent (Lane et al., 2007), we selected the 2D RS formalism, as it has the advantage of summarizing the impact of waves on the currents in a single additional stress term in the hydrodynamic model equations.

SLIM's governing equations are integrated using an implicit time integration scheme while SWAN is unconditionally stable (Dietrich et al., 2012), allowing both models to be run with relatively large time steps. In this study, the stationary version of SWAN was used, i.e. the first term of Eq. (5.5) was set to zero. This resulted in reduced scaling and convergence rates than with the nonstationary version of SWAN but increased the model stability. The wave spectra at each node of the mesh was saved at the end of each iteration to serve as initial conditions for the next one. Both models were run sequentially using a time step of 600 s, so that each computational core was alternatively running either SLIM or SWAN. As in the coupling between SWAN and the Advanced CIRCulation model (ADCIRC) (Dietrich et al., 2012), both models use the same local sub-mesh, allowing for a one-to-one correspondence between the geographic locations of the mesh vertices. No interpolation is therefore needed when passing the discretised variables from one model to the other, which allows an efficient inter-model communication.

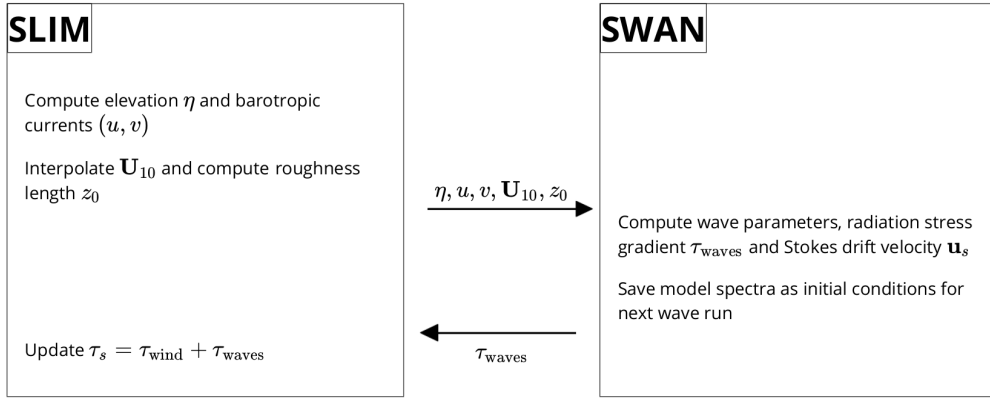


Fig. 5.3: Schematic illustration of the coupled SLIM+SWAN model.

However, as SLIM is based on a discontinuous Galerkin finite element method, an additional conversion step to a continuous framework was required to transfer SLIM nodal quantities to SWAN. The coupling increases the computation time by 3% as compared to the sum of the uncoupled SLIM and SWAN simulations wall-clock times for the same number of CPUs and the same simulation period.

5.2.6 Quantifying the effect of wave-current interactions on transport

To quantify the impact of wave-current interactions on transport processes, we compared the trajectories of passive particles advected by the uncoupled SLIM and coupled SLIM+SWAN currents during the passage of Irma in the Lower Keys. Furthermore, the depth-averaged Stokes drift was computed using the wave spectra of the coupled model SLIM+SWAN run as well as those of an uncoupled SWAN run. Particles were released on the inner and outer shelves at the points highlighted by red and blue dots in Fig. 5.4 on Sept. 7 at 0000 UTC and then tracked until Sept. 15. These initial particle positions were found using backtracking methods (Spivakovskaya et al., 2005) to ensure that the release particles would intersect the path of Irma during its passage through the Florida Keys. We first defined two 25 km^2 circular regions on the trajectory of the hurricane (see red and blue circles in Fig. 5.4). Particles within these two regions were then tracked backward in time using uncoupled SLIM currents from the exact time of the passage of the hurricane until Sept. 7 at 0000 UTC. Their positions at the end of the backward simulation (see red and blue particle clouds in Fig. 5.4) corresponds to the initial condition of the forward transport simulations described below. We then compared the trajectories of particles originating from these regions and advected forward in time by different sets of currents: (i) uncoupled SLIM currents alone; (ii) coupled SLIM+SWAN currents; (iii) SLIM currents with the addition of the depth-averaged Stokes drift computed with the coupled wave-current model (Stokes-C); (iv) SLIM+SWAN currents with Stokes-C; and (v) SLIM currents with the depth-

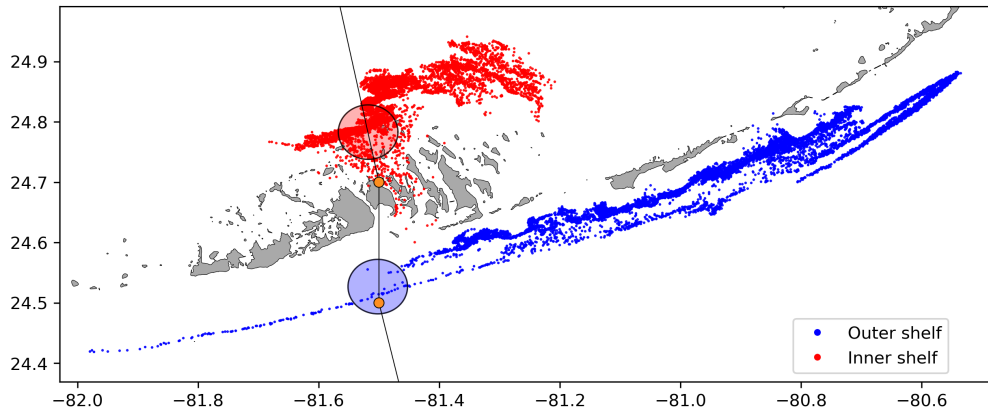


Fig. 5.4: Release regions of the passive particles on the inner and outer shelves on Sept 7 at 0000 UTC (red and blue clouds) obtained by backtracking particles released in the red and blue circular areas during the passage of Irma.

Experiment name	Eulerian currents from	Stokes drift from
SLIM	uncoupled SLIM simulation	None
SLIM+SWAN	coupled SLIM+SWAN simulation (impacted by RS gradient)	None
SLIM+Stokes-U	uncoupled SLIM simulation	uncoupled SWAN simulation
SLIM+Stokes-C	uncoupled SLIM simulation	coupled SLIM+SWAN simulation
SLIM+SWAN+Stokes-C	coupled SLIM+SWAN simulation (impacted by RS gradient)	coupled SLIM+SWAN simulation

Table 5.1: Summary of the different combinations of Eulerian currents and Stokes drifts used to model the transport of passive drifters on the passage of Hurricane Irma in the Lower Keys

averaged Stokes drift computed with the uncoupled wave model (Stokes-U). The different combinations of Eulerian currents and Stokes drifts used to model the transport of passive drifters in the Lower Keys during the passage of Irma are summarized in Table 5.1. Particle trajectories are compared by computing the distances between the centers of mass of the particle clouds through time.

5.3 Results

We first validated the reconstructed atmospheric fields of Hurricane Irma as well as the outputs of our coupled wave-current model against field measurements. We then used the validated model outputs to simulate the transport of passive particles in the Lower Keys during the passage of Hurricane Irma. These particles were advected by the sets of currents described in Table 5.1 and their trajectories were compared to evaluate the impact of the wave-current interactions and the Stokes drift on the transport processes during the passage of Irma.

5.3.1 Model validation

H*Wind winds and hybrid pressure field agree well with station measurements at Vaca Key station (Fig. 5.5). The hybrid pressure field shows a better agreement with observations than ERA-5 pressure as it successfully reproduces the storm depression. ERA-5 fields, on the other hand, fail to reproduce the low pressure at the core of the hurricane due to their coarser grid, leading to an overestimation of 8 mbar of the storm depression. Both H*Wind and ERA-5 agree well with observed wind speeds although both data sets tend to slightly overestimate the width and intensity of the wind peak. However, H*Wind profiles better reproduce the timing of the observed peak, as ERA-5 winds tend to anticipate it. H*wind also exhibits a slightly narrower peak in wind speed, which better agrees with observations.

Hydrodynamic outputs of the coupled wave-current model agree well with tide gauge (Fig. 5.6) and ADCP measurements (Fig. 5.7). The coupled model reproduces well the timing of the positive and negative storm surges at all tide gauge locations. The amplitude of the positive surges are especially well captured at Naples and Vaca Key, with errors of 2 and 6 centimeters respectively. However, the model underestimates the positive surges at Virginia Key and Key West by 24% and 15% at the peak respectively. The amplitude of the negative surge at Naples is also underestimated by about 16% at the peak. Nonetheless, on average, the absolute error between the model and observations does not exceed 10 cm (Table 5.2). Modeled 2D currents were validated against depth-averaged ADCP measurements at mooring stations C10, C12 and C13 (Fig. 5.7). As in Liu et al. (2020), we performed the vector correlation analysis of Kundu (1976) to compare modeled and observed current velocity vectors. Correlation coefficients (ρ) between simulated and observed depth-averaged currents are 0.87, 0.84 and 0.81 at stations C10, C12 and C13, respectively. The average veering angles are below 12°, as in (Liu et al., 2020). Furthermore, the positive bias in Table 5.2 indicates that our model tends to underestimate the southward component of the currents at the different stations. As expected from a depth-averaged model, the best fit with observations is obtained at the shallowest mooring C10, located on the 25 m isobath.

The simulated significant wave height agrees well with observations at all buoy locations (Fig. 5.8). The timing of the peak in wave height is well captured at all buoys, while the amplitude is better reproduced on the WFS (buoys 42036

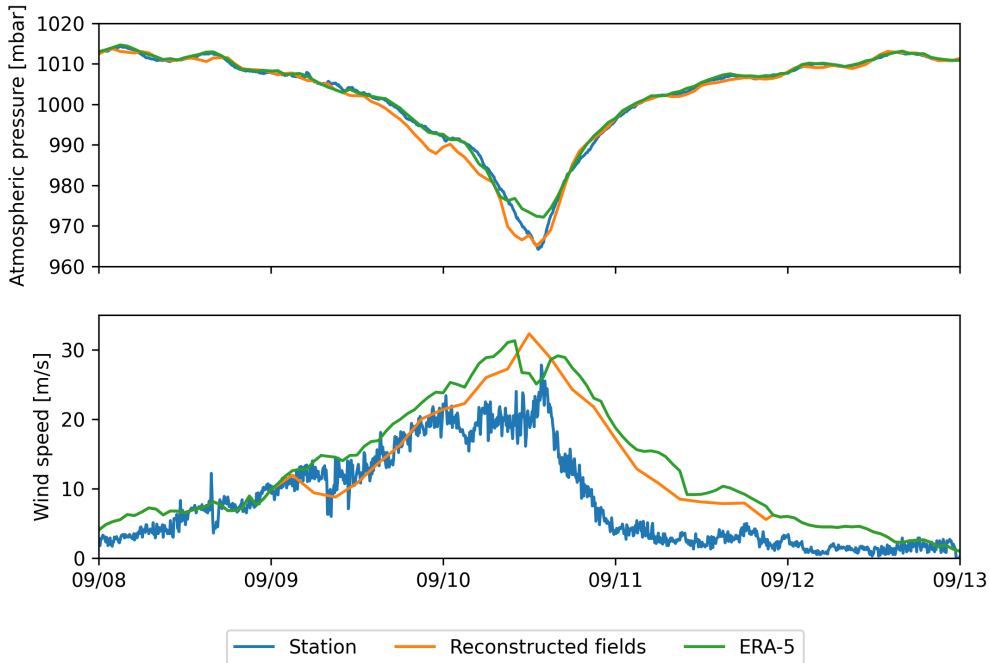


Fig. 5.5: Comparison of reconstructed atmospheric pressure (top) and wind speed (bottom)

with field measurements and coarser ECMWF ERA-5 profiles at Vaca Key station. The generated hybrid atmospheric forcings better reproduce the observed storm depression while H*wind winds better reproduce the measured peak in wind speed.

and 42097) with errors below 10%. The error on the peak amplitude on Florida's eastern shelf is of 13% and 21% at buoys 4114 and 4113, respectively. On average, observed significant wave height and wave period are better reproduced on the WFS while wave direction is better captured by the model on Florida's eastern shelf (Table 5.2). The fit is especially good at buoy 41113, where the mostly westward-northwestward wave propagation is less perturbed by Irma's wind field.

5.3.2 Impact of waves on currents and transport

We evaluated the impact of the RS gradient on the modeled currents during the passage of Irma in the Lower Keys, between Sept. 7 and 13, 2017. First, we computed the maximum difference between currents modeled by SLIM and SLIM+SWAN during this period (Fig. 5.9A). The largest differences in current speed were observed over the reefs, on the shelf break and around islands. They locally reach 1 m/s, with the coupled SLIM+SWAN model yielding the largest amplitudes. The regions where the differences were the largest correspond to areas that experienced large maximum values of the RS gradient τ_{wave} (Fig. 5.9B). These areas of large RS gradient are located on the shelf break and over coral reefs, where important wave energy dissipation occurred through depth-induced

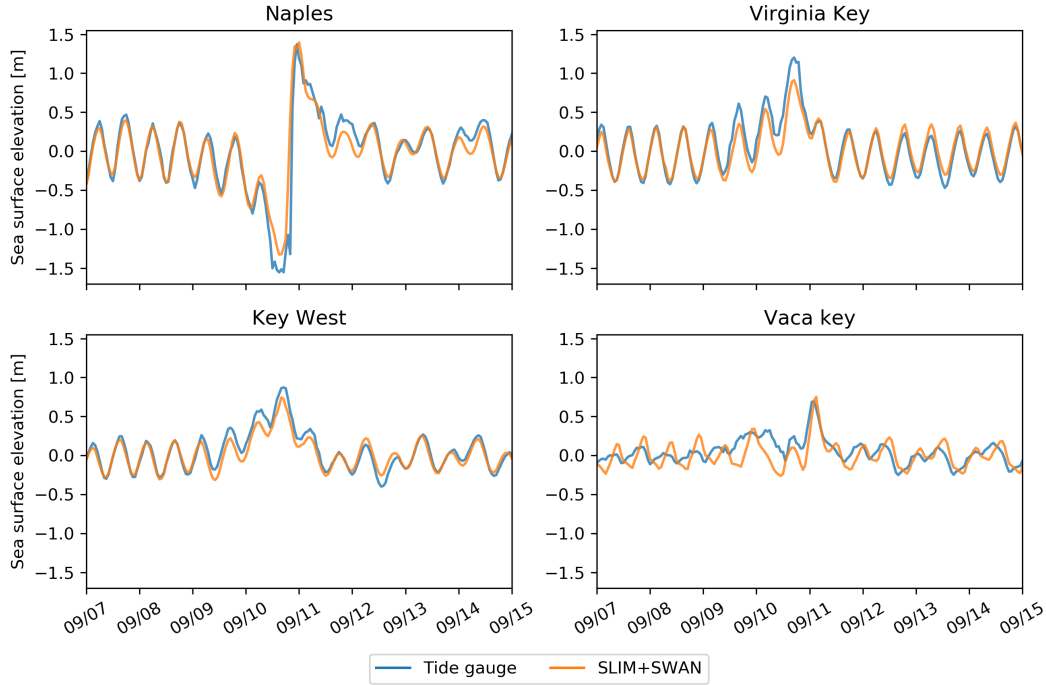


Fig. 5.6: Comparison of modeled sea surface elevation at the 4 tide gauges shown in Fig. 5.1B. The timing and amplitude of the storm surges are well reproduced by the model

wave breaking and bottom dissipation (Longuet-Higgins and Stewart, 1964). This highlights the important protective role of the barrier formed by the offshore reefs, that require a fine spatial resolution to be accurately represented by the model. RS-induced differences in current speed were amplified by the action of the wind stress τ_{wind} (Fig. 5.9C). Wind speeds were larger in the front right quadrant of the hurricane (Zedler et al., 2009), yielding larger differences on the right-hand side of the storm trajectory. This is especially clear in the area between the Florida Keys and the Everglades, where relatively small values of τ_{wave} produce current speed differences larger than 0.5 m/s because of the wind stress.

Our results suggest that the RS gradient alone can deflect particle trajectories by up to 1 km on the inner shelf and 5 km on the outer shelf (Fig. 5.10A,B). The RS mainly affects transport processes during the passage of the hurricane, as the distance between particle cloud advected by SLIM and SLIM+SWAN currents remains roughly constant afterwards. The Stokes drift, however, has a longer-lasting effect on the particle trajectories on the outer shelf. When adding a Stokes drift component to the Eulerian currents, the distances between the particle cloud centers keeps increasing during 2 days after the passage of Irma (Fig. 5.10B). Under the effect of the Stokes drift, particles from the outer shelf can be moved inshore on the passage of the hurricane. This motion is less pronounced for particles that are advected by Eulerian currents only. The particle cloud thus moves quickly northeastward under the action of the FC. After 2 days, the particles advected

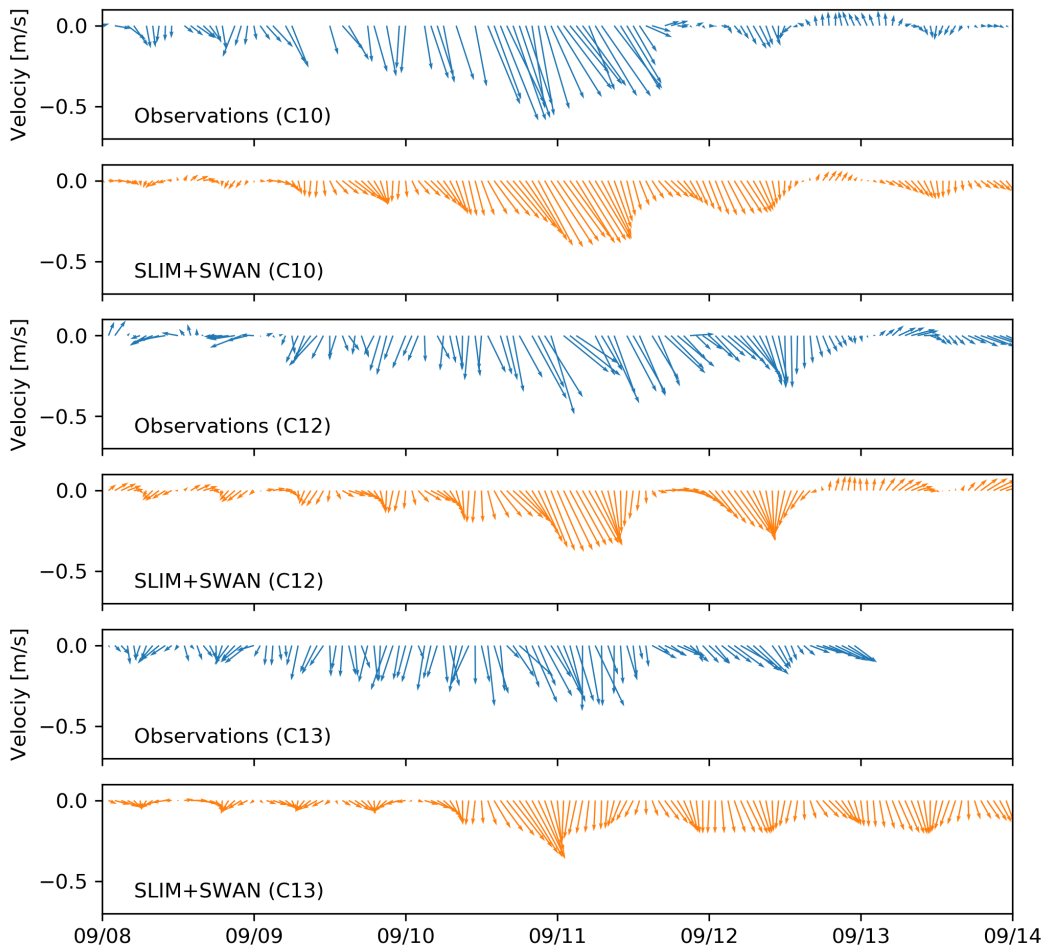


Fig. 5.7: Comparison of modeled current velocity with observed velocity at the moorings (see Fig. 5.1B for their location). Modeled current velocities agree well with observations, with a correlation coefficient of 0.87, 0.83 and 0.81 at moorings C10, C12 and C13, respectively. The corresponding veering angles are 5.4° , 0.07° and 10.5° , respectively.

inshore under the action of the Stokes drift are in turn entrained by the FC and the distance between the clouds of particles starts decreasing. The impact of the Stokes drift on particle motion appears to be five times larger than the one of the RS on the inner shelf (Fig. 5.10A). However, both processes yield a similar impact on the particle trajectories at the moment of the passage of Hurricane Irma on the outer shelf (Fig. 5.10B).

Taking wave-currents interactions into account appears to significantly impact the modeled Stokes drift (Fig. 5.10C,D). Our results suggest that neglecting the wave-current coupling when computing the Stokes drift in storm conditions can yield deflections of the particle trajectories by up to 5 km on both the inner and outer shelves. On the outer shelf, differences in particle trajectories mostly appear during the two days following the passage of the hurricane. This is explained by the stronger shoreward component of the coupled SLIM+SWAN Stokes drift

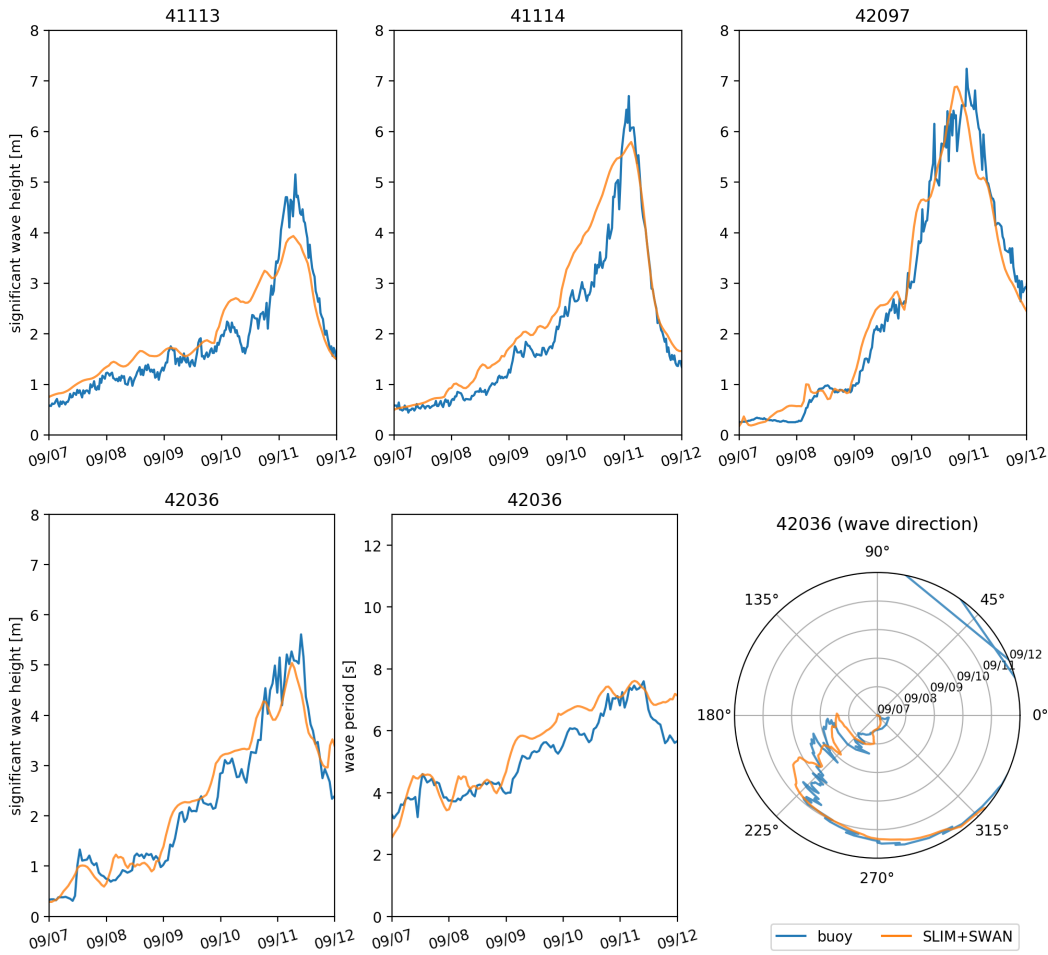


Fig. 5.8: Comparison of modeled wave parameters with observation at the 4 buoys location (locations shown in Fig. 5.1B). Overall, the modeled significant wave heights agree well with field measurement (mean error < 25%).

compared to the uncoupled one. On the inner shelf, however, differences in particle trajectories of up to 5 km occur at the moment of the passage of Hurricane Irma. The distance between the particle clouds then stabilizes directly after the passage of the hurricane.

5.4 Discussion

The coupled SLIM+SWAN model correctly reproduced the hydrodynamics and wave dynamics during Hurricane Irma. Such good agreement with field measurements could only be achieved using accurate forcings and adequate wave parameterizations. By comparing coupled and uncoupled model runs, we showed that neglecting wave radiation stress gradient can induce differences of up to 1 m/s in modeled current velocities. The radiation stress gradient during the hurricane was especially large over the shelf break, where waves are strongly dissipated by the

Station	Variable	Bias	MAE	RMSE
Vaca Key	sse (m)	0	0.112	0.142
	U_{10} (m/s)	1.51	1.85	2.61
	p_{atm} (hPa)	-0.21	0.59	1.03
Key West	sse (m)	0	0.066	0.085
Virginia Key	sse (m)	0	0.087	0.120
Naples	sse (m)	0	0.099	0.180
C10	u (m/s)	0.002	0.045	0.056
	v (m/s)	0.039	0.102	0.121
C12	u (m/s)	0.002	0.059	0.074
	v (m/s)	0.047	0.073	0.094
C13	u (m/s)	-0.009	0.065	0.077
	v (m/s)	0.039	0.086	0.102
41113	H_s (m)	0.150	0.357	0.430
	T_m (s)	1.608	1.671	1.878
	θ_m (degree)	-1.555	7.036	9.250
41114	H_s (m)	0.361	0.424	0.560
	T_m (s)	0.899	1.506	1.594
	θ_m (degree)	-8.236	14.616	22.560
42036	H_s (m)	0.082	0.312	0.398
	T_m (s)	0.430	0.528	0.645
	θ_m (degree)	-2.307	17.144	22.734
42097	H_s (m)	0.048	0.326	0.432
	T_m (s)	0.476	0.755	0.892
	θ_m (degree)	2.538	34.760	55.892

Table 5.2: Error statistics on the wave-current model outputs as compared to the measured sea surface elevation (sse), eastward and northward depth-average current velocities (u, v), significant wave height (H_s), zero-crossing mean wave period (T_m) and mean wave direction (θ_m). Model bias, mean absolute error (MAE), and root mean squared error (RMSE) are listed by variable (unit) and value.

offshore coral reef barrier. The radiation stress gradient alone can deflect drifting particles by up to 5 km during the passage of the hurricane. The impact of the Stokes drift dominates the effects of the radiation stress gradient on transport processes, except during the passage of the hurricane, when both contributions are similar on the outer shelf. The Stokes drift induces a shoreward transport during the passage of the hurricane that moves particles towards the inner shelf, and hence away from the FC. Finally, neglecting wave-current interactions when computing Stokes drift leads to variations of up to 5 km in modeled trajectories on the passage of the hurricane.

The coupled wave-current model correctly reproduced the timing of the observed storm surges and captured the elevation peaks with a 15% accuracy at every tide gauge except Virginia Key. Such accuracy is key to predict the damages

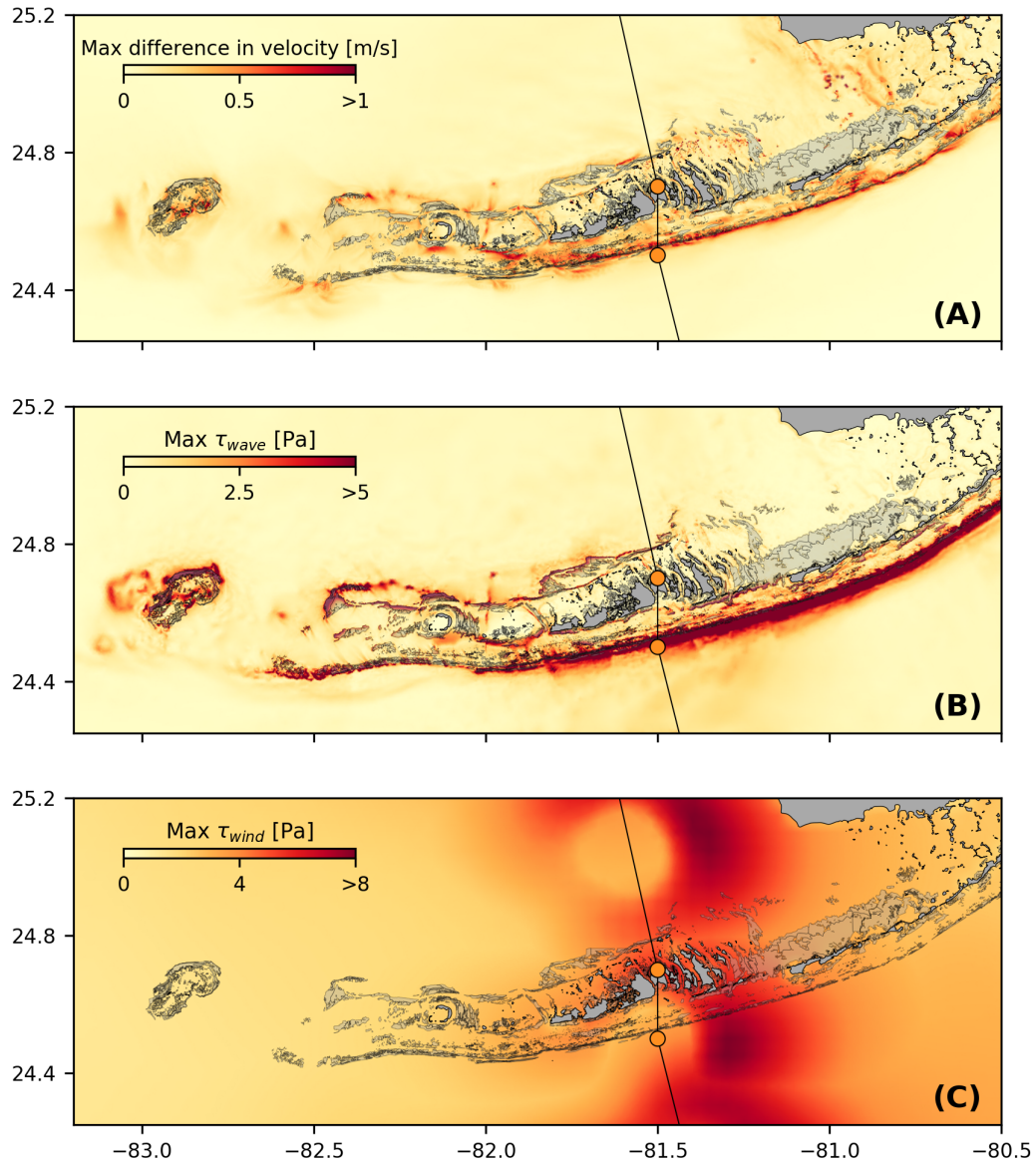


Fig. 5.9: (A). Maximum difference between SLIM and SLIM+SWAN currents during the passage of Irma in the Lower Florida Keys; (B) Maximum wave radiation stress gradient τ_{wave} and (C) maximum wind stress τ_{wind} (C) generated by the hurricane. Radiation stress gradient yields currents speed differences reaching 1 m/s, especially over offshore reefs.

caused by the hurricane, as they were mostly due to the storm surge and high waves (Xian et al., 2018). Furthermore, by using a high-resolution model, we can explicitly reproduce the circulation between all the reefs and islands of the Florida Keys. The fine-scale details of the storm surge, and hence the associated risk, are thus accurately represented. In addition to accurately capturing positive surges, the model also reproduced the observed negative surge in Naples. This result is of interest from a biological point of view as negative surges, although less studied,

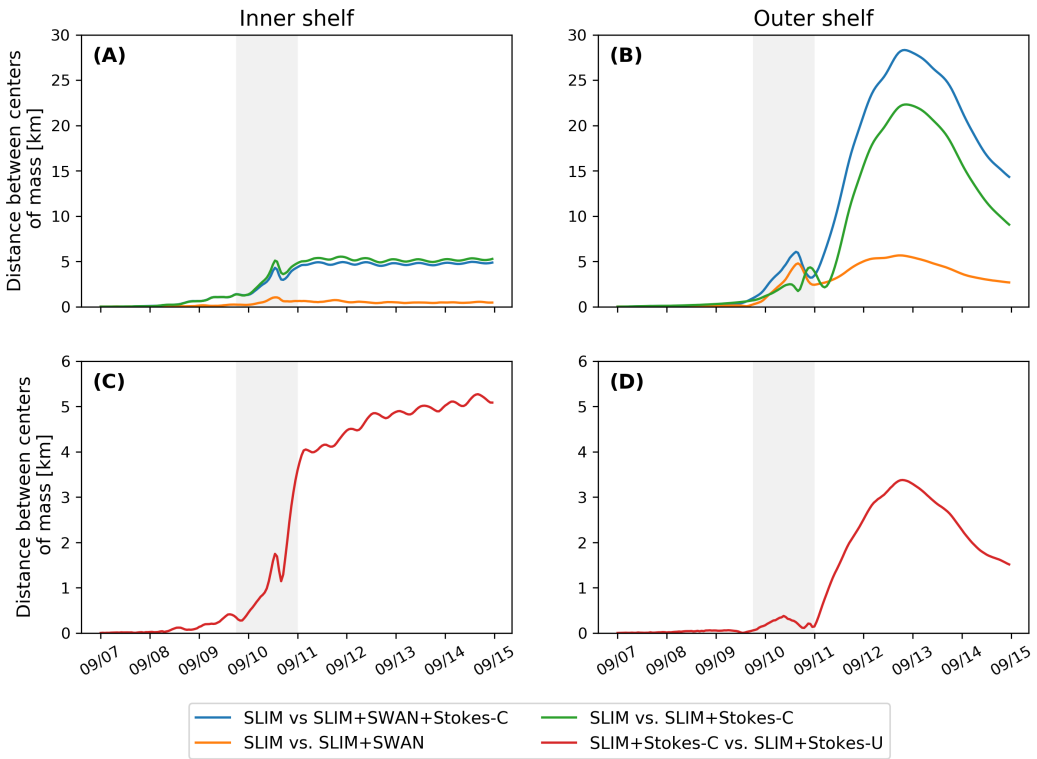


Fig. 5.10: Difference between the centers of mass of the particle clouds released from the regions highlighted in Fig. 5.4 and advected by the different combinations of Eulerian currents and Stokes drifts described in Table 5.1

affect water exchanges between the estuaries and the coastal ocean and disturb the benthic ecosystems (Liu et al., 2020). Such rapid decrease in water level followed by a positive surge cause massive freshwater inflows, causing a significant decrease in water salinity (Wachnicka et al., 2019). Surface waters are also significantly impacted by storms and hurricanes through induced cooling, upwelling and mixing (Varlas et al., 2020), but these processes were not accounted for in our model.

Strong currents such as the Gulf Stream affect waves through refraction over gradients in current velocity, shoaling and breaking of opposing waves or lengthening of following waves (Hegermiller et al., 2019). Under hurricane conditions, these interactions can cause numerical instabilities in the wave model if the parameterizations are not appropriate and the model resolution not sufficient. Hegermiller et al. (2019), for instance, used a 5-km model grid and 48 directional bins to capture spatial gradients in wave height induced by wave-currents interactions in the Gulf Stream during Hurricane Matthew (2016). We followed these guidelines when defining the coarsest mesh resolution as the wave model spectral discretization. Boundary conditions and directional spreading of the incident waves also play a significant role when modeling wave-current interactions at meso- and submesoscales (Villas Bôas et al., 2020), which motivated our choice of imposing full spectra on the boundary of the wave model instead of bulk parameters.

Tropical cyclones interact with the Gulf Stream and the FC through cooling and mixing of the upper ocean. These interactions can momentarily disrupt these currents and cause a significant reduction of their transport (Oey et al., 2007; Ezer et al., 2017; Ezer, 2020). As a 2D barotropic model, SLIM does not explicitly capture the vertical structure of the FC and Gulf Stream. Furthermore, a coupling with an atmospheric model would be required to represent heat fluxes between the upper ocean and the hurricane. However, we argue that a 2D model is sufficient for the scope of this study, that focuses on nearshore processes on the shelf and the shelf slope. Furthermore, by coupling the model with HYCOM, SLIM is able to represent indirectly the baroclinic features such as the meandering of the FC and eddy formation (Frys et al., 2020b). Furthermore, using a 2D model allows us to capture the impact of wave-current interactions on transport processes at the reef scale in the topologically complex coastal system of the FRT. Such a fine resolution is key to estimate the amount of wave energy dissipated over offshore reefs and accurately capture the generated RS gradient.

The RS gradient significantly impacts currents during the passage of the hurricane. It can induce differences of up to 1 m/s in the current speed on the shelf break. In this region, waves are strongly dissipated due to action of depth-induced breaking and bottom dissipation on coral reefs. This link between wave breaking, RS gradient and wave-induced nearshore currents is consistent with previous studies on wave-current dynamics during storms (Mao and Xia, 2017, 2018, 2020). Furthermore, our results highlight the protective role of coral reefs against strong incoming waves (Lowe et al., 2005), which requires a sufficiently fine spatial resolution to be explicitly represented in the model. As wave energy mostly dissipates on the shelf break, the impact of the RS gradient on transport processes is 5 times larger on the outer shelf. In the sheltered area of the inner shelf, wave impact on transport processes is dominated by the Stokes drift. Trajectory deflection under the influence of wave-induced motions mostly occurs at the moment of the passage of the hurricane on the inner shelf. After that moment, the distance between the clouds of particles remained roughly constant through time. On the outer shelf, RS and Stokes drift have a similar impact on transport processes at the moment of the passage of the cyclone and deflect particle trajectories by up to 5 km. However, by inducing shoreward transport, the Stokes drift delayed the advection of particles by the FC, therefore causing differences in trajectories of up to 20 km during the days following the passage of the hurricane. The dominance of the Stokes drift on particle transport in storm conditions was also observed in Lake Michigan by Mao and Xia (2020). Finally, neglecting wave-current coupling in Stokes drift computation leads to differences in modeled trajectories of the order of 5 km on both the inner and the outer shelves. This fact, coupled with the impact of RS-induced currents strongly advocates for the use of coupled wave-current models when studying transport processes in storm conditions.

5.5 Conclusion

We developed a coupled wave-current model to study the impact of waves on transport processes during Hurricane Irma. In order to accurately represent the wind and pressure profiles of the hurricane, we built hybrid fields by combining coarser ERA-5 data with high-resolution H*Wind data for the wind speed and idealized Holland profiles for the pressure. Comparing these hybrid profiles with field observations showed that they were better at reproducing the observed central depression of the hurricane as well as the peak in wind speed than ERA-5 data. Using these hybrid fields as forcings, our coupled model accurately reproduced the storm surge at tide gauge locations and produced currents and wave parameters in good agreement with field observations. The modeled currents and Stokes drift were then used to evaluate the impact of wave-current coupling on the modeled trajectories of passive drifters on the passage of the hurricane through the Florida Keys. Our results show that waves had a significant impact on heavy-wind transport processes and caused deflections of the drifters trajectories by more than 20 km on the outer shelf.

Despite its good agreement with observations, our model could be further refined by improving the representation of wind-wave interactions. In particular, we did not consider the momentum loss due to the action of surface waves, which can lead to overestimations of the momentum flux from the atmosphere to the ocean under hurricane conditions. Our model could therefore be further improved by using a wave-dissipative stress instead of the full wind stress as the momentum flux from the atmosphere to the ocean. As a 2D barotropic model, SLIM does not explicitly represent heat fluxes between the ocean and the atmosphere and the vertical structure of the ocean. However, our study focused on relatively shallow and vertically homogeneous coastal waters using a reef-scale resolution throughout the whole FRT. Such fine resolution allows to explicitly represent wave dissipation over coral reefs and is only achievable using a 2D model due to computational resource limitations.

Wave coupling needs to be taken into account during heavy-wind events but not necessarily in milder conditions. While the RS gradient plays an important role and can lead to differences of up to 5 km, the Stokes drift is about 4 times more intense and is thus the most important wave-induced transport process. Nonetheless, neglecting wave-current coupling through RS when modeling Stokes drift leads to differences of up to 5 km in predicted drifter trajectories. Such discrepancies reveal the strong influence of wave-current interactions on transport under storm conditions. This study brings new insight on the impact of waves on the transport processes nearshore during a tropical cyclone. Due to its fine spatial resolution, our coupled wave-current model can be used to accurately represent the dispersal of pollutants, sediments or larvae in topologically complex coastal areas in heavy-wind conditions.

Conclusions and perspectives

Lorem ipsum dolor sit amet, consectetuer adipiscing elit. Ut purus elit, vestibulum ut, placerat ac, adipiscing vitae, felis. Curabitur dictum gravida mauris. Nam arcu libero, nonummy eget, consectetuer id, vulputate a, magna. Donec vehicula augue eu neque. Pellentesque habitant morbi tristique senectus et netus et malesuada fames ac turpis egestas. Mauris ut leo. Cras viverra metus rhoncus sem. Nulla et lectus vestibulum urna fringilla ultrices. Phasellus eu tellus sit amet tortor gravida placerat. Integer sapien est, iaculis in, pretium quis, viverra ac, nunc. Praesent eget sem vel leo ultrices bibendum. Aenean faucibus. Morbi dolor nulla, malesuada eu, pulvinar at, mollis ac, nulla. Curabitur auctor semper nulla. Donec varius orci eget risus. Duis nibh mi, congue eu, accumsan eleifend, sagittis quis, diam. Duis eget orci sit amet orci dignissim rutrum.

Nam dui ligula, fringilla a, euismod sodales, sollicitudin vel, wisi. Morbi auctor lorem non justo. Nam lacus libero, pretium at, lobortis vitae, ultricies et, tellus. Donec aliquet, tortor sed accumsan bibendum, erat ligula aliquet magna, vitae ornare odio metus a mi. Morbi ac orci et nisl hendrerit mollis. Suspendisse ut massa. Cras nec ante. Pellentesque a nulla. Cum sociis natoque penatibus et magnis dis parturient montes, nascetur ridiculus mus. Aliquam tincidunt urna. Nulla ullamcorper vestibulum turpis. Pellentesque cursus luctus mauris.

Nulla malesuada porttitor diam. Donec felis erat, congue non, volutpat at, tincidunt tristique, libero. Vivamus viverra fermentum felis. Donec nonummy pellentesque ante. Phasellus adipiscing semper elit. Proin fermentum massa ac quam. Sed diam turpis, molestie vitae, placerat a, molestie nec, leo. Maecenas lacinia. Nam ipsum ligula, eleifend at, accumsan nec, suscipit a, ipsum. Morbi blandit ligula feugiat magna. Nunc eleifend consequat lorem. Sed lacinia nulla vitae enim. Pellentesque tincidunt purus vel magna. Integer non enim. Praesent euismod nunc eu purus. Donec bibendum quam in tellus. Nullam cursus pulvinar

lectus. Donec et mi. Nam vulputate metus eu enim. Vestibulum pellentesque felis eu massa.

Quisque ullamcorper placerat ipsum. Cras nibh. Morbi vel justo vitae lacus tincidunt ultrices. Lorem ipsum dolor sit amet, consectetur adipiscing elit. In hac habitasse platea dictumst. Integer tempus convallis augue. Etiam facilisis. Nunc elementum fermentum wisi. Aenean placerat. Ut imperdiet, enim sed gravida sollicitudin, felis odio placerat quam, ac pulvinar elit purus eget enim. Nunc vitae tortor. Proin tempus nibh sit amet nisl. Vivamus quis tortor vitae risus porta vehicula.

Fusce mauris. Vestibulum luctus nibh at lectus. Sed bibendum, nulla a faucibus semper, leo velit ultricies tellus, ac venenatis arcu wisi vel nisl. Vestibulum diam. Aliquam pellentesque, augue quis sagittis posuere, turpis lacus congue quam, in hendrerit risus eros eget felis. Maecenas eget erat in sapien mattis porttitor. Vestibulum porttitor. Nulla facilisi. Sed a turpis eu lacus commodo facilisis. Morbi fringilla, wisi in dignissim interdum, justo lectus sagittis dui, et vehicula libero dui cursus dui. Mauris tempor ligula sed lacus. Duis cursus enim ut augue. Cras ac magna. Cras nulla. Nulla egestas. Curabitur a leo. Quisque egestas wisi eget nunc. Nam feugiat lacus vel est. Curabitur consectetur.

Suspendisse vel felis. Ut lorem lorem, interdum eu, tincidunt sit amet, laoreet vitae, arcu. Aenean faucibus pede eu ante. Praesent enim elit, rutrum at, molestie non, nonummy vel, nisl. Ut lectus eros, malesuada sit amet, fermentum eu, sodales cursus, magna. Donec eu purus. Quisque vehicula, urna sed ultricies auctor, pede lorem egestas dui, et convallis elit erat sed nulla. Donec luctus. Curabitur et nunc. Aliquam dolor odio, commodo pretium, ultricies non, pharetra in, velit. Integer arcu est, nonummy in, fermentum faucibus, egestas vel, odio.

Sed commodo posuere pede. Mauris ut est. Ut quis purus. Sed ac odio. Sed vehicula hendrerit sem. Duis non odio. Morbi ut dui. Sed accumsan risus eget odio. In hac habitasse platea dictumst. Pellentesque non elit. Fusce sed justo eu urna porta tincidunt. Mauris felis odio, sollicitudin sed, volutpat a, ornare ac, erat. Morbi quis dolor. Donec pellentesque, erat ac sagittis semper, nunc dui lobortis purus, quis congue purus metus ultricies tellus. Proin et quam. Class aptent taciti sociosqu ad litora torquent per conubia nostra, per inceptos hymenaeos. Praesent sapien turpis, fermentum vel, eleifend faucibus, vehicula eu, lacus.

Pellentesque habitant morbi tristique senectus et netus et malesuada fames ac turpis egestas. Donec odio elit, dictum in, hendrerit sit amet, egestas sed, leo. Praesent feugiat sapien aliquet odio. Integer vitae justo. Aliquam vestibulum fringilla lorem. Sed neque lectus, consectetur at, consectetur sed, eleifend ac, lectus. Nulla facilisi. Pellentesque eget lectus. Proin eu metus. Sed porttitor. In hac habitasse platea dictumst. Suspendisse eu lectus. Ut mi mi, lacinia sit amet, placerat et, mollis vitae, dui. Sed ante tellus, tristique ut, iaculis eu, malesuada ac, dui. Mauris nibh leo, facilisis non, adipiscing quis, ultrices a, dui.

Morbi luctus, wisi viverra faucibus pretium, nibh est placerat odio, nec commodo wisi enim eget quam. Quisque libero justo, consectetur a, feugiat vitae, porttitor eu, libero. Suspendisse sed mauris vitae elit sollicitudin malesuada. Mae-

cenas ultricies eros sit amet ante. Ut venenatis velit. Maecenas sed mi eget dui varius euismod. Phasellus aliquet volutpat odio. Vestibulum ante ipsum primis in faucibus orci luctus et ultrices posuere cubilia Curae; Pellentesque sit amet pede ac sem eleifend consectetur. Nullam elementum, urna vel imperdierit sodales, elit ipsum pharetra ligula, ac pretium ante justo a nulla. Curabitur tristique arcu eu metus. Vestibulum lectus. Proin mauris. Proin eu nunc eu urna hendrerit faucibus. Aliquam auctor, pede consequat laoreet varius, eros tellus scelerisque quam, pellentesque hendrerit ipsum dolor sed augue. Nulla nec lacus.

Suspendisse vitae elit. Aliquam arcu neque, ornare in, ullamcorper quis, commodo eu, libero. Fusce sagittis erat at erat tristique mollis. Maecenas sapien libero, molestie et, lobortis in, sodales eget, dui. Morbi ultrices rutrum lorem. Nam elementum ullamcorper leo. Morbi dui. Aliquam sagittis. Nunc placerat. Pellentesque tristique sodales est. Maecenas imperdierit lacinia velit. Cras non urna. Morbi eros pede, suscipit ac, varius vel, egestas non, eros. Praesent malesuada, diam id pretium elementum, eros sem dictum tortor, vel consectetur odio sem sed wisi.

Sed feugiat. Cum sociis natoque penatibus et magnis dis parturient montes, nascetur ridiculus mus. Ut pellentesque augue sed urna. Vestibulum diam eros, fringilla et, consectetur eu, nonummy id, sapien. Nullam at lectus. In sagittis ultrices mauris. Curabitur malesuada erat sit amet massa. Fusce blandit. Aliquam erat volutpat. Aliquam euismod. Aenean vel lectus. Nunc imperdierit justo nec dolor.

Etiam euismod. Fusce facilisis lacinia dui. Suspendisse potenti. In mi erat, cursus id, nonummy sed, ullamcorper eget, sapien. Praesent pretium, magna in eleifend egestas, pede pede pretium lorem, quis consectetur tortor sapien facilisis magna. Mauris quis magna varius nulla scelerisque imperdierit. Aliquam non quam. Aliquam porttitor quam a lacus. Praesent vel arcu ut tortor cursus volutpat. In vitae pede quis diam bibendum placerat. Fusce elementum convallis neque. Sed dolor orci, scelerisque ac, dapibus nec, ultricies ut, mi. Duis nec dui quis leo sagittis commodo.

Bibliography

- Abdolali, A., Roland, A., Van Der Westhuysen, A., Meixner, J., Chawla, A., Hesser, T.J., Smith, J.M., Sikiric, M.D., 2020. Large-scale hurricane modeling using domain decomposition parallelization and implicit scheme implemented in WAVEWATCH III wave model. *Coastal Engineering* 157, 103656.
- Aeby, G., Ushijima, B., Campbell, J.E., Jones, S., Williams, G., Meyer, J.L., Hase, C., Paul, V., 2019. Pathogenesis of a tissue loss disease affecting multiple species of corals along the Florida Reef Tract. *Frontiers in Marine Science* 6, 678.
- Aijaz, S., Ghantous, M., Babanin, A., Ginis, I., Thomas, B., Wake, G., 2017. Nonbreaking wave-induced mixing in upper ocean during tropical cyclones using coupled hurricane-ocean-wave modeling. *Journal of Geophysical Research: Oceans* 122, 3939–3963.
- Alvarez-Filip, L., Estrada-Saldívar, N., Pérez-Cervantes, E., Molina-Hernández, A., González-Barrios, F.J., 2019. A rapid spread of the stony coral tissue loss disease outbreak in the Mexican Caribbean. *PeerJ* 7, e8069.
- Ardhuin, F., Jenkins, A.D., Belibassakis, K.A., 2008. Comments on “The three-dimensional current and surface wave equations”. *Journal of Physical Oceanography* 38, 1340–1350.
- Ardhuin, F., Marié, L., Rascle, N., Forget, P., Roland, A., 2009. Observation and estimation of Lagrangian, Stokes, and Eulerian currents induced by wind and waves at the sea surface. *Journal of Physical Oceanography* 39, 2820–2838.
- Ardhuin, F., Suzuki, N., McWilliams, J.C., Aiki, H., 2017. Comments on “A combined derivation of the integrated and vertically resolved, coupled wave-current equations”. *Journal of Physical Oceanography* 47, 2377–2385.
- Aronson, R.B., Precht, W.F., 2001. White-band disease and the changing face of Caribbean coral reefs, in: *The ecology and etiology of newly emerging marine diseases*. Springer, pp. 25–38.
- Aronson, R.B., Precht, W.F., 2006. Conservation, precaution, and Caribbean reefs. *Coral reefs* 25, 441–450.

- Ault, J.S., Smith, S.G., Bohnsack, J.A., Luo, J., Harper, D.E., McClellan, D.B., 2006. Building sustainable fisheries in Florida's coral reef ecosystem: Positive signs in the Dry Tortugas. *Bulletin of Marine Science* 78, 633–654.
- Ault, J.S., Smith, S.G., Bohnsack, J.A., Luo, J., Zurcher, N., McClellan, D.B., Ziegler, T.A., Hallac, D.E., Patterson, M., Feeley, M.W., et al., 2013. Assessing coral reef fish population and community changes in response to marine reserves in the Dry Tortugas, Florida, USA. *Fisheries Research* 144, 28–37.
- Barnes, B.B., Hu, C., Kovach, C., Silverstein, R.N., 2015. Sediment plumes induced by the Port of Miami dredging: Analysis and interpretation using Landsat and MODIS data. *Remote Sensing of Environment* 170, 328–339.
- Bever, A.J., MacWilliams, M.L., 2013. Simulating sediment transport processes in San Pablo Bay using coupled hydrodynamic, wave, and sediment transport models. *Marine Geology* 345, 235–253.
- Bhatia, K.T., Vecchi, G.A., Knutson, T.R., Murakami, H., Kossin, J., Dixon, K.W., Whitlock, C.E., 2019. Recent increases in tropical cyclone intensification rates. *Nature Communications* 10, 1–9.
- Bidegain, G., Powell, E., Klinck, J., Ben-Horin, T., Hofmann, E., 2016a. Microparasitic disease dynamics in benthic suspension feeders: infective dose, non-focal hosts, and particle diffusion. *Ecological Modelling* 328, 44–61.
- Bidegain, G., Powell, E.N., Klinck, J.M., Ben-Horin, T., Hofmann, E.E., 2016b. Marine infectious disease dynamics and outbreak thresholds: contact transmission, pandemic infection, and the potential role of filter feeders. *Ecosphere* 7, e01286.
- Blondeau, J., Brandt, M., Donovan, C., Eakin, M., Edwards, K., Edwards, K., Edwards, P., Enochs, I., Feeley, M., Fleming, C., et al., 2020. Coral reef condition: A status report for the US Virgin Islands .
- Booij, N., Ris, R.C., Holthuijsen, L.H., 1999. A third-generation wave model for coastal regions: 1. Model description and validation. *Journal of Geophysical Research: Oceans* 104, 7649–7666.
- Brandt, M.E., McManus, J.W., 2009. Dynamics and impact of the coral disease white plague: insights from a simulation model. *Diseases of aquatic organisms* 87, 117–133.
- Breivik, Ø., Allen, A.A., Maisondieu, C., Olagnon, M., 2013. Advances in search and rescue at sea. *Ocean Dynamics* 63, 83–88.
- Brown, J.M., Bolaños, R., Wolf, J., 2013. The depth-varying response of coastal circulation and water levels to 2D radiation stress when applied in a coupled wave–tide–surge modelling system during an extreme storm. *Coastal Engineering* 82, 102–113.

- Burgess, S.C., Kingsford, M.J., Black, K.P., 2007. Influence of tidal eddies and wind on the distribution of presettlement fishes around One Tree Island, Great Barrier Reef. *Marine Ecology Progress Series* 341, 233–242.
- Cangialosi, J.P., Latto, A.S., Berg, R., 2018. National Hurricane Center Tropical Cyclone Report: Hurricane Irma (30 August–12 September 2017). https://www.nhc.noaa.gov/data/tcr/AL112017_Irma.pdf.
- Chassignet, E.P., Hurlburt, H.E., Smedstad, O.M., Halliwell, G.R., Hogan, P.J., Wallcraft, A.J., Baraille, R., Bleck, R., 2007. The HYCOM (hybrid coordinate ocean model) data assimilative system. *Journal of Marine Systems* 65, 60–83.
- Craik, A.D., Leibovich, S., 1976. A rational model for Langmuir circulations. *Journal of Fluid Mechanics* 73, 401–426.
- Csardi, G., Nepusz, T., et al., 2006. The igraph software package for complex network research. *InterJournal, complex systems* 1695, 1–9.
- Cunning, R., Silverstein, R.N., Barnes, B.B., Baker, A.C., 2019. Extensive coral mortality and critical habitat loss following dredging and their association with remotely-sensed sediment plumes. *Marine pollution bulletin* 145, 185–199.
- Curcic, M., 2015. Explicit air-sea momentum exchange in coupled atmosphere-wave-ocean modeling of tropical cyclones. Ph.D. thesis. University of Miami.
- Curcic, M., Chen, S.S., Özgökmen, T.M., 2016. Hurricane-induced ocean waves and stokes drift and their impacts on surface transport and dispersion in the Gulf of Mexico. *Geophysical Research Letters* 43, 2773–2781.
- Curcic, M., Haus, B.K., 2020. Revised estimates of ocean surface drag in strong winds. *Geophysical Research Letters* 47, e2020GL087647.
- Dietrich, J., Bunya, S., Westerink, J., Ebersole, B., Smith, J., Atkinson, J., Jensen, R., Resio, D., Luettich, R., Dawson, C., et al., 2010. A high-resolution coupled riverine flow, tide, wind, wind wave, and storm surge model for southern Louisiana and Mississippi. Part II: Synoptic description and analysis of Hurricanes Katrina and Rita. *Monthly Weather Review* 138, 378–404.
- Dietrich, J., Westerink, J., Kennedy, A., Smith, J., Jensen, R., Zijlema, M., Holthuijsen, L., Dawson, C., Luettich, R., Powell, M., et al., 2011. Hurricane Gustav (2008) waves and storm surge: Hindcast, synoptic analysis, and validation in southern Louisiana. *Monthly Weather Review* 139, 2488–2522.
- Dietrich, J.C., Tanaka, S., Westerink, J.J., Dawson, C., Luettich, R., Zijlema, M., Holthuijsen, L.H., Smith, J., Westerink, L., Westerink, H., 2012. Performance of the unstructured-mesh, SWAN+ ADCIRC model in computing hurricane waves and surge. *Journal of Scientific Computing* 52, 468–497.

- Dobbelaere, T., Holstein, D.M., Muller, E.M., Gramer, L.J., McEachron, L., Williams, S.D., Hanert, E., 2022. Connecting the dots: Transmission of stony coral tissue loss disease from the Marquesas to the Dry Tortugas. *Frontiers in Marine Science* URL: <https://www.frontiersin.org/article/10.3389/fmars.2022.778938>, doi:10.3389/fmars.2022.778938.
- Dobbelaere, T., Muller, E.M., Gramer, L.J., Holstein, D.M., Hanert, E., 2020. Coupled epidemi-hydrodynamic modeling to understand the spread of a deadly coral disease in Florida. *Frontiers in Marine Science* 7, 1016.
- Domeier, M.L., 2004. A potential larval recruitment pathway originating from a Florida marine protected area. *Fisheries Oceanography* 13, 287–294.
- Donelan, M., Haus, B., Reul, N., Plant, W., Stiassnie, M., Gruber, H., Brown, O., Saltzman, E., 2004. On the limiting aerodynamic roughness of the ocean in very strong winds. *Geophysical Research Letters* 31.
- Drivdal, M., Broström, G., Christensen, K., 2014. Wave-induced mixing and transport of buoyant particles: Application to the Statfjord A oil spill. *Ocean Science* 10, 977–991.
- Dustan, P., Halas, J.C., 1987. Changes in the reef-coral community of Carysfort Reef, Key Largo, Florida: 1974 to 1982. *Coral Reefs* 6, 91–106.
- Eaton, K.R., Landsberg, J.H., Kiryu, Y., Peters, E.C., Muller, E.M., 2021. Measuring stony coral tissue loss disease induction and lesion progression within two intermediately susceptible species, Montastraea cavernosa and Orbicella faveolata. *Frontiers in Marine Science* , 1287.
- Erftemeijer, P.L., Riegl, B., Hoeksema, B.W., Todd, P.A., 2012. Environmental impacts of dredging and other sediment disturbances on corals: a review. *Marine pollution bulletin* 64, 1737–1765.
- Estrada-Saldívar, N., Molina-Hernández, A., Pérez-Cervantes, E., Medellín-Maldonado, F., González-Barrios, F.J., Alvarez-Filip, L., 2020. Reef-scale impacts of the stony coral tissue loss disease outbreak. *Coral Reefs* 39, 861–866.
- Estrada-Saldívar, N., Quiroga-García, B.A., Pérez-Cervantes, E., Rivera-Garibay, O.O., Alvarez-Filip, L., 2021. Effects of the stony coral tissue loss disease outbreak on coral communities and the benthic composition of cozumel reefs. *Frontiers in Marine Science* 8, 306.
- Ezer, T., 2018. On the interaction between a hurricane, the Gulf Stream and coastal sea level. *Ocean Dynamics* 68, 1259–1272.
- Ezer, T., 2020. The long-term and far-reaching impact of hurricane dorian (2019) on the gulf stream and the coast. *Journal of Marine Systems* 208, 103370.

- Ezer, T., Atkinson, L.P., Tuleya, R., 2017. Observations and operational model simulations reveal the impact of Hurricane Matthew (2016) on the Gulf Stream and coastal sea level. *Dynamics of Atmospheres and Oceans* 80, 124–138.
- Figueiredo, J., Baird, A.H., Connolly, S.R., 2013. Synthesizing larval competence dynamics and reef-scale retention reveals a high potential for self-recruitment in corals. *Ecology* 94, 650–659.
- Fourney, F., Figueiredo, J., 2017. Additive negative effects of anthropogenic sedimentation and warming on the survival of coral recruits. *Scientific reports* 7, 1–8.
- Fratantoni, P.S., Lee, T.N., Podesta, G.P., Muller-Karger, F., 1998. The influence of Loop Current perturbations on the formation and evolution of Tortugas eddies in the southern Straits of Florida. *Journal of Geophysical Research: Oceans* 103, 24759–24779.
- Fringer, O.B., Dawson, C.N., He, R., Ralston, D.K., Zhang, Y.J., 2019. The future of coastal and estuarine modeling: Findings from a workshop. *Ocean Modelling* 143, 101458.
- FRRP, 2018. Florida Reef Resilience Program Disturbance Response Monitoring Quick Look Report: Summer 2018. URL: <https://ocean.floridamarine.org/FRRP/TrainingDocs/2018%20DRM%20Summer%20Quick%20Look%20Report.pdf>. Accessed on August 24, 2021.
- FRRP, 2019. Florida Reef Resilience Program Disturbance Response Monitoring Quick Look Report: Summer 2019. URL: <https://ocean.floridamarine.org/FRRP/TrainingDocs/2019%20Summer%20DRM%20Quick%20Look%20Report.pdf>. Accessed on August 24, 2021.
- FRRP, 2020. Florida Reef Resilience Program Disturbance Response Monitoring Quick Look Report: Summer 2020. URL: <https://ocean.floridamarine.org/FRRP/TrainingDocs/2020%20DRM%20Summer%20Quick%20Look%20Report.pdf>. Accessed on August 24, 2021.
- Frys, C., Saint-Amand, A., Le Hénaff, M., Figueiredo, J., Kuba, A., Walker, B., Lambrechts, J., Vallaeyns, V., Vincent, D., Hanert, E., 2020a. Fine-scale coral connectivity pathways in the Florida Reef Tract: Implications for conservation and restoration. *Frontiers in Marine Science* 7, 312.
- Frys, C., Saint-Amand, A., Le Hénaff, M., Figueiredo, J., Kuba, A., Walker, B., Lambrechts, J., Vallaeyns, V., Vincent, D., Hanert, E., 2020b. Fine-scale coral connectivity pathways in the Florida Reef Tract: Implications for conservation and restoration. *Frontiers in Marine Science* 7, 312.
- FWC-FWRI, 2017. Unified Reef Map v2. 0. FWC-FWRI (Florida Fish and Wildlife Conservation Commission-Fish and Wildlife Research Institute).

- Gardner, T.A., Côté, I.M., Gill, J.A., Grant, A., Watkinson, A.R., 2003. Long-term region-wide declines in Caribbean corals. *Science* 301, 958–960.
- Geuzaine, C., Remacle, J.F., 2009. Gmsh: A 3-d finite element mesh generator with built-in pre-and post-processing facilities. *International journal for numerical methods in engineering* 79, 1309–1331.
- Gintert, B.E., Precht, W.F., Fura, R., Rogers, K., Rice, M., Precht, L.L., D'Alessandro, M., Croop, J., Vilmar, C., Robbart, M.L., 2019. Regional coral disease outbreak overwhelms impacts from a local dredge project. *Environmental monitoring and assessment* 191, 1–39.
- Gray, J.R., 2000. Comparability of suspended-sediment concentration and total suspended solids data. 4191, US Department of the interior, US Geological Survey.
- Hamilton, E.L., Bachman, R.T., 1982. Sound velocity and related properties of marine sediments. *The Journal of the Acoustical Society of America* 72, 1891–1904.
- Harper, B., Kepert, J., Ginger, J., 2010. Guidelines for converting between various wind averaging periods in tropical cyclone conditions.
- Harvell, D., Jordán-Dahlgren, E., Merkel, S., Rosenberg, E., Raymundo, L., Smith, G., Weil, E., Willis, B., 2007. Coral disease, environmental drivers, and the balance between coral and microbial associates. *Oceanography* 20, 172–195.
- Hegermiller, C.A., Warner, J.C., Olabarrieta, M., Sherwood, C.R., 2019. Wave-current interaction between Hurricane Matthew wave fields and the Gulf Stream. *Journal of Physical Oceanography* 49, 2883–2900.
- Heres, M.M., Farmer, B.H., Elmer, F., Hertler, H., 2021. Ecological consequences of stony coral tissue loss disease in the turks and caicos islands. *Coral Reefs* 40, 609–624.
- Hoefel, F., Elgar, S., 2003. Wave-induced sediment transport and sandbar migration. *Science* 299, 1885–1887.
- Holthuijsen, L.H., Powell, M.D., Pietrzak, J.D., 2012. Wind and waves in extreme hurricanes. *Journal of Geophysical Research: Oceans* 117.
- Hope, M.E., Westerink, J.J., Kennedy, A.B., Kerr, P., Dietrich, J.C., Dawson, C., Bender, C.J., Smith, J., Jensen, R.E., Zijlema, M., et al., 2013. Hindcast and validation of Hurricane ike (2008) waves, forerunner, and storm surge. *Journal of Geophysical Research: Oceans* 118, 4424–4460.
- Janssen, P.A., 1991. Quasi-linear theory of wind-wave generation applied to wave forecasting. *Journal of Physical Oceanography* 21, 1631–1642.

- Johns, W.E., Schott, F., 1987. Meandering and transport variations of the Florida Current. *Journal of Physical Oceanography* 17, 1128–1147.
- Jones, R., Bessell-Browne, P., Fisher, R., Klonowski, W., Slivkoff, M., 2016. Assessing the impacts of sediments from dredging on corals. *Marine Pollution Bulletin* 102, 9–29.
- Jones, R., Ricardo, G., Negri, A., 2015. Effects of sediments on the reproductive cycle of corals. *Marine Pollution Bulletin* 100, 13–33.
- Keeling, M., Rohani, P., 2007. Stochastic dynamics. *Modeling Infectious Diseases in Humans and Animals*, 190–230.
- Kermack, W.O., McKendrick, A.G., 1927. A contribution to the mathematical theory of epidemics. *Proceedings of the Royal Society of London. Series A, Containing papers of a mathematical and physical character* 115, 700–721.
- Knaff, J.A., Sampson, C.R., Musgrave, K.D., 2018. Statistical tropical cyclone wind radii prediction using climatology and persistence: Updates for the western North Pacific. *Weather and Forecasting* 33, 1093–1098.
- Knutson, T., Camargo, S.J., Chan, J.C., Emanuel, K., Ho, C.H., Kossin, J., Mo-hapatra, M., Satoh, M., Sugi, M., Walsh, K., et al., 2020. Tropical cyclones and climate change assessment: Part II: Projected response to anthropogenic warming. *Bulletin of the American Meteorological Society* 101, E303–E322.
- Komen, G., Hasselmann, S., Hasselmann, K., 1984. On the existence of a fully developed wind-sea spectrum. *Journal of Physical Oceanography* 14, 1271–1285.
- Koopman, B., Heaney, J.P., Cakir, F.Y., Rembold, M., Indeglia, P., Kini, G., 2006. Ocean outfall study. Florida Department of Environmental Protection, Tallahassee .
- Kourafalou, V.H., Androulidakis, Y., Kang, H., Smith, R., Valle-Levinson, A., 2018. Physical connectivity between Pulley Ridge and Dry Tortugas coral reefs under the influence of the Loop Current/Florida Current system. *Progress in oceanography* 165, 75–99.
- Kourafalou, V.H., Kang, H., 2012. Florida current meandering and evolution of cyclonic eddies along the Florida Keys Reef Tract: Are they interconnected? *Journal of Geophysical Research: Oceans* 117.
- Kramer, P., Roth, L., Lang, J., 2019. Map of stony coral tissue loss disease outbreak in the Caribbean. URL: www.agrra.org. ArcGis Online. (accessed June 12, 2020).
- Kuffner, I.B., Lidz, B.H., Hudson, J.H., Anderson, J.S., 2015. A century of ocean warming on Florida Keys coral reefs: historic in situ observations. *Estuaries and Coasts* 38, 1085–1096.

- Kundu, P.K., 1976. Ekman veering observed near the ocean bottom. *Journal of Physical Oceanography* 6, 238–242.
- Kuta, K., Richardson, L., 1996. Abundance and distribution of black band disease on coral reefs in the northern Florida Keys. *Coral reefs* 15, 219–223.
- Lambrechts, J., Hanert, E., Deleersnijder, E., Bernard, P.E., Legat, V., Remacle, J.F., Wolanski, E., 2008. A multi-scale model of the hydrodynamics of the whole Great Barrier Reef. *Estuarine, Coastal and Shelf Science* 79, 143–151.
- Landsberg, J.H., Kiryu, Y., Gray, C., Wilson, P., Perry, N., Waters, Y., 2018. MCAV disease lab analyses update. URL: https://floridadep.gov/sites/default/files/Copy%20of%20FWC-FWRI_MCAV_disease_update_041118.pdf. Consulted on 2020-07-20.
- Landsea, C.W., Franklin, J.L., 2013. Atlantic hurricane database uncertainty and presentation of a new database format. *Monthly Weather Review* 141, 3576–3592.
- Lane, E.M., Restrepo, J., McWilliams, J.C., 2007. Wave–current interaction: A comparison of radiation-stress and vortex-force representations. *Journal of Physical Oceanography* 37, 1122–1141.
- Langmuir, I., 1938. Surface motion of water induced by wind. *Science* 87, 119–123.
- Le, H.A., Lambrechts, J., Ortaleb, S., Gratiot, N., Deleersnijder, E., Soares-Frazão, S., 2020. An implicit wetting–drying algorithm for the discontinuous galerkin method: application to the tonle sap, mekong river basin. *Environmental Fluid Mechanics*, 1–29.
- Le Hénaff, M., Kourafalou, V.H., Paris, C.B., Helgers, J., Aman, Z.M., Hogan, P.J., Srinivasan, A., 2012. Surface evolution of the Deepwater Horizon oil spill patch: Combined effects of circulation and wind-induced drift. *Environmental Science & Technology* 46, 7267–7273.
- Lee, T.N., Clarke, M., Williams, E., Szmant, A.F., Berger, T., 1994. Evolution of the Tortugas Gyre and its influence on recruitment in the Florida Keys. *Bulletin of Marine Science* 54, 621–646.
- Lee, T.N., Leaman, K., Williams, E., Berger, T., Atkinson, L., 1995. Florida Current meanders and gyre formation in the southern Straits of Florida. *Journal of Geophysical Research: Oceans* 100, 8607–8620.
- Lee, T.N., Mayer, D.A., 1977. Low-frequency current variability and spin-off eddies along the shelf off southeast Florida. *Collected Reprints* 1, 344.
- Lee, T.N., Smith, N., 2002. Volume transport variability through the Florida Keys tidal channels. *Continental Shelf Research* 22, 1361–1377.

- Lee, T.N., Williams, E., 1988. Wind-forced transport fluctuations of the Florida Current. *Journal of Physical Oceanography* 18, 937–946.
- Leipper, D.F., 1970. A sequence of current patterns in the Gulf of Mexico. *Journal of Geophysical Research* 75, 637–657.
- Li, Z., Johns, B., 1998. A three-dimensional numerical model of surface waves in the surf zone and longshore current generation over a plane beach. *Estuarine, Coastal and Shelf Science* 47, 395–413.
- Lin, N., Chavas, D., 2012. On hurricane parametric wind and applications in storm surge modeling. *Journal of Geophysical Research: Atmospheres* 117.
- Liu, Y., Weisberg, R.H., 2012. Seasonal variability on the West Florida shelf. *Progress in Oceanography* 104, 80–98.
- Liu, Y., Weisberg, R.H., Lenes, J.M., Zheng, L., Hubbard, K., Walsh, J.J., 2016. Offshore forcing on the "pressure point" of the West Florida Shelf: Anomalous upwelling and its influence on harmful algal blooms. *Journal of Geophysical Research: Oceans* 121, 5501–5515.
- Liu, Y., Weisberg, R.H., Zheng, L., 2020. Impacts of hurricane Irma on the circulation and transport in Florida Bay and the Charlotte Harbor estuary. *Estuaries and Coasts* 43, 1194–1216.
- Liubartseva, S., Coppini, G., Lecci, R., Clementi, E., 2018. Tracking plastics in the Mediterranean: 2D Lagrangian model. *Marine Pollution Bulletin* 129, 151–162.
- Longuet-Higgins, M.S., 1970. Longshore currents generated by obliquely incident sea waves. *Journal of Geophysical Research* 75, 6778–6789.
- Longuet-Higgins, M.S., Stewart, R., 1964. Radiation stresses in water waves; a physical discussion, with applications, in: *Deep Sea Research and Oceanographic Abstracts*, Elsevier. pp. 529–562.
- Lowe, R.J., Falter, J.L., Bandet, M.D., Pawlak, G., Atkinson, M.J., Monismith, S.G., Koseff, J.R., 2005. Spectral wave dissipation over a barrier reef. *Journal of Geophysical Research: Oceans* 110.
- MacDonald, N.J., Davies, M.H., Zundel, A.K., Howlett, J.D., Demirbilek, Z., Gailani, J.Z., Lackey, T.C., Smith, J., 2006. PTM: particle tracking model. Report 1: Model theory, implementation, and example applications. Technical Report. Engineer Research And Development Center Vicksburg MS Coastal And Hydraulics Lab.
- Madsen, O.S., Poon, Y.K., Gruber, H.C., 1989. Spectral wave attenuation by bottom friction: Theory, in: *Coastal Engineering* 1988, pp. 492–504.

- Malmstadt, J., Scheitlin, K., Elsner, J., 2009. Florida hurricanes and damage costs. *Southeastern Geographer* 49, 108–131.
- Manzello, D.P., 2015. Rapid recent warming of coral reefs in the Florida Keys. *Scientific reports* 5, 16762.
- Mao, M., Xia, M., 2017. Dynamics of wave–current–surge interactions in lake michigan: A model comparison. *Ocean Modelling* 110, 1–20.
- Mao, M., Xia, M., 2018. Wave–current dynamics and interactions near the two inlets of a shallow lagoon–inlet–coastal ocean system under hurricane conditions. *Ocean Modelling* 129, 124–144.
- Mao, M., Xia, M., 2020. Particle dynamics in the nearshore of Lake Michigan revealed by an observation-modeling system. *Journal of Geophysical Research: Oceans* 125, e2019JC015765.
- Maul, G.A., 1977. The Annual Cycle of the Gulf Loop Current: Part 1: Observations During a One-year Time Series.
- McWilliams, J.C., Restrepo, J.M., Lane, E.M., 2004. An asymptotic theory for the interaction of waves and currents in coastal waters. *Journal of Fluid Mechanics* 511, 135.
- McWilliams, J.C., Sullivan, P.P., 2000. Vertical mixing by Langmuir circulations. *Spill Science & Technology Bulletin* 6, 225–237.
- Mei, C.C., 1989. The applied dynamics of ocean surface waves. volume 1. World scientific.
- Meiling, S.S., Muller, E.M., Lasseigne, D., Rossin, A., Veglia, A.J., MacKnight, N., Dimos, B., Huntley, N., Correa, A., Smith, T.B., et al., 2021. Variable species responses to experimental stony coral tissue loss disease (SCTLD) exposure. *Frontiers in Marine Science* 8, 464.
- Mellor, G., 2013. Waves, circulation and vertical dependence. *Ocean Dynamics* 63, 447–457.
- Mellor, G., 2015. A combined derivation of the integrated and vertically resolved, coupled wave–current equations. *Journal of Physical Oceanography* 45, 1453–1463.
- Miller, J., Muller, E., Rogers, C., Waara, R., Atkinson, A., Whelan, K., Patterson, M., Witcher, B., 2009. Coral disease following massive bleaching in 2005 causes 60% decline in coral cover on reefs in the US Virgin Islands. *Coral Reefs* 28, 925.
- Miller, M.W., Karazsia, J., Groves, C.E., Griffin, S., Moore, T., Wilber, P., Gregg, K., 2016. Detecting sedimentation impacts to coral reefs resulting from dredging the Port of Miami, Florida USA. *PeerJ* 4, e2711.

- Moon, I.J., Ginis, I., Hara, T., Thomas, B., 2007. A physics-based parameterization of air-sea momentum flux at high wind speeds and its impact on hurricane intensity predictions. *Monthly Weather Review* 135, 2869–2878.
- Muller, E.M., Sartor, C., Alcaraz, N.I., van Woesik, R., 2020. Spatial epidemiology of the Stony-Coral-Tissue-Loss Disease in Florida. *Frontiers in Marine Science* 7, 163.
- Murphy, B.S., 2014. Pykrige: development of a kriging toolkit for Python. AGUFM 2014, H51K-0753.
- Murray, J.D., 2007. Mathematical biology: I. An introduction. volume 17. Springer Science & Business Media.
- Neely, K., 2018. Surveying the Florida Keys southern coral disease boundary. Florida DEP. Miami, FL , 1–15.
- Niu, Q., Xia, M., 2017. The role of wave-current interaction in Lake Erie's seasonal and episodic dynamics. *Journal of Geophysical Research: Oceans* 122, 7291–7311.
- NOAA, 2018. Stony Coral Tissue Loss Disease Case Definition. URL: <https://nmsfloridakeys.blob.core.windows.net/floridakeys-prod/media/docs/20181002-stony-coral-tissue-loss-disease-case-definition.pdf>. Accessed on June 4, 2020.
- Oey, L.Y., Ezer, T., Wang, D.P., Yin, X.Q., Fan, S.J., 2007. Hurricane-induced motions and interaction with ocean currents. *Continental Shelf Research* 27, 1249–1263.
- Perlin, A., Moum, J., Klymak, J., Levine, M., Boyd, T., Kosro, P., 2007. Organization of stratification, turbulence, and veering in bottom Ekman layers. *Journal of Geophysical Research: Oceans* 112.
- Pinelli, J.P., Roueche, D., Kijewski-Correa, T., Plaz, F., Prevatt, D., Zisis, I., Elawady, A., Haan, F., Pei, S., Gurley, K., et al., 2018. Overview of damage observed in regional construction during the passage of Hurricane Irma over the State of Florida, in: *Forensic Engineering 2018: Forging Forensic Frontiers*. American Society of Civil Engineers Reston, VA, pp. 1028–1038.
- Porter, J.W., Meier, O.W., 1992. Quantification of loss and change in floridian reef coral populations. *American Zoologist* 32, 625–640.
- Powell, M.D., Houston, S.H., Amat, L.R., Morisseau-Leroy, N., 1998. The HRD real-time hurricane wind analysis system. *Journal of Wind Engineering and Industrial Aerodynamics* 77, 53–64.
- Powell, M.D., Vickery, P.J., Reinhold, T.A., 2003. Reduced drag coefficient for high wind speeds in tropical cyclones. *Nature* 422, 279–283.

- Precht, W.F., Gintert, B.E., Robbart, M.L., Fura, R., Van Woesik, R., 2016. Unprecedented disease-related coral mortality in Southeastern Florida. *Scientific Reports* 6, 1–11.
- Richardson, L.L., Goldberg, W.M., Carlton, R.G., Halas, J.C., 1998a. Coral disease outbreak in the Florida Keys: plague type II. *Revista de Biología tropical*, 187–198.
- Richardson, L.L., Goldberg, W.M., Kuta, K.G., Aronson, R.B., Smith, G.W., Ritchie, K.B., Halas, J.C., Feingold, J.S., Miller, S.L., 1998b. Florida's mystery coral-killer identified. *Nature* 392, 557–558.
- Röhrs, J., Christensen, K.H., Hole, L.R., Broström, G., Drivdal, M., Sundby, S., 2012. Observation-based evaluation of surface wave effects on currents and trajectory forecasts. *Ocean Dynamics* 62, 1519–1533.
- Rosales, S.M., Clark, A.S., Huebner, L.K., Ruzicka, R.R., Muller, E., 2020. Rhodobacterales and Rhizobiales are associated with stony coral tissue loss disease and its suspected sources of transmission. *Frontiers in Microbiology* 11, 681.
- Ruzicka, R., Colella, M., Porter, J., Morrison, J., Kidney, J., Brinkhuis, V., Lunz, K., Macaulay, K., Bartlett, L., Meyers, M., et al., 2013. Temporal changes in benthic assemblages on Florida Keys reefs 11 years after the 1997/1998 El Niño. *Marine Ecology Progress Series* 489, 125–141.
- Schott, F.A., Lee, T.N., Zantopp, R., 1988. Variability of structure and transport of the Florida Current in the period range of days to seasonal. *Journal of Physical Oceanography* 18, 1209–1230.
- Sebastian, A., Proft, J., Dietrich, J.C., Du, W., Bedient, P.B., Dawson, C.N., 2014. Characterizing hurricane storm surge behavior in Galveston Bay using the swan+ adcirc model. *Coastal Engineering* 88, 171–181.
- Shore, A., Caldwell, J.M., 2019. Modes of coral disease transmission: How do diseases spread between individuals and among populations? *Marine Biology* 166, 45.
- Siadatmousavi, S.M., Jose, F., Stone, G., 2011. Evaluation of two WAM white capping parameterizations using parallel unstructured SWAN with application to the Northern Gulf of Mexico, USA. *Applied Ocean Research* 33, 23–30.
- Sikirić, M.D., Roland, A., Janeković, I., Tomazić, I., Kuzmić, M., 2013. Coupling of the Regional Ocean Modeling System (ROMS) and Wind Wave Model. *Ocean Modelling* 72, 59–73.
- Smith, N.P., 1982. Response of Florida Atlantic shelf waters to hurricane David. *Journal of Geophysical Research: Oceans* 87, 2007–2016.

- Smith, N.P., 2009. The influence of wind forcing on across-shelf transport in the Florida Keys. *Continental Shelf Research* 29, 362–370.
- Sokolow, S.H., Foley, P., Foley, J.E., Hastings, A., Richardson, L.L., 2009. Editor's choice: Disease dynamics in marine metapopulations: modelling infectious diseases on coral reefs. *Journal of Applied Ecology* 46, 621–631.
- Soulsby, R., Whitehouse, R., et al., 1997. Threshold of sediment motion in coastal environments, in: *Pacific Coasts and Ports'97*. Proceedings, pp. 149–154.
- Spivakovskaya, D., Heemink, A., Milstein, G., Schoenmakers, J., 2005. Simulation of the transport of particles in coastal waters using forward and reverse time diffusion. *Advances in water resources* 28, 927–938.
- Sponaugle, S., Lee, T., Kourafalou, V., Pinkard, D., 2005. Florida Current frontal eddies and the settlement of coral reef fishes. *Limnology and Oceanography* 50, 1033–1048.
- Sponaugle, S., Paris, C., Walter, K., Kourafalou, V., Alessandro, E., 2012. Observed and modeled larval settlement of a reef fish to the Florida Keys. *Marine Ecology Progress Series* 453, 201–212.
- Stokes, G.G., 1880. On the theory of oscillatory waves. *Transactions of the Cambridge Philosophical Society* .
- Studivan, M.S., Rossin, A.M., Rubin, E., Soderberg, N., Holstein, D.M., Enochs, I.C., 2022. Reef sediments can act as a stony coral tissue loss disease vector. *Frontiers in Marine Science* , 2046.
- Sutherland, K.P., Porter, J.W., Torres, C., 2004. Disease and immunity in Caribbean and Indo-Pacific zooxanthellate corals. *Marine Ecology Progress Series* 266, 273–302.
- Team, A.B.R., 2005. Atlantic Acropora status review document. Report to National Marine Fisheries Service , 152.
- Thackston, E., Palermo, M.R., 2000. Improved methods for correlating turbidity and suspended solids for monitoring. US Army Engineer Research and Development Center.
- Thomas, C.J., Bridge, T.C., Figueiredo, J., Deleersnijder, E., Hanert, E., 2015. Connectivity between submerged and near-sea-surface coral reefs: Can submerged reef populations act as refuges? *Diversity and Distributions* 21, 1254–1266.
- Thomas, C.J., Lambrechts, J., Wolanski, E., Traag, V.A., Blondel, V.D., Deleersnijder, E., Hanert, E., 2014. Numerical modelling and graph theory tools to study ecological connectivity in the Great Barrier Reef. *Ecological Modelling* 272, 160–174.

- Tolman, H.L., et al., 2009. User manual and system documentation of WAVEWATCH III TM version 3.14. Technical note, MMAB Contribution 276, 220.
- U.S. Army Corps of Engineers, 2017. Water and Air Research, Inc. 2017. Contract W912EP-15-A-0002-0003 Final Miami Task 1 Report. URL: <https://usace.contentdm.oclc.org/utils/getfile/collection/p16021coll7/id/11844>. Accessed on February 8, 2022.
- Van Den Bremer, T., Breivik, Ø., 2018. Stokes drift. Philosophical Transactions of the Royal Society A: Mathematical, Physical and Engineering Sciences 376, 20170104.
- Varlas, G., Vervatis, V., Spyrou, C., Papadopoulou, E., Papadopoulos, A., Katsafados, P., 2020. Investigating the impact of atmosphere–wave–ocean interactions on a Mediterranean tropical-like cyclone. Ocean Modelling 153, 101675.
- Vaz, A.C., Paris, C.B., Olascoaga, M.J., Kourafalou, V.H., Kang, H., Reed, J.K., 2016. The perfect storm: match-mismatch of bio-physical events drives larval reef fish connectivity between Pulley Ridge mesophotic reef and the Florida Keys. Continental Shelf Research 125, 136–146.
- Viehman, S., Gittings, S., Groves, S., Moore, J., Moore, T., Stein, J., 2018. NCCOS Assessment: Coral Disturbance Response Monitoring (DRM) Along the Florida Reef Tract Following Hurricane Irma From 2017-10-09 to 2017-10-18 (NCEI Accession 0179071). NOAA National Centers for Environmental Information . Silver Spring, MD: National Centers for Coastal Ocean Science. Available online at: <https://doi.org/10.25921/sscd-6h41> (accessed June 22, 2020).
- Villas Bôas, A.B., Cornuelle, B.D., Mazloff, M.R., Gille, S.T., Ardhuin, F., 2020. Wave–current interactions at meso-and submesoscales: Insights from idealized numerical simulations. Journal of Physical Oceanography 50, 3483–3500.
- Vukovich, F.M., 1988. Loop Current boundary variations. Journal of Geophysical Research: Oceans 93, 15585–15591.
- Wachnicka, A., Browder, J., Jackson, T., Louda, W., Kelble, C., Abdelrahman, O., Stabenau, E., Avila, C., 2019. Hurricane Irma's impact on water quality and phytoplankton communities in Biscayne Bay (Florida, USA). Estuaries and Coasts , 1–18.
- Walton, C.J., Hayes, N.K., Gilliam, D.S., 2018. Impacts of a regional, multi-year, multi-species coral disease outbreak in Southeast Florida. Frontiers in Marine Science 5, 323.
- WAMDI Group, 1988. The WAM model – A third generation ocean wave prediction model. Journal of Physical Oceanography 18, 1775–1810.

- Warner, J.C., Armstrong, B., He, R., Zambon, J.B., 2010. Development of a coupled ocean–atmosphere–wave–sediment transport (COAWST) modeling system. *Ocean modelling* 35, 230–244.
- Weber, M., De Beer, D., Lott, C., Polerecky, L., Kohls, K., Abed, R.M., Ferdelman, T.G., Fabricius, K.E., 2012. Mechanisms of damage to corals exposed to sedimentation. *Proceedings of the National Academy of Sciences* 109, E1558–E1567.
- Weisberg, R., Liu, Y., Mayer, D., 2009. Mean circulation on the west Florida continental shelf observed with long-term moorings. *Geophys. Res. Lett* 36, L19610.
- Weisberg, R.H., He, R., 2003. Local and deep-ocean forcing contributions to anomalous water properties on the West Florida Shelf. *Journal of Geophysical Research: Oceans* 108.
- Weisberg, R.H., Liu, Y., 2017. On the Loop Current penetration into the Gulf of Mexico. *Journal of Geophysical Research: Oceans* 122, 9679–9694.
- Weisberg, R.H., Zheng, L., 2006. Hurricane storm surge simulations for Tampa Bay. *Estuaries and Coasts* 29, 899–913.
- Williams, S.D., Walter, C.S., Muller, E.M., 2021. Fine scale temporal and spatial dynamics of the stony coral tissue loss disease outbreak within the lower Florida Keys. *Frontiers in Marine Science* .
- Wolanski, E., 1994. Physical oceanographic processes of the Great Barrier Reef. CRC Press.
- Wolanski, E., Fabricius, K., Spagnol, S., Brinkman, R., 2005. Fine sediment budget on an inner-shelf coral-fringed island, Great Barrier Reef of Australia. *Estuarine, Coastal and Shelf Science* 65, 153–158.
- Wu, L., Chen, C., Guo, P., Shi, M., Qi, J., Ge, J., 2011. A FVCOM-based unstructured grid wave, current, sediment transport model, I. Model description and validation. *Journal of Ocean University of China* 10, 1–8.
- WW3DG, 2019. User Manual and System Documentation of WAVEWATCH III Version 6.07, the WAVEWATCH III Development Group. Technical Note 316. NOAA/NWS/ NCEP/MMAB url: <https://github.com/NOAA-EMC/WW3/wiki/files/manual.pdf>.
- Xia, M., Mao, M., Niu, Q., 2020. Implementation and comparison of the recent three-dimensional radiation stress theory and vortex-force formalism in an unstructured-grid coastal circulation model. *Estuarine, Coastal and Shelf Science* 240, 106771.

- Xian, S., Feng, K., Lin, N., Marsooli, R., Chavas, D., Chen, J., Hatzikyriakou, A., 2018. Brief communication: Rapid assessment of damaged residential buildings in the Florida Keys after Hurricane Irma. *Natural Hazards and Earth System Sciences* 18, 2041–2045.
- Zedler, S., Niiler, P., Stammer, D., Terrill, E., Morzel, J., 2009. Ocean's response to Hurricane Frances and its implications for drag coefficient parameterization at high wind speeds. *Journal of Geophysical Research: Oceans* 114.
- Zhang, C., Durgan, S.D., Lagomasino, D., 2019. Modeling risk of mangroves to tropical cyclones: A case study of Hurricane Irma. *Estuarine, Coastal and Shelf Science* 224, 108–116.